UNIVERSITY OF MINNESOTA
ST. ANTHONY FALLS LABORATORY
Engineering, Environmental and Geophysical Fluid Dynamics

PROJECT REPORT 516

Physical Model Study of the Fairfax Water Off-Shore Intake:

New Modifications and the Study of the Flow Patterns around the Sand Barrier

By

Omid Mohseni, Adam Howard and Matthew Lueker

Prepared for
Fairfax Water, VA

September 2008
Minneapolis, Minnesota

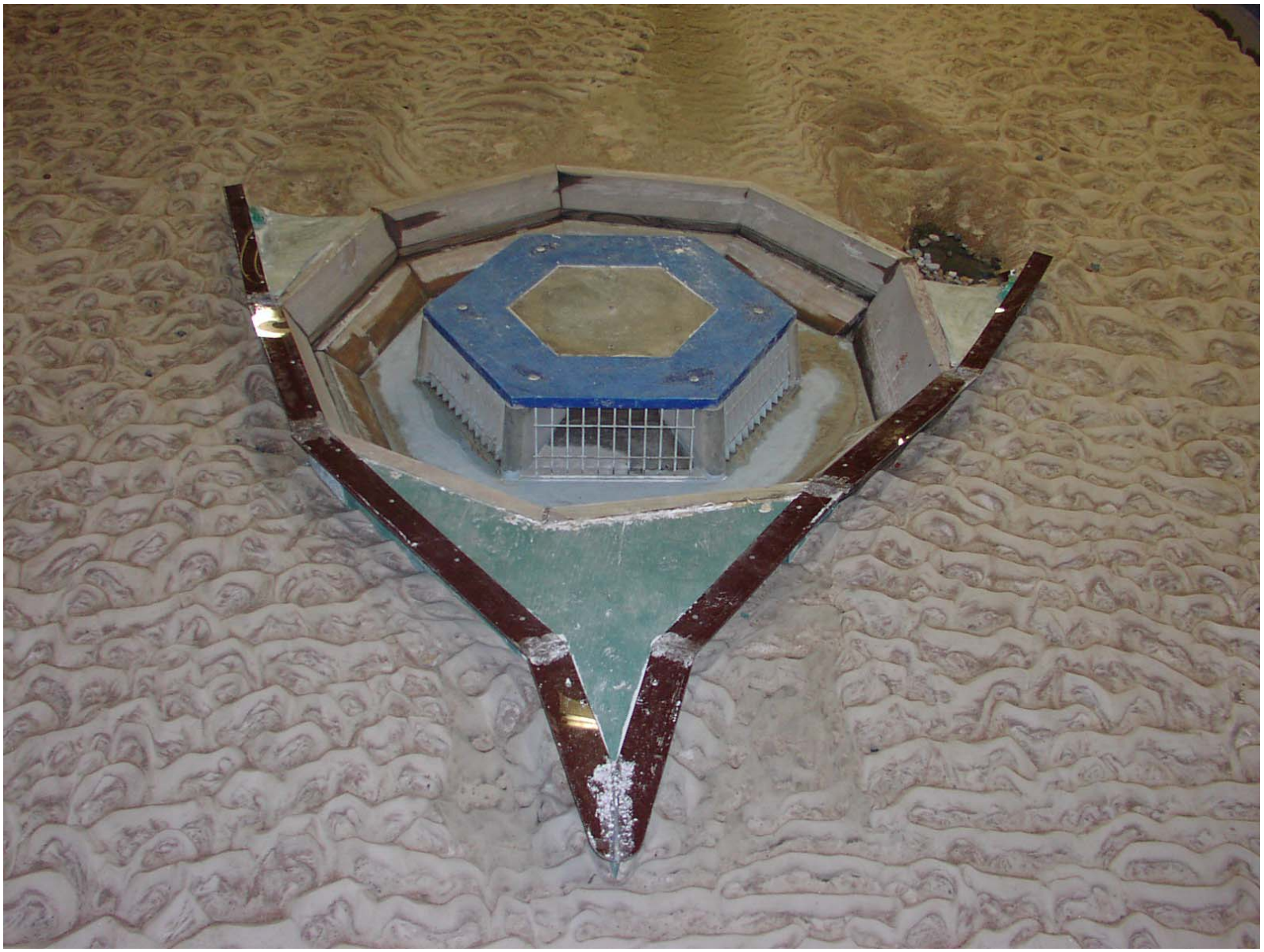

Abstract

To withdraw better water quality from the Potomac River for a water treatment plant during flow conditions under 20,000 cfs, Fairfax Water in VA had an off-shore river intake built in 2004. The intake was comprised of a 36-ft diameter hexagon concrete structure sitting on the bed of the river with a sand barrier around it to minimize the sand withdrawal. The sand barrier is a nonagon concrete structure with approximately a 54 ft diameter.

Since the intake started operating in late 2004, it has exhibited a significant amount of sand withdrawal. In 2007, a 1:10 scale model of the intake was built at the St. Anthony Falls Laboratory (SAFL) to study the causes of sand withdrawal, to modify the structure and to minimize the amount of sand withdrawal. The modifications conducted on the sand barrier resulted in a new geometry for the sand barrier, which was comprised of two wingwalls at the downstream end, a nose wall at the upstream end and a crown over the entire structure. The results of the tests conducted on this geometry showed that by building the new geometry for the sand barrier, the prototype bedload withdrawal should decrease by more than 60%. To further reduce the sediment withdrawal, a new study was required which is the subject of the current report.

In this study, three more modifications were made to the sand barrier and tested. A total of 11 tests were conducted on the new geometries and the original geometry. In addition, the flow patterns around the original geometry of the sand barrier as well as the modified geometry were studied to determine if any further modification could decrease the bedload withdrawal.

By studying the flow patterns and turbulence intensities around the structure, the final geometry was designed to include the crown, wingwalls and nose wall of the sixth geometry with a screen mounted on the half height of the walls around the structure. The screen was designed to prevent the eddies from dispersing the resuspended sediments in the water column along the height of the wall. The results of the tests conducted on this geometry suggest that the prototype bedload withdrawal should decrease by approximately 70%.

Acknowledgements

The work reported herein was supported by Fairfax Water and Mr. Dale Kovach from Fairfax Water was the project manager. We would like to thank Ben Plante for his contribution to the model construction and data collection.

Table of Contents

List of Figures

List of Tables

1. Introduction

1.1. Background

In 2004, Fairfax Water added an off-shore intake structure to its intake system in the Seneca Pool upstream of Dam no. 2 in the Potomac River (Figure 1.1). The idea of an off-shore intake was to withdraw water with better quality when the turbidity along the shoreline increases during the localized rain and run-off events. Fairfax Water currently withdraws 170 MGPD (millions of gallons per day) with a maximum of 300 MGPD from the off-shore intake when the Potomac River discharge is less than 20,000 cfs, i.e. when the quality of the river flow near the shoreline is suspected to be poor. The off-shore intake was a 36-ft diameter hexagon concrete structure sitting on the bed of the Potomac River with a 10×8 ft vertical shaft connected to a 10-ft diameter pipe laid under the river bed. The intake concrete structure was surrounded by a 54-ft nonagon sand barrier of the same height to minimize the amount of sand withdrawal. The Potomac River is relatively wide along that reach; approximately 2000 ft.

Since the beginning of operation, the intake has been filled with sand and silt quite frequently. A physical model study was conducted at the St. Anthony Falls Laboratory in 2006 and 2007 to modify the sand barrier or the intake structure to effectively minimize the rate of sediment withdrawal by the intake (Mohseni and Lueker, 2007).

1.2. Summary of the Previous Study

The model was built at a scale of 1:10. Froude similarity was used to scale all model parameters (Table 1.1), except for the flow depth. The flow depth was set lower to develop the bed forms observed in the field.

Table 1.1. Model-prototype scales used for a number of parameters in the physical model study.

Length	1:10
Area	1:100
Volume	1:1000
Flow rate	1:316.2
Velocity	1:3.16
Time	1:3.16
Shear stress	1:10

The final design of the structure in that model study was comprised of the existing structure with two wingwalls at the downstream end of the sand barrier to divert the dunes away from the structure, a broken nose wall to streamline the structure and to minimize scour holes at the upstream end of the sand barrier, and a crown over the entire structure to suppress the vortices responsible for lifting the bed particles over the walls (Figure 1.2).

The results of the tests conducted on the original and final designs are given again here in Table 1.2. As it was shown by Mohseni and Lueker (2007), the 120 micron particles could be assumed as the lower limit of the bedload materials at the model scale. Based on the sieve analyses conducted on the withdrawn materials (Figure 1.3), 60% of the materials withdrawn by the original intake design were bedload (0.6×3933=2360 grams). Under the final design of the intake structure, only 45% of the materials were bedload (0.45×2166=974 grams). Therefore, the final design decreased the bedload withdrawal by approximately 60%. Mohseni and Lueker (2007) also showed that the ratio of suspended load to bed load at the model scale was 8 to 1 while it was 5 to 1 for the prototype, therefore, regarding the suspended load, the results of the model study was conservative i.e. the bedload withdrawal at the prototype scale would decrease by more than 60%.

Table 1.2. Summary of the final results for 2-hour duration and a 10-hour pre-run (Mohseni and Lueker, 2007).

Geometry	150 MGPD Withdrawal rate	300 MGPD Withdrawal Rate
	Settling Tank (grams)	Settling Tank (grams)
Original	1730	3933
Nose wall and wingwalls with the crown	903	2166

A 60% reduction in bedload withdrawal did not meet the Fairfax Water plans for the improvement of the intake structure, and SAFL was asked to test another modification to the sand barrier. The goal of the new modification was further improvement to the geometry of the crown along the entire structure.

Figure 1.1. Aerial photo of the Potomac River and the approximate location of the off-shore intake in the Seneca Pool.

Figure 1.2. Sixth geometry: A long nose wall, with wingwalls, and a crown around the nose wall, the sand barrier and the wingwalls. In this figure, the crown was removed to scan the bed forms around the structure.

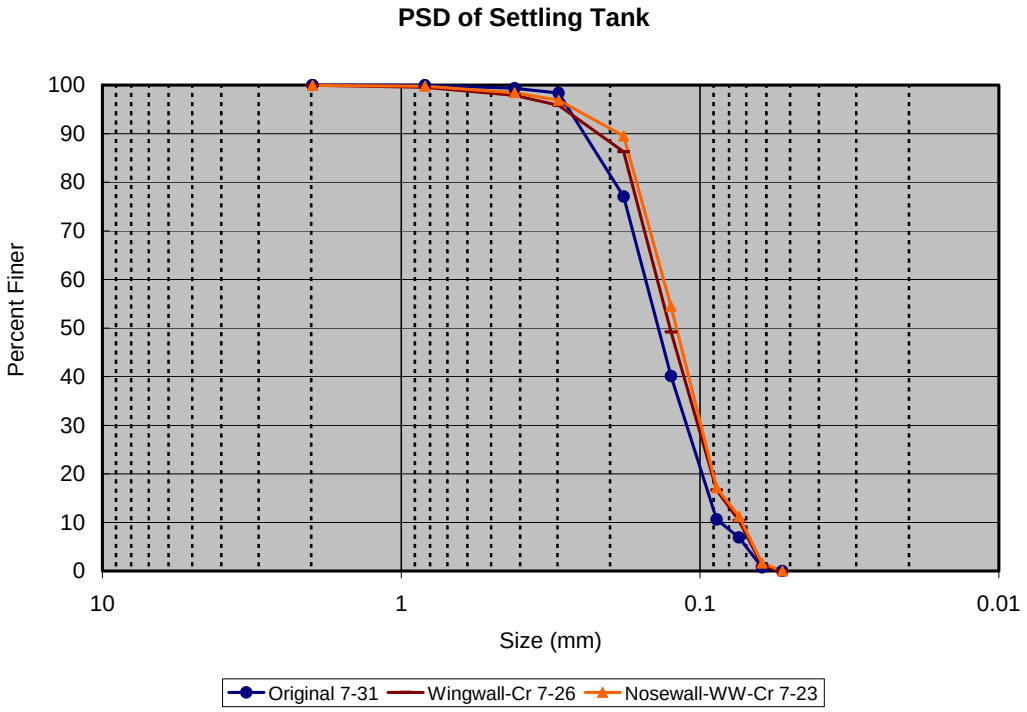

Figure 1.3. Particle size distributions (PSD) of all the materials collected from the settling tank during the two-hour tests with 2-hr pre-runs.

1.3. Scope of the Current Study

This report presents the results of two more tests conducted on the original design and the 6th geometry to verify the final results of the previous study. In addition, this report gives the results of the tests conducted on modified crowns. Overall, three modifications were made and 9 tests were conducted on the modified systems and one new test was conducted on the original design. In addition, velocities were measured along the sand barrier to further understand the strength of the vortices and turbulence intensities around the structure.

This report is organized as follows: In section 2, a brief description of the model features and the new instrumentation is given. In section 3, the results of the repeated tests on the original geometry as well as the sixth geometry are presented. In section 4, the three modifications made to the crown and the results of the tests and velocity measurements are given. Section 5 is a brief summary of the report.

2. The Physical Model Characteristics

2.1. Model Features

The physical model had already been built on the second floor (Model floor) of the St. Anthony Falls Laboratory (SAFL) for initial testing. Since the reach of the Potomac River upstream of the intake was relatively straight and wide, and the off-shore intake capture zone was small in comparison to the approach flow, only a 180 foot wide span of the river was modeled. The physical model consisted of a head tank and an 18×39 ft rectangular basin representing 180×390 ft of the Potomac River, and included the intake structure, a tail tank and a settling tank. Mississippi River water was discharged into the head tank using two different sources. Downstream of the head tank a rock crib wall was built to uniformly distribute the flow across the 18-ft basin.

The intake structure and sand barrier had been built from wood and Plexiglas, and the intake vertical shaft and its bell mouth were built from sheet metal. The intake structure was placed on a wooden platform to facilitate the future modifications to the structure. Subsequently, the model basin was filled with cinder blocks and a 2-inch layer of rocks (pebbles) on top. A geo-synthetic membrane was placed on top of the river rocks and then more than 4 inches of sediments representing the river bed materials at the model scale were placed on top of the membrane to create the bed forms observed in the field (Figure 2.1). For further information on the model construction see Mohseni and Lueker (2007).

The maximum modeled river flow was 7 cfs which corresponded to 22,000 cfs for the prototype across the entire width of the river, and the maximum modeled intake withdrawal rate was 0.95 MGPD (1.47 cfs), which corresponded to 300 MGPD (464 cfs) for the prototype.

Figure 2.1. The original geometry and the bed forms created at the model scale.

2.2. Instrumentation

To measure the flow rate through the model, a sharp-crested weir was built at the downstream end of the tail tank and was calibrated against the SAFL weighing tanks. Water level upstream of the weir was measured using a pressure tap mounted orthogonal to the flow direction to give the hydrostatic pressure and which was connected to a wet well with a point gage via a ¼" plastic tube. The point gage had a precision of 0.001 ft.

To measure the flow rate through the intake, a second weir was built at the outlet of the settling tank. A valve was mounted downstream of the intake to adjust the flow over the second weir, i.e. to meet the target withdrawal by the intake (Mohseni and Lueker, 2007).

To scan the bed forms after each test, a laser profiler was mounted on a towing carriage. Scanning was conducted every two inches (5 cm) for an area of about 13'×13' (400×400 cm), with the intake at the center of the area. The laser profiler had an accuracy of 0.02 inches (0.5 mm).

A Nortek Vectrino+ ADV was used to measure the velocity around the intake (Figure 2.2). All

of the tests were conducted using a side mounted probe which measured the velocity in a control volume located 1.97 inches (50 mm) away from the probe (Vectrino). This allowed for accurate velocity measurements without flow disruption from the probe itself.

The ADV measures the flow velocity in all three directions by measuring the Doppler shift from particles in the flow. It is often necessary to seed the flow in order to ensure particles are present in the water. Due to the use of sediment laden water directly from the Mississippi River and the movement of suspended sediments in the model, it was not necessary to seed the flow.

Figure 2.2. The Nortek Vectrino+ ADV used for velocity measurement.

The Nortek Vectrino+ ADV uses two pulse pairs for each velocity measurement. This allows for a calculation of correlation coefficient for each velocity measured (Clunie et al., 2007). It is important to have a correlation coefficient above 0.70 for instantaneous velocities and above 0.40 for average velocities (Sontek, 2008). The Vectrino+ had a maximum sampling rate of 200 Hz, which was used on all tests. With a frequency of 200 Hz, 36,000 velocity measurements were taken over a period of one minute at every point in three directions (each point measurement was comprised of three components of velocity in three directions: x-component or streamwise direction, y-component or widthwise direction, and z-component or vertical direction).

Data processing was done in large part through the use of the software package WinADV.

WinADV is produced by the Bureau of Reclamation specifically for processing the ADV data. It allows for the viewing of time series, correlation coefficients, signal to noise ratios and histogram plots of probability density functions, cumulative density functions and power spectrum series. A phase-space threshold despiking filter as described by Goring & Nikora (2002) and modified by Wahl (2003) was used to eliminate outliers.

2.3. Experimental Setup

To measure the sediment withdrawal by the intake, a settling tank was built on the lower floor of the St. Anthony Falls Laboratory and after each test, the tank was drained, and all sediments removed by the settling tank were collected by a shop-vac. The sediments were then placed in an oven for 24 hours to dry. The dry sediments were weighed using a scale with a precision of 0.0002 lbs (0.1 grams). The settling tank had a removal efficiency of about 100% for particles larger than 0.003 inches (0.075 mm), i.e. the settling tank could be used to measure the bedload withdrawal.

All tests were conducted at 22,000 cfs which corresponded to 7 cfs at the model scale. To determine the flow patterns (using the ADV) around the structures the inlet was kept closed except for the test on January 14, 2008, which had an intake flow rate of 464 cfs (1.47 cfs at the model scale). During the tests, the Mississippi water temperature varied between 33.2 ^{o}F (0.7 ^{o}C) and 35.6 ^{o}F (2 ^{o}C) in January, was at 39 ^{o}F (3.9 ^{o}C) in March, 49 ^{o}F (9.4 ^{o}C) in May, and 64.4 ^{o}F (18 ^{o}C) in June.

All velocity measurements were stationary, i.e. the probe was fixed at each location during the data collection. The ADV could be moved vertically, and parallel and perpendicular to the flow on a horizontal plane. This allowed for the creation of a grid which could measure velocity at various depths and locations around the sand barrier. Measurements were taken at five fixed depths. The bed forms would not allow a well established bed elevation to be the datum, therefore, the depths were based on the water surface elevation which remained fairly constant. The model depths, where velocity measurements were conducted, were 4.92″, 3.84″, 2.76″, 1.68″, and 0.6″ from the water surface at the model scale, which “somewhat” corresponded to 4.1', 3.2', 2.3', 1.4', and 0.5' for the prototype. In order to accurately model the bed forms and the bed shear stress at the model scale, the model depths were not necessarily representative of the

prototype depths associated with the 22,000 cfs flow condition (Mohseni and Lueker, 2007). For the 22,000 cfs flow condition, the 2.30' (2.76″ model) depth was located near the top of the sand barrier.

The measurements around the sand barrier were taken ¼ inch from the intake, i.e. 0.2 ft for the prototype. Any measurements taken away from the structure included only three depths. These depths were 4.10', 2.30', and 0.5' for the prototype. The ADV locations in the horizontal plane across the width of the river were 10' apart (one foot at the model scale) and along the flow direction 5 ft apart (0.5 ft at the model scale). This created a grid with 417 points, including depths, when the entire grid was used for flow velocity measurement. The measurement grid is shown in Figure 2.3. At each grid point near the structure five numbers are printed which represent the five grid numbers along the depth at each location (4.1', 3.2', 2.3', 1.4', and 0.5'). For the grid points away from the structure, only three numbers are given which represent the three grid numbers along the depth (4.10', 2.30', and 0.5'). When measurements were only taken along the modified sand barrier, the grid was comprised of 160 points.

The two sides of the structure were defined as Virginia Side and Maryland Side. The Virginia Side (south side) is defined as the right side of the structure when facing downstream and the Maryland Side (north side) is defined as the left side of the structure when facing downstream.

The ADV was always oriented with the probe facing perpendicular to the flow and always facing the structure. In the figures, a positive X velocity represents the downstream direction, a negative Y velocity represents the flow away from the structure, and a positive Z velocity is towards the water surface.

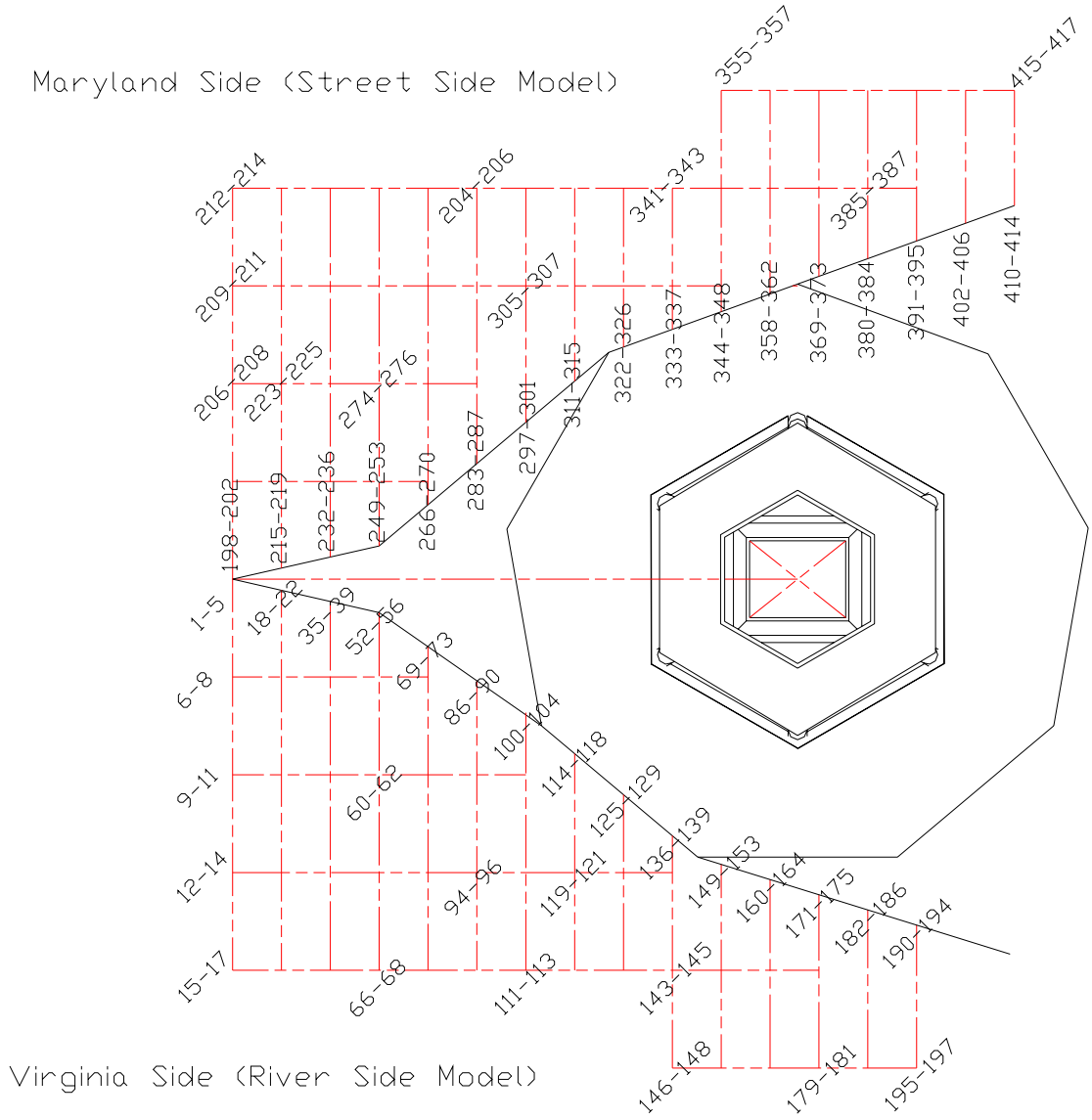

Figure 2.3. The grid and some of the grid numbers where velocities were measured. Along the structure, at each grid point, five grid numbers are given, e.g. 1 - 5, which are associated with five depths where velocities were measured. Away from the structure, at each grid point, three grid numbers are given, e.g. 15 – 17, which represent the three depths where velocities were measured.

3. Verifying the Rate of Sediment Withdrawal by the Sixth Geometry

The last two tests conducted in the previous study exhibited some errors, due to seepage through the membrane underneath the bed materials. Therefore, it was decided to conduct one more test on the sixth geometry (Figure 1.2) with a crown shown in Figure 3.1. The crown extended 9 inches into the river and 6 inches upward at the prototype scale. In addition, since the water temperature had dropped and could impact the settling of the suspended particles as well as turbulence in the flow, one more test was conducted on the original geometry to ensure a fair comparison between the original geometry and the sixth geometry.

In both tests, prior to tests, the bed was flattened to remove any memory from the past tests and ensure similar initial conditions. Then the intake valve was kept closed and the model was run at 22,000 cfs for 12 hours, after which the valve was opened and the model was run at 22,000 cfs with a 300 MGPD withdrawal for 4 hours. After the tests, the bed was scanned (Figures 3.2 and 3.3) and the sediments collected in the settling tank were dried and weighed. The results of these two tests are given in Table 3.1 and show that the sediment withdrawal is twice as much as the tests shown in Table 1.2 due to the longer duration of the tests. The values shown in Table 3.1 are not in complete agreement with those in Table 2.1, because the temperature was about 30 ^{o}F lower than when these tests were initially conducted, i.e. both turbulence and particle settling were different than the tests conducted in summer. Nevertheless, the percent reduction reconfirm that the sixth geometry removed more than 60% of the bedload (using the particle size distributions shown in Figure 1.3, the sixth geometry reduced the bedload withdrawal by 66%). Because the tests on new geometries were conducted in winter the results of these two tests were used as a reference for assessing the improvements to the structure.

Table 3.1. Summary of the tests with 4-hour duration and 12-hour pre-runs at 22,000 cfs flow rate in the river, and a 300 MGPD intake withdrawal.

Test Number and Geometry	Settling Tank (grams)	Date
Test no. 1 on the original geometry	10,841	10/08/2007
Test no. 2 on the sixth geometry (nose wall and wingwalls with the crown)	4,888	10/15/2007

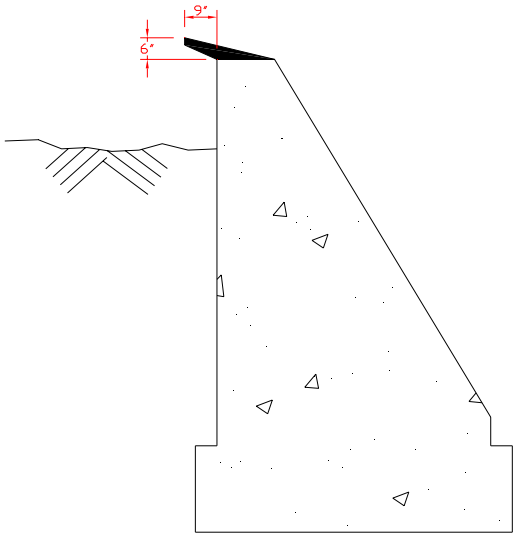

Figure 3.1. The crown installed along the sand barrier, nose wall and wingwalls.

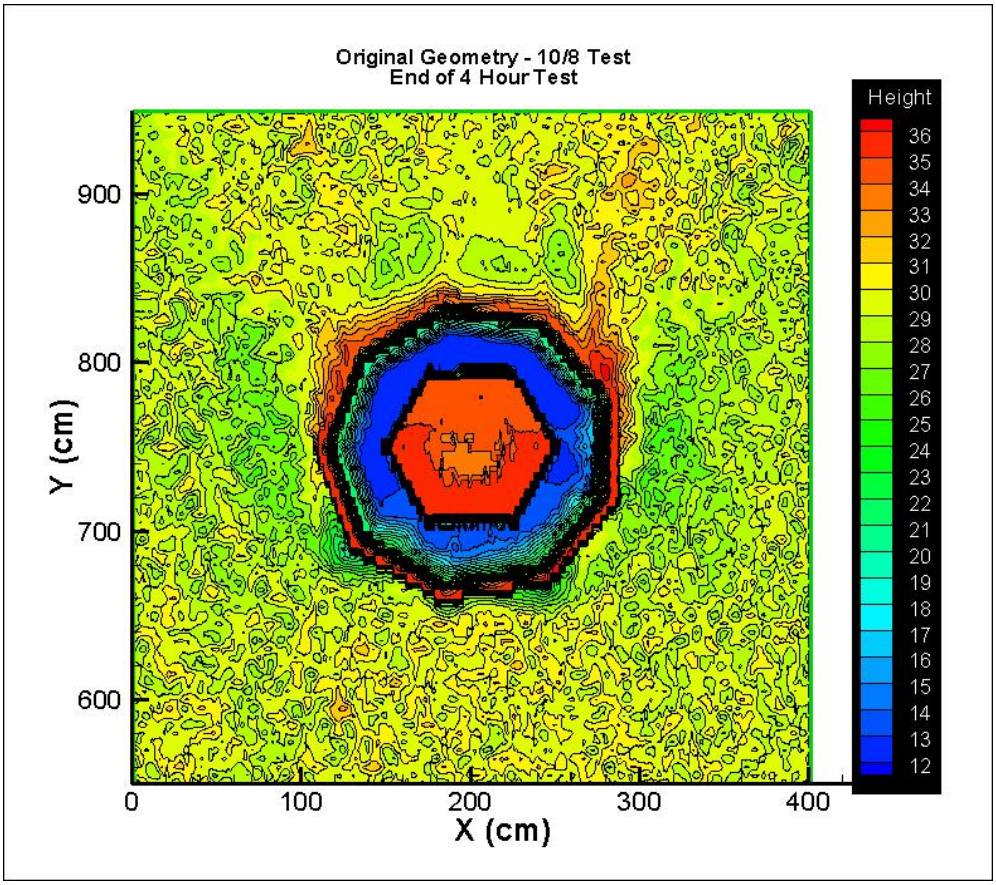

Figure 3.2. Results of the topographical scan of the bed after the test was conducted on the original geometry on 10/08. The intake flow rate was 300 MGPD (1.47 cfs). It was a 4-hour duration test with a 12-hour pre-run.

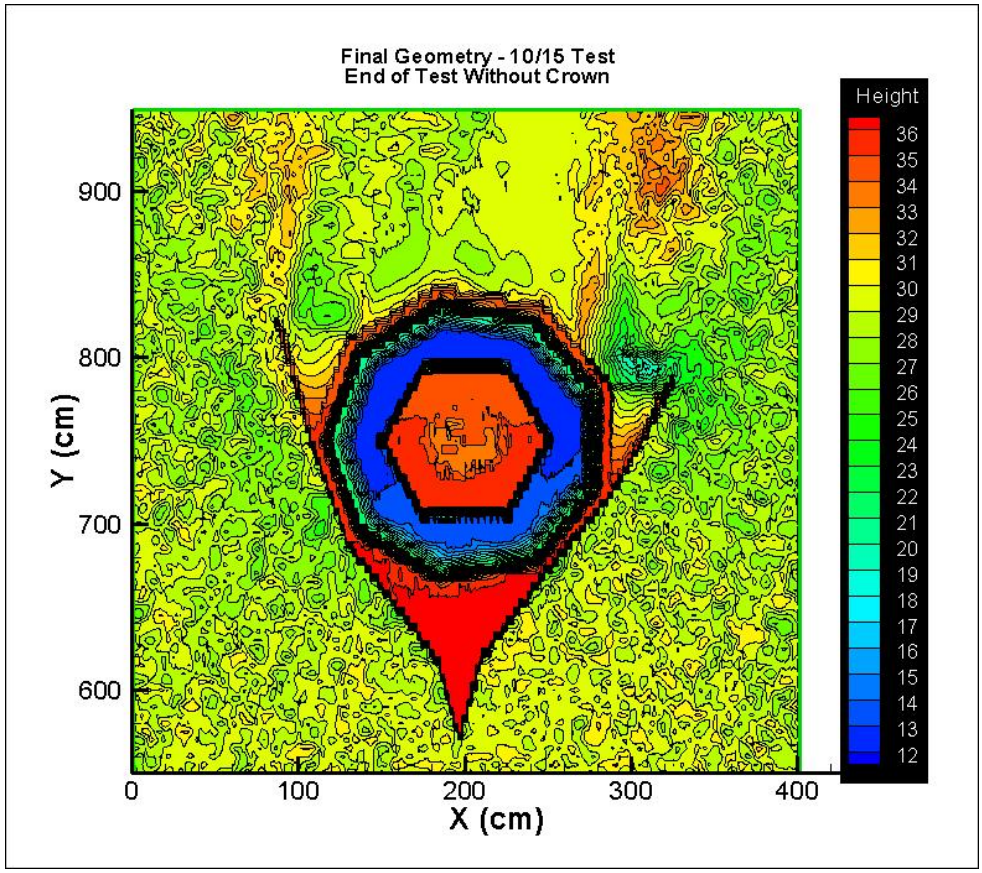

Figure 3.3. Results of the topographical scan of the bed after the test was conducted on the sixth geometry on 10/15. The intake flow rate was 300 MGPD (1.47 cfs). It was a 4-hour duration test with a 12-hour pre-run.

4. Testing New Geometries

To improve the reduction in sediment withdrawal, it was decided to slightly modify the sixth geometry. The nose wall had already streamlined the flow patterns at the upstream end of the sand barrier and the wingwalls had diverted the dunes away from the structure. Therefore, it was decided to modify the crown to suppress the vortices along the structure which would resuspend the bedload. A total of three modifications were made to the structure, and since in the report prepared by Mohseni and Lueker (2007), the geometries were numbered from one to eight, it was decided to number these three geometries from nine to eleven.

4.1. The 9th Geometry

The ninth geometry (first modification in this study) was a significant deviation from the sixth geometry. It was decided to increase the width of the crown, i.e. the length extended into the river, from 9 to 18 inches and then slope it at 5% away from the structure. The new crown was extended 6 inches upward to the maximum depth required for navigation over the structure (Figure 4.1). The additional length was to keep the vortices near the structure and the 5% downward slope was to allow the suspended particles which would settle over the crown (because of low flow velocities over the crown) to move towards the river. Therefore, the ninth geometry was comprised of a nose wall, an 18-inch crown sloped downward and wingwalls.

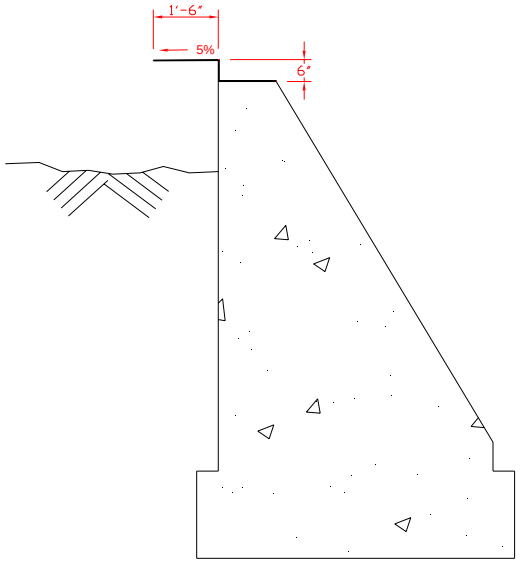

Figure 4.1. The ninth geometry crown installed along the sand barrier, nose wall and wingwalls.

Two tests were conducted in November. Prior to each test, the bed was flattened. The model was run for 8 hours at 22,000 cfs (7 cfs for the model) with the intake valve closed, and then it was run for an additional 4 hours at 22,000 cfs with an intake withdrawal of 300 MGPD (1.47 cfs for the model). The pre-run duration was set at 8 hours because no change was evident after 8 hours.

After the first test, a couple of seepage points through the membrane underneath the bed sediment near the structure were identified. The seepage points were repaired for the second test, and the sediment withdrawal decreased. The results of the two tests are given in Table 4.2. Despite the repair, the reduction in sediment withdrawal was not as good as the sixth geometry.

Table 4.1. Summary of the tests with 4-hour duration and 8-hour pre-runs at 22,000 cfs flow rate in the river, and a 300 MGPD intake withdrawal.

Ninth Geometry (nose wall and wingwalls with a crown sloped outward)	Settling Tank (grams)	Date
Test no. 3	7762	11/06/2007
Test no. 4	5884	11/21/2007

4.2. The 10th Geometry

Since the downward slope of the crown in the ninth geometry did not lead to better results, it was decided to slightly modify the sixth geometry (Mohseni and Lueker, 2007) by only extending the crown by 18 inches (Figure 4.2) and conduct two tests on this geometry. However, prior to the modification of the structure, it was decided to measure the three components of velocity around the structure as was explained in Section 2.3 and determine the flow patterns, and the intensity of turbulence and vorticity around the structure.

4.2.1. Velocity Measurements

The velocity data were collected over a long period, therefore it was difficult to capture eddies forming along the structure. Furthermore, the movement of dunes created a mobile bed during the velocity measurement thus making the near bed conditions too dynamic to capture average velocities near the bed. In addition, the measuring grid was fairly coarse, i.e. the eddies and vortices could not be well captured in the measurement. With these limitations in mind, it is important to look at the data with a more holistic approach. Even though the grid was comprised of either 417 or 160 points, one could not confidently define the detailed characteristics of the

flow at any given instant or location. However, the overall characteristics of the flow can be assessed from the data.

All charts presented in the main body of this report provide the instrument depth at the prototype scale. The actual measured data are presented in the appendix at the model scale. Each chart provides the overall characteristics of the flow patterns, whether it is presented at the model scale or the prototype scale.

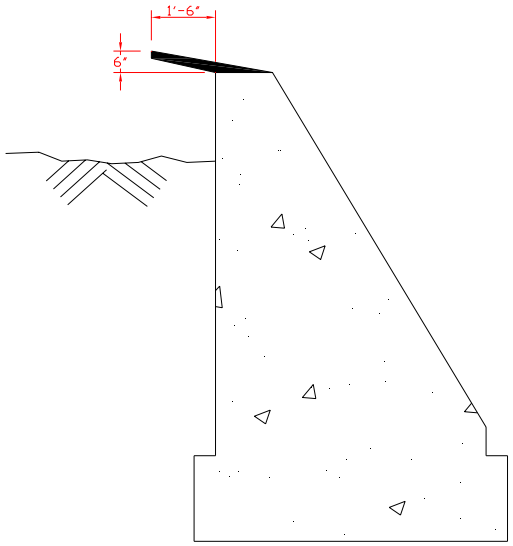

Figure 4.2. The tenth geometry crown installed along the sand barrier, nose wall and wingwalls.

The first set of velocity measurements was conducted on January 9-11, 2008 with the wingwalls and the nose wall in place and with no crown. The flow was set at 22,000 cfs (7 cfs at the model scale) with the intake valve closed. The velocities were measured for the entire grid of 417 points. Each measurement took one minute, which provided approximately 12,000 velocity measurements at each point in each direction.

The second set of velocities was measured on January 14, 2008 with the intake valve open to withdraw 464 cfs (1.47 cfs at the model scale). The flow rate before opening the intake valve was set at 22,000 cfs (7 cfs at the model scale), and the wingwalls and nose wall were in place, but the crown was removed, i.e. the same as in the January 9-11, 2008 test. All measurements

were only taken along the structure at every other point, which resulted in measurements every foot in the direction of flow (at the model scale). The goal of this test was to see if the flow patterns along the structure would change from the first set when the intake valve was open. The results showed that velocities measured along the height of the structure in this set were not significantly different from those collected in the first set. Therefore, it was decided to keep the intake valve closed in the subsequent tests.

The third set of velocities was measured on January 24-25, 2008. The wing walls and nose walls were in place and the 10^{th} geometry crown (Figure 4.2) was mounted. The flow rate was set at 22,000 cfs with the intake valve closed. Velocity data were collected for 30 seconds at each location. This provided approximately 6,000 velocity measurements in each direction.

The velocity vectors along the walls show a very uniform flow above the structure when the crown is not present. But from the top of the structure down to the bed, a lot of fluctuations are evident (Figure 4.3). From the fluctuations, it is possible to observe the presence of vortices along the structure. Nearly the opposite is true for the velocity vectors with the crown in place. There are no fluctuations at depths greater than the structure, but near the top of the structure (a depth of 1.4 ft) there are more fluctuations than were present without the crown (Figure 4.4). In addition, there is a strong upward direction at the 1.4 ft depth at the upstream end of the structure which tends to dissipate along the length of the structure. Nevertheless, the direction is upward and this indicates that resuspended particles may go over the barrier and enter the intake.

The velocities at lower depths are crucial for scouring and transport of sediment. Large velocity vectors scour the bed, and more fluctuations mean more likelihood for sediment resuspension and upward transport. The velocities with the crown show fewer fluctuations at lower depths. It is important to note that with the crown in place, velocities were not measured as close to the structure as velocities measured without the crown. Nevertheless, the vector plot with the crown (Figure 4.3) shows that it is less likely for the particles which move away from the crown to be lifted upward, i.e. the fluctuations were somewhat suppressed. With the crown in place, only the particles which moved away from the structure at a depth near the top of the crown were likely to stay in suspension and be withdrawn into the intake.

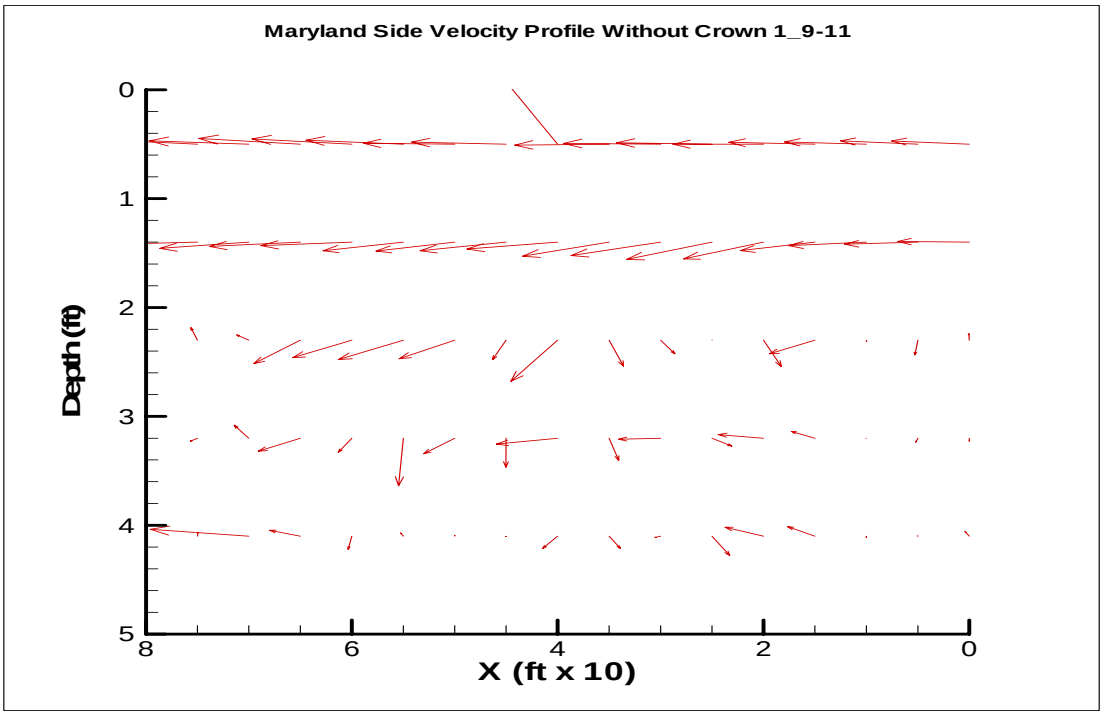

Figure 4.3. Velocity vectors along the nose wall, sand barrier and wingwalls with no crown in place and the intake valve closed. X increases in the direction of flow. The sizes of the vectors represent the relative magnitude of velocities. Depth and distance are given at the prototype scale.

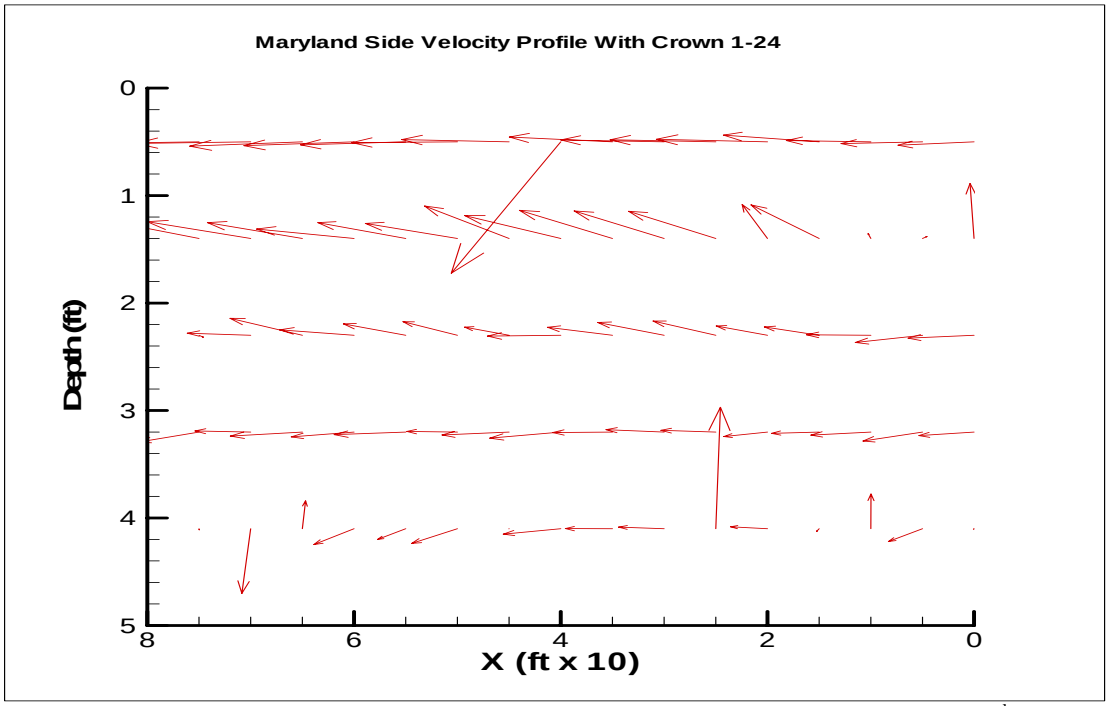

Figure 4.4. Velocity vectors along the nose wall, sand barrier and wingwalls with the 10th geometry crown in place and the intake valve closed. X increases in the direction of flow. The sizes of the vectors represent the relative magnitude of velocities. Depth and distance are given at the prototype scale.

The average velocities measured at a depth of 3.2 ft from the surface, i.e. below the top of the structure, without the crown in place (first set) are shown in Figure 4.5. The fluctuations evident in x- and z-component of the flow velocity indicate the formation of horizontal vortices along the structure. Velocity components at other depths (at the model scale) are shown in Figures A.1 to A.10. The summary of the average x-, y- and z-components of velocity are given in Figures A.11 to A.13. There is a mild increasing trend in the x-component of velocity at depths above the structure (0.6 and 1.68 inches at the model scale), which is due to the change in the cross-sectional area, i.e. the structure has blocked part of the river (Figures A.1 to A.4 and A.11). The maximum fluctuations occur at the top of the structure, where horizontal vortices disperse into the water column. The y-components of velocity are near zero with little fluctuations (Figure A.12). The z-components of velocity are near zero at most locations with the largest fluctuations evident at the top of the structure (2.76 inches from the surface at the model scale).

Similarly, the largest turbulence intensity is at the top of the structure (Figures A.18 and A.19), and it is primarily due to turbulence in the z direction. Estimates of vorticity about the three axes are shown in Figures A.24 to A.29. Vorticity about x- and z-axes are very small. Vorticity about the y-axis is significant larger with the maximum near the top of the structure (Figures A.26 and A.27), which is due to the presence of horizontal vortices along the structure.

With the crown in place (the 10^{th} geometry), the fluctuations at a depth of 3.2 ft below the surface (roughly at the mid height of the structure) are suppressed (Figure 4.6). Velocities near the surface (Figures B.1 and B.2) do not fluctuate, however there is a dip in the x-component at point 149 (Figure B.1) on the river side of the structure which is also evident for the condition with no crown (Figure A.1). This persisting reduction in the x-component is due to the separation of flow at that location. An increase in the magnitude of z- and y-components reflects the presence of a circulation in that location. Therefore, where the separation occurs, the z-component of velocity increases and more scouring can occur, regardless of the presence of the crown.

With the crown in place, fluctuations in velocity increase above the top of the structure (Figures B.3 and B.4) and near the bed (Figure B.9 and B.10), i.e. more scouring may occur along the structure and if the particles are lifted all the way to the top of the crown, there is a good chance

that the particles will be pulled into the intake. Overall the velocities are slightly higher with the crown in place than without the crown (Figure B.11 to B.16). However, turbulence is somewhat suppressed at depths near or below the crown (Figures B.21 to B.24). The largest turbulence intensity is estimated to be near the bed (Figures 4.7, B.25 and B.26). The y-components of velocity near the bed increase in the mid-section of the structure (Figures B.13 and B.14) and are towards the river. This is due to horizontal vortices which disperse along the stream width and can potentially transport the bed materials away from the structure. However, the y-components of velocity increase slightly at the mid-section above the structure which may transport some of the lighter suspended sediments towards the intake. The magnitude of the y-component of velocity does not seem to be large enough to be effective in moving the resuspended bedload towards the intake. Overall, with the crown in place, the shear stresses near the bed seem to be slightly higher, more scouring is likely, but turbulence above the bed is not as strong without the crown, therefore the resuspended bedload may not stay in resuspension.

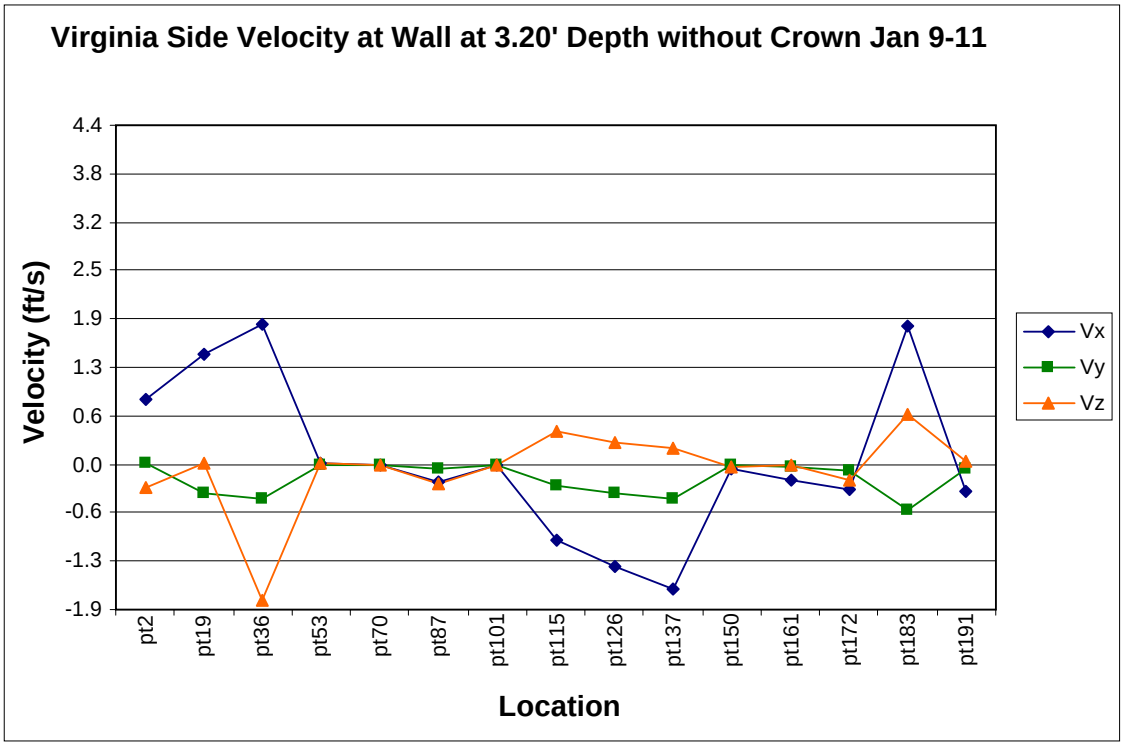

Figure 4.5. Average velocity components along the structure without the crown at a depth of 3.2 ft from the surface. Streamflow is from left to right. Location numbers are shown in Figure 2.3.

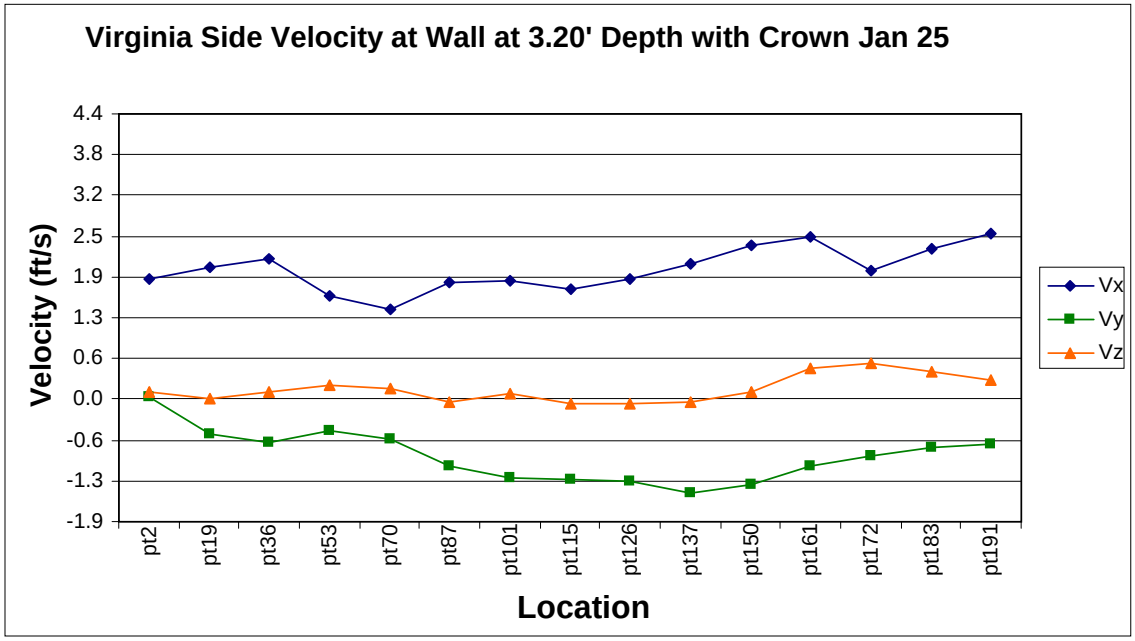

Figure 4.6. Average velocity components along the structure with the crown in place (10th geometry) at a depth of 3.2 ft from the surface. Streamflow is from left to right. Location numbers are shown in Figure 2.3.

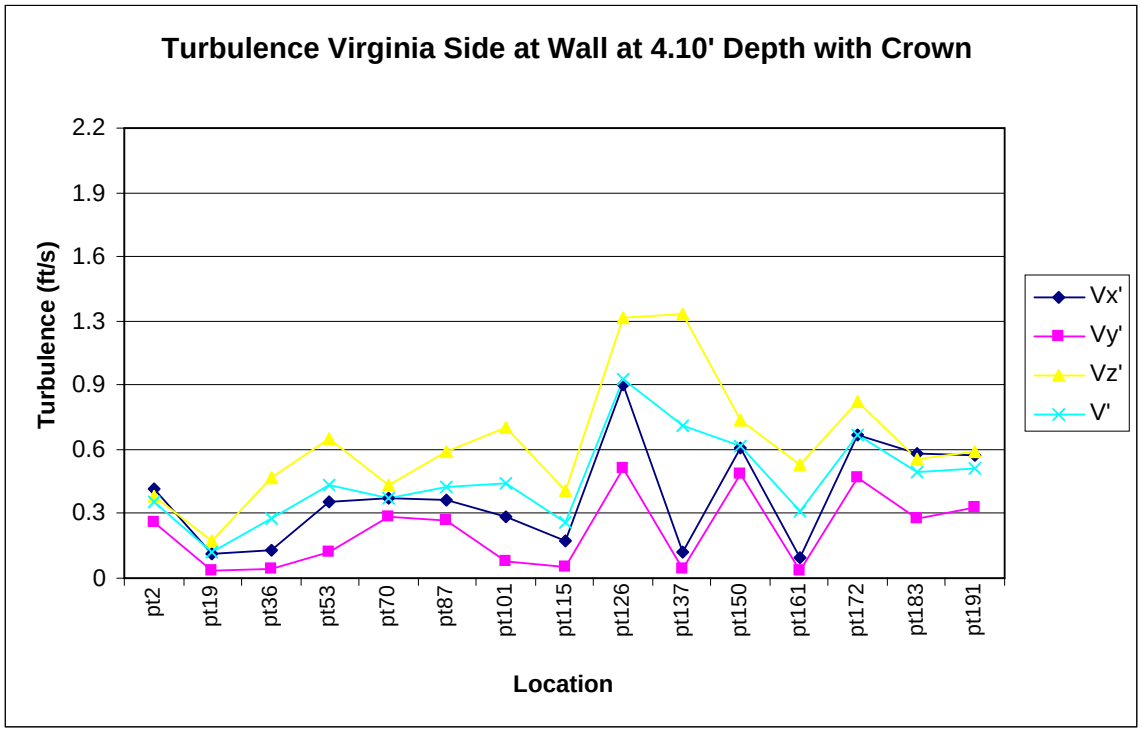

Figure 4.7. Turbulence intensities along the structure with the crown in place (10th geometry) at a depth of 4.1 ft from the surface. Streamflow is from left to right. Location numbers are shown in Figure 2.3.

4.2.2. Sediment Withdrawal

After completing the velocity measurement, three tests were conducted on the 10th geometry. In addition, one more test was conducted on the original geometry since water temperature had changed which would impact the settling velocity of the sediments as well as turbulence. Figures 4.8 and 4.9 show the bed scans prior to the test with the new crown and with the original geometry, i.e. the bed was flattened to create similar initial condition. Figure 4.10 is the photo of the original geometry prior to the test.

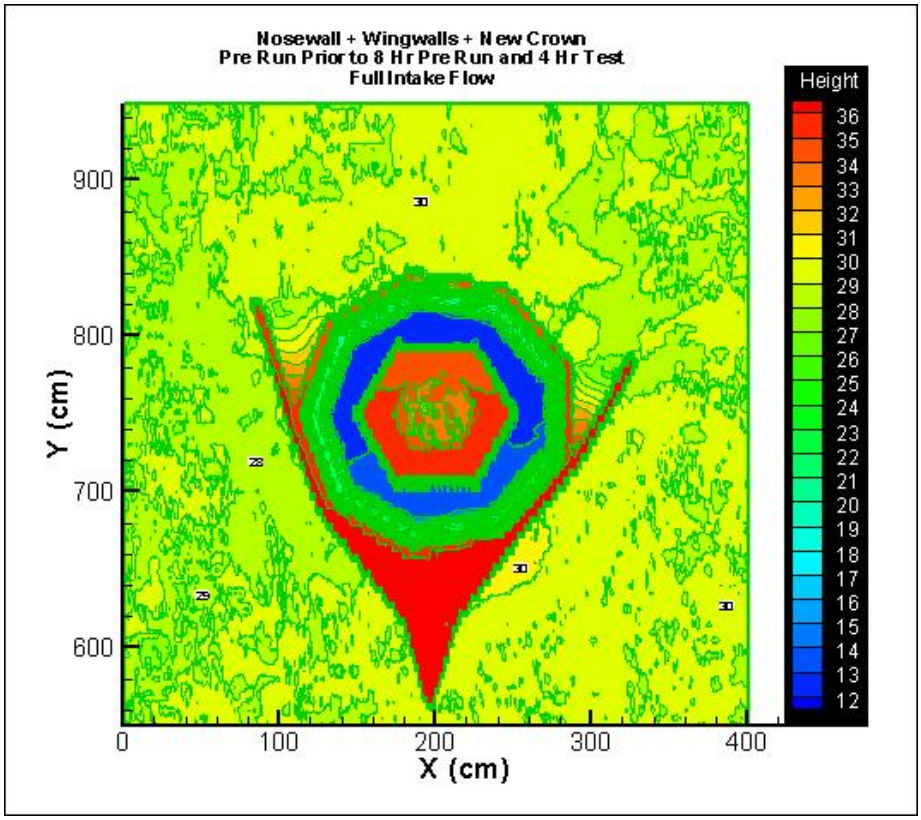

Figure 4.8. Bed elevations prior to Test no. 5 with the new crown in place.

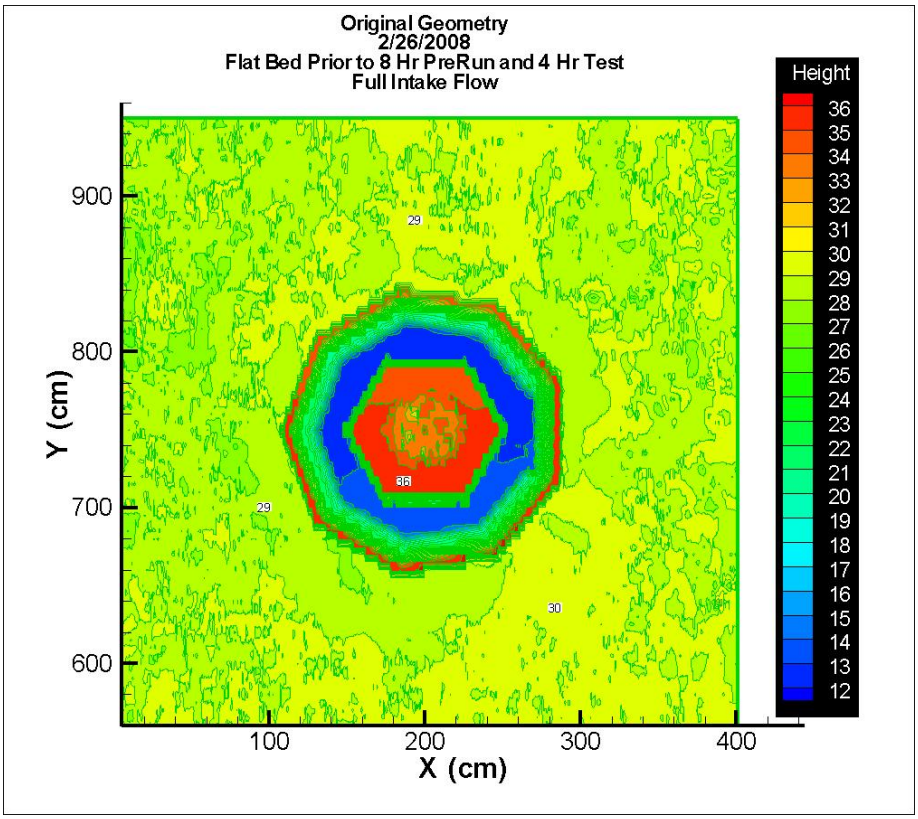

Figure 4.9. Bed elevations prior to Test no. 8 on the original geometry.

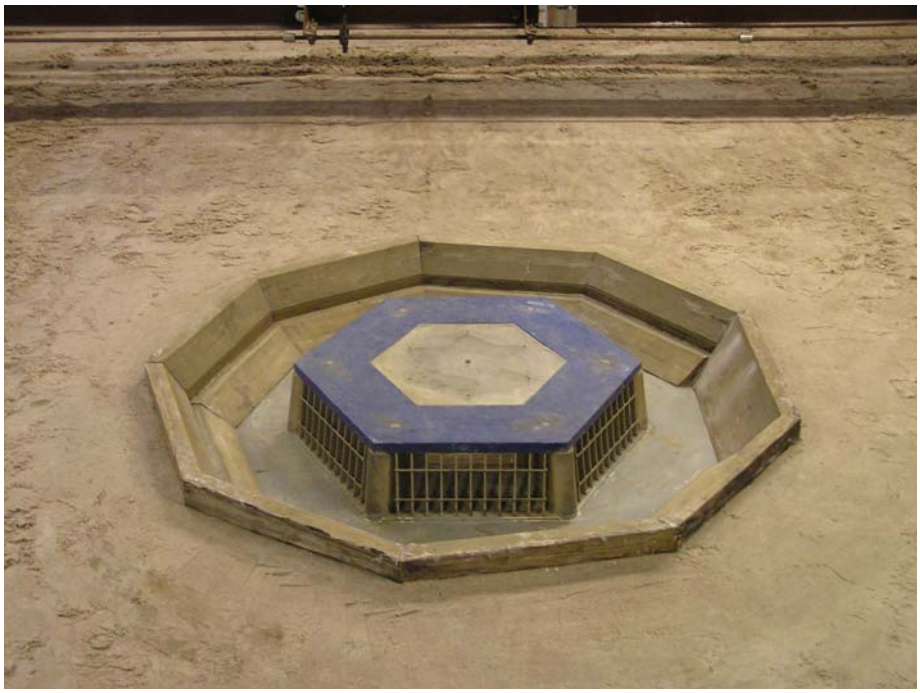

Figure 4.10. Photo of the flat bed prior to Test no. 8.

The first test on the 10th geometry (Test no.5), resulted in a significant withdrawal of sediment in comparison to the previous tests. After close inspection, a couple of seepage points were spotted. Therefore, the seepage points were repaired and the test was repeated two more times (Tests nos. 6 and 7).

A reduction in scour holes is evident from the pictures taken from the bed after each test (Figures 4.11 through 4.14). There are drastic improvements in the scour holes developed on the upstream vertexes of the sand barrier (Figures 4.11 and 4.12) and there is a significant reduction in deposition at the downstream end of the system as was evident from the sixth geometry (Mohseni and Lueker, 2007).

The reductions in scour holes were quantified using the bed scans. The lowest bed elevation around the 10the geometry was 25 cm at the model scale (Figure 4.15), while the lowest bed elevation around the original geometry was 19 cm at the model scale (Figure 4.16). As expected and speculated from the velocity measurements, at the vertexes where the nose walls meet the existing sand barrier the scour holes can be seen to be the worst. The average depth below the top of the structure on the left (Maryland side) of these two scour holes is reduced from 17 cm (5.6 ft for the prototype) to 11 cm (3.6 ft for the prototype). For the right scour hole (Virginia side), these values are 14 cm (4.6 ft for the prototype) and 7 cm (2.3 ft for the prototype) respectively.

The results of the tests are summarized in Table 4.2. The results of Test nos. 6 and 7 were close and repeatable and show a significant improvement over the 9th geometry. However, the 10th geometry did not show any improvement over the sixth geometry (Table 3.1).

Table 4.2. Summary of the tests with 4-hour duration and 8-hour pre-runs at 22,000 cfs flow rate in the river, and a 300 MGPD intake withdrawal.

Test number and geometry	Settling Tank (grams)	Date
Test no. 5 on the 10th geometry	6168	2/1/08
Test no. 6 on the 10th geometry	4891	2/5/08
Test no. 7 on the 10th geometry	4905	2/15/08
Test no. 8 on the original geometry	8802	2/26/08

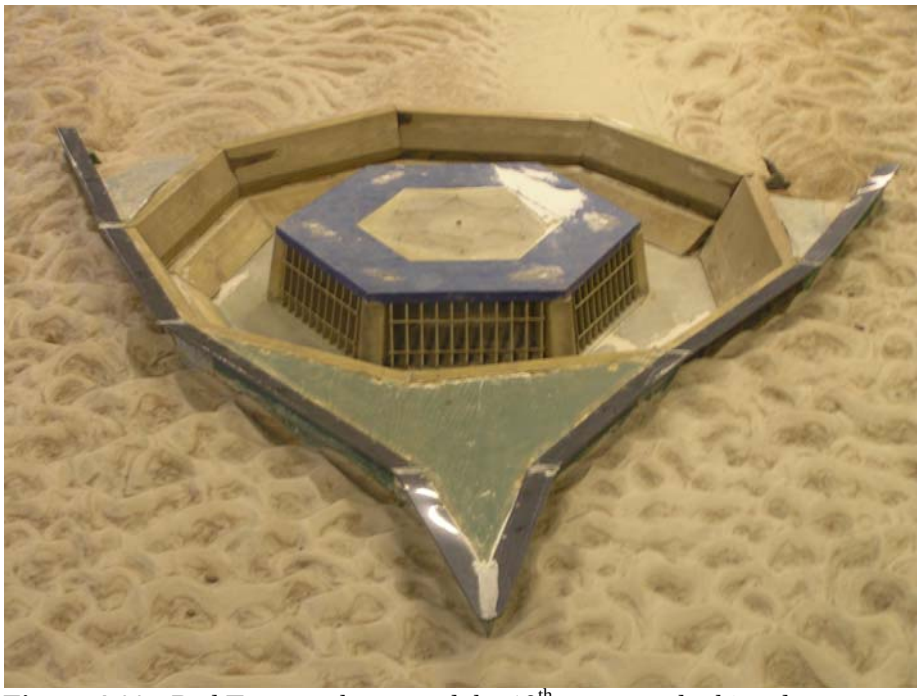

Figure 4.11. Bed Topography around the 10th geometry looking downstream

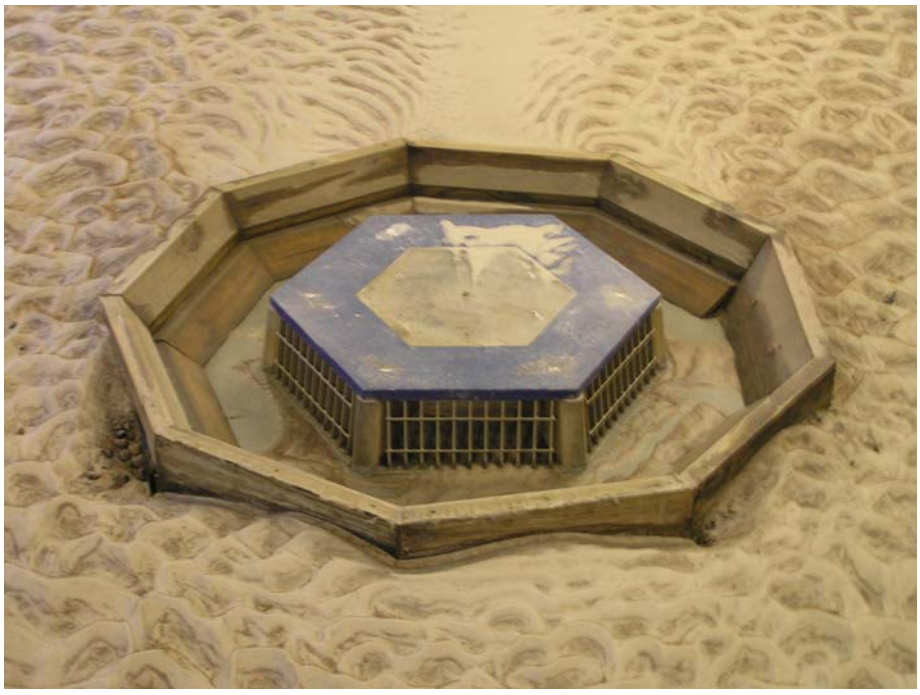

Figure 1.12. Bed Topography around the original geometry looking downstream (same angle as in Figure 4.11)

Figure 4.13. Bed topography around the 10th geometry looking from the Virginia shoreline.

Figure 4.14. Bed topography around the original geometry looking from the Virginia shoreline (same angle as in Figure 4.13).

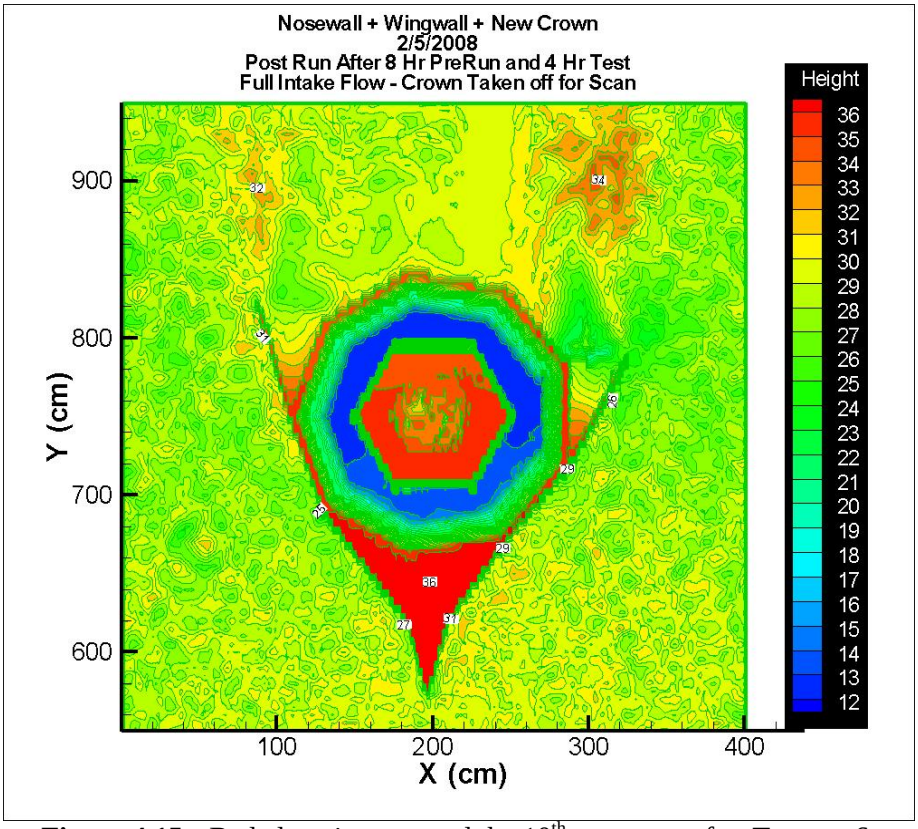

Figure 4.15. Bed elevations around the 10th geometry after Test no. 6.

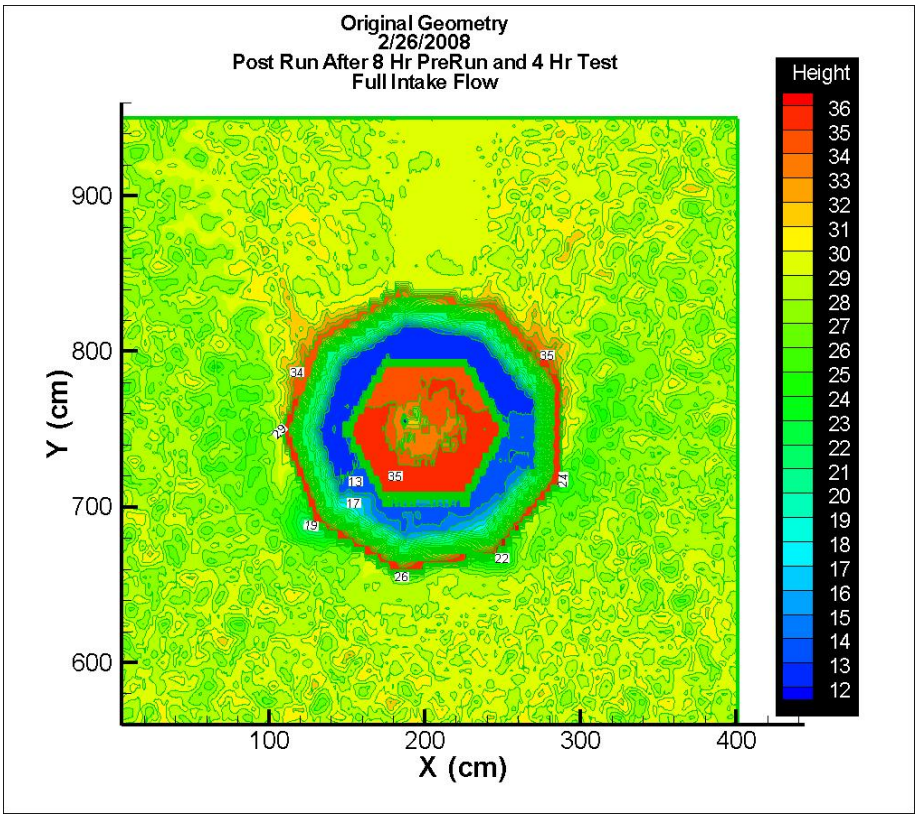

Figure 4.16. Bed elevations around the original geometry after Test no. 8.

4.3. The 11th Geometry

The velocity data collected with the crown in place showed no significant difference in turbulence from the test done with the crown in place. Even though the crown had an impact in the reduction of sediment withdrawal it was concluded that a wider crown could not necessarily reduce the withdrawal any further.

To suppress the turbulence under the crown and to minimize the upwelling of the resuspended sediments, it was decided to mount a screen at the mid height of the wall along the nose wall and the sand barrier of the sixth geometry, therefore, the original crown was used. The idea of the screen was to make the eddies near the bed smaller and dissipate the eddies which tend to cross the perforation of the screen, i.e. to keep the eddies near the bed and prevent the dispersion of the particles in the water column near the wall. The schematic of the screen is shown in Figure 4.17 and the photo of the mounted screen is shown in Figure 4.18.

4.3.1. Velocity Measurements

The x-component of the velocity exhibited an increase of nearly one ft/s near the bed (Figure 4.19). Unlike the 10h geometry, very little fluctuation in the x-component of velocity was evident near the bed. The increase in the x-component velocity was due to a smaller flow conduit under the screen. At a depth of 3.2 ft (3.84" at the model scale), more fluctuations were evident (Figure 4.20) because the probe was at a depth near the screen height. At a depth of 2.3 ft (top of the crown), the velocities were similar to those measured with no screen in place, i.e. the 10th geometry (Figures B.5 and B.6). Model scale velocities are shown in Figures C.1 to C10.

With the screen in place, turbulence intensity exhibited a significant decrease near the bed (Figure 4.22), i.e. the screen had a significant impact on suppressing the diffusion of the resuspended bedload materials (see Figures B21 and B.22). Turbulence intensity at the top of the crown, however, did not seem to change (Figures 4.23 with screen and Figures B.25 and B.26 the 10th geometry). Model scale turbulence intensities are shown in Figures C.11 to C.20.

Vorticity about the y-axis did not change with the screen in place (Figure 4.24) and only its direction changed which might lead to an increase in particles movement away from the structure. Nevertheless, it is difficult to assess the impact of the change in vorticity on the

sediment withdrawal. Another set of velocity measurements were conducted to ensure that the measurements were repeatable. While some data appeared nearly identical, most of the data showed small differences which were due to the transient character of the bed. The overall characteristics of the flow patterns remained similar between the two sets of velocity measurements. Model scale vorticities about the y-axis are shown in Figures C.21 and C.21.

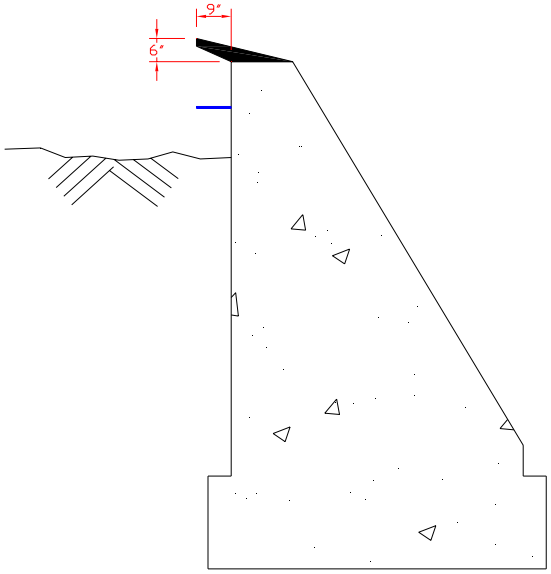

Figure 4.17. The crown and screen were installed along the sand barrier, nose wall and wingwalls.

Figure 4.18. The screen installed at the mid height of the wall around the structure.

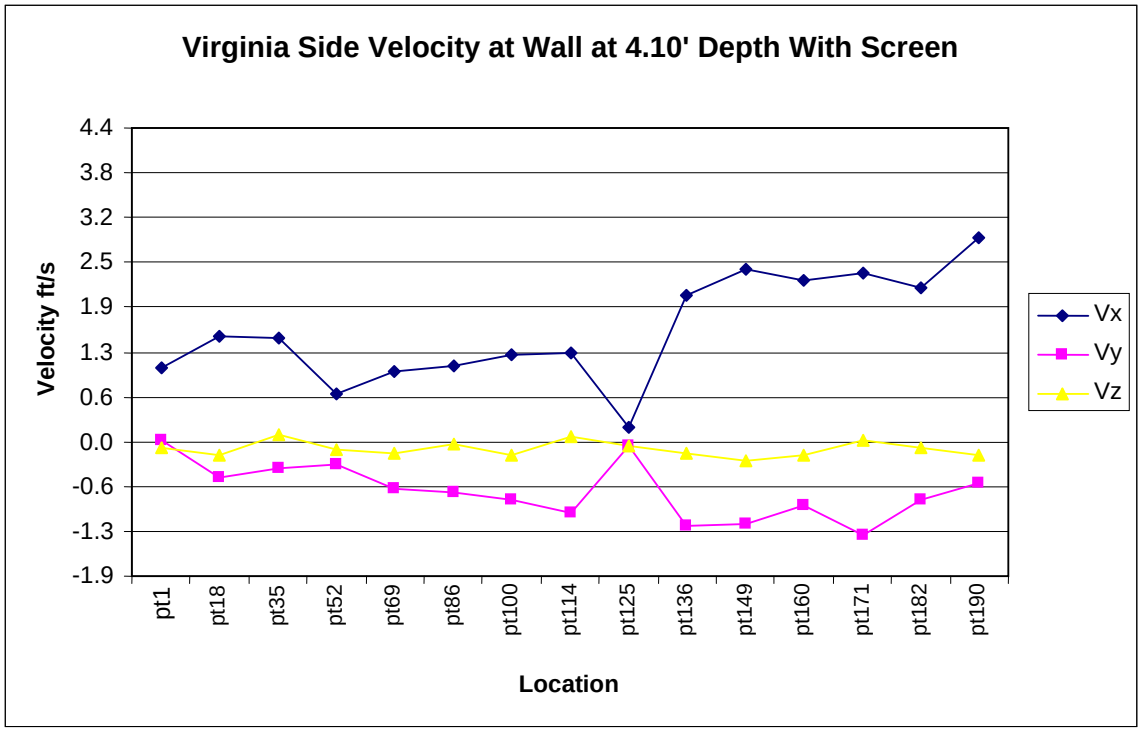

Figure 4.19. Average velocity components along the Virginia side of the 11th geometry with a screen (river side at SAFL) at a depth of 4.1 ft from the surface. Streamflow is from left to right. Location numbers are shown in Figure 2.3.

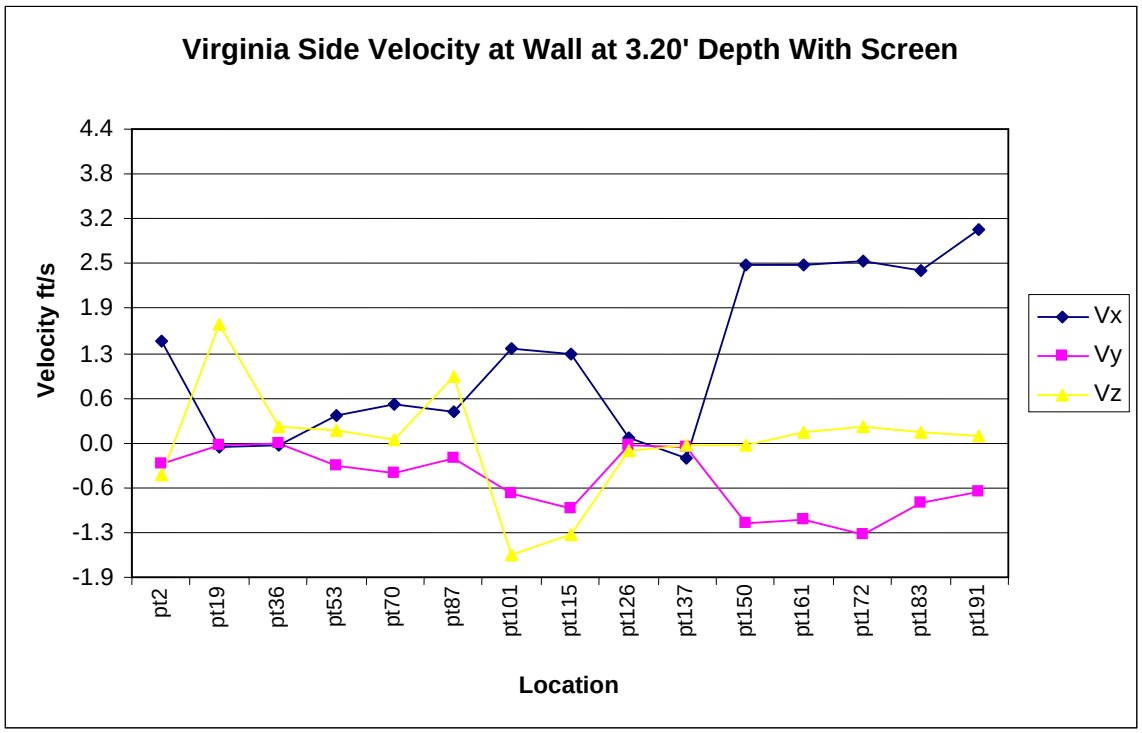

Figure 4.20. Average velocity components along the Virginia side of the 11th geometry with a screen (river side at SAFL) at a depth of 3.2 ft from the surface. Streamflow is from left to right. Location numbers are shown in Figure 2.3.

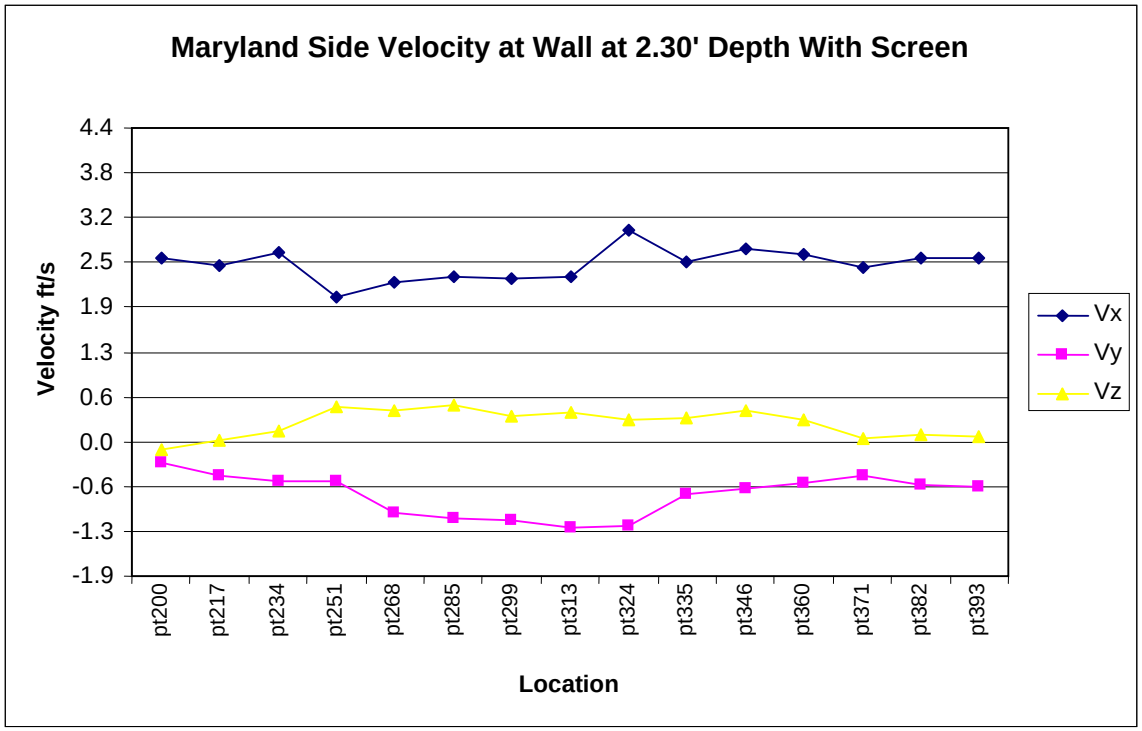

Figure 4.21. Average velocity components along the Maryland side of the 11th geometry with a screen (street side at SAFL) at a depth of 2.3 ft from the surface. Streamflow is from left to right. Location numbers are shown in Figure 2.3.

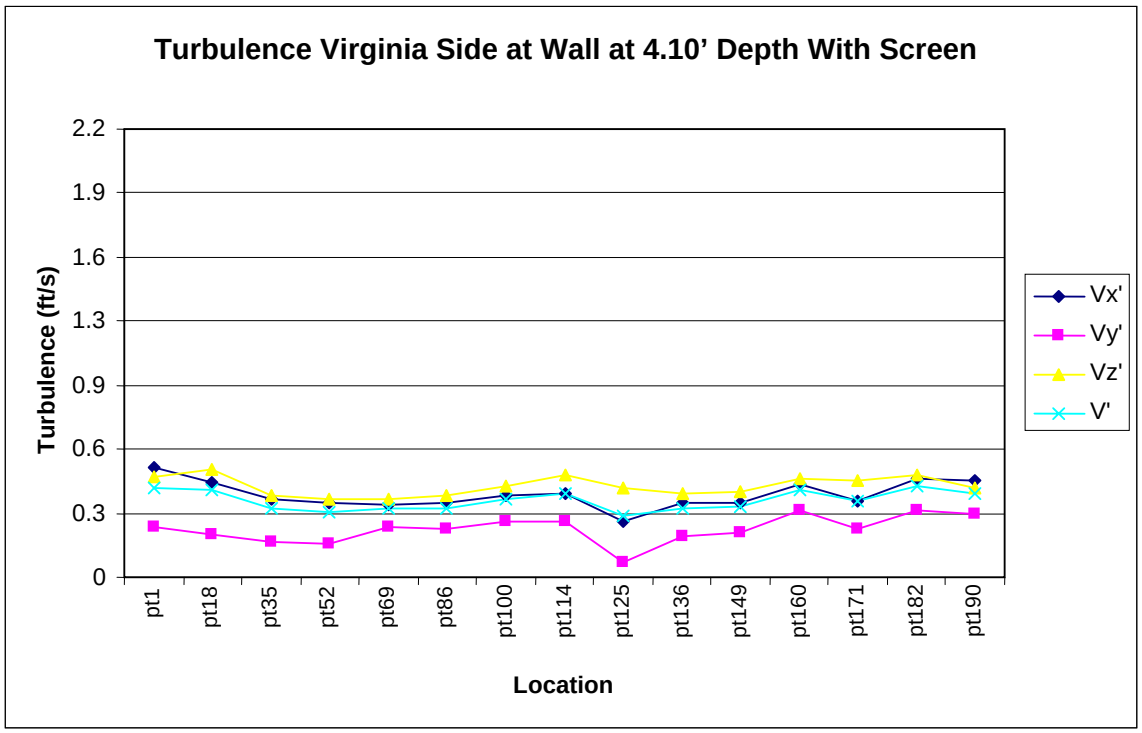

Figure 4.22. Turbulence intensity along the Virginia side of the11th geometry with a screen (river side at SAFL) at a depth of 4.1 ft from the surface. Streamflow is from left to right. Location numbers are shown in Figure 2.3.

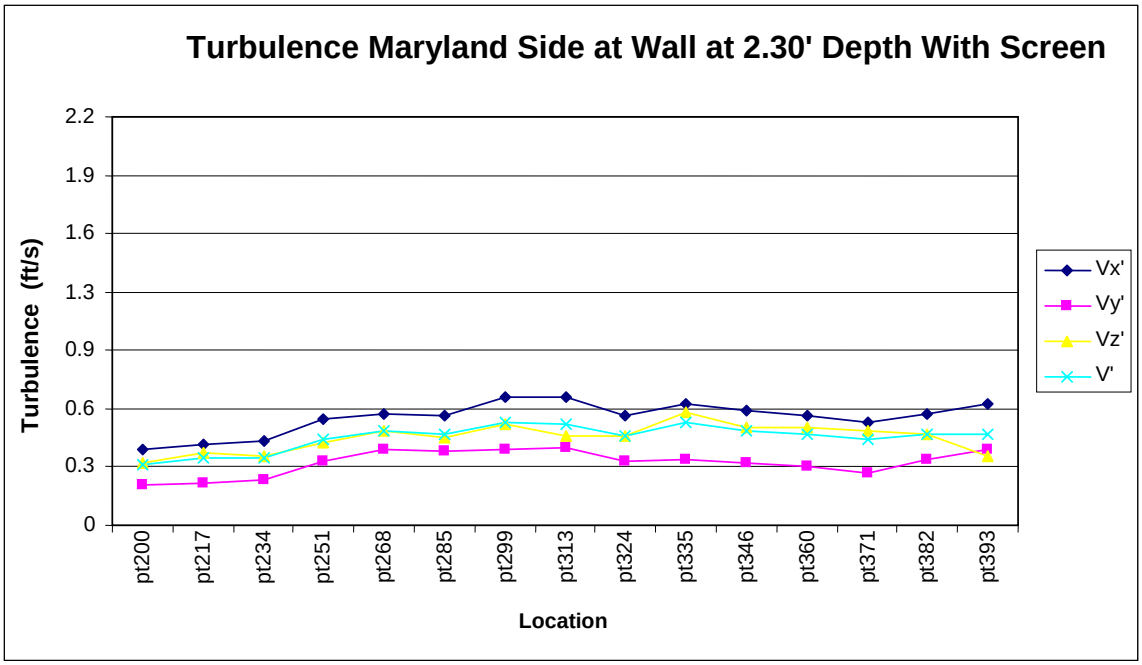

Figure 4.23. Turbulence intensity along the Maryland side of the11th geometry with a screen (street side at SAFL) at a depth of 2.3 ft from the surface. Streamflow is from left to right. Location numbers are shown in Figure 2.3.

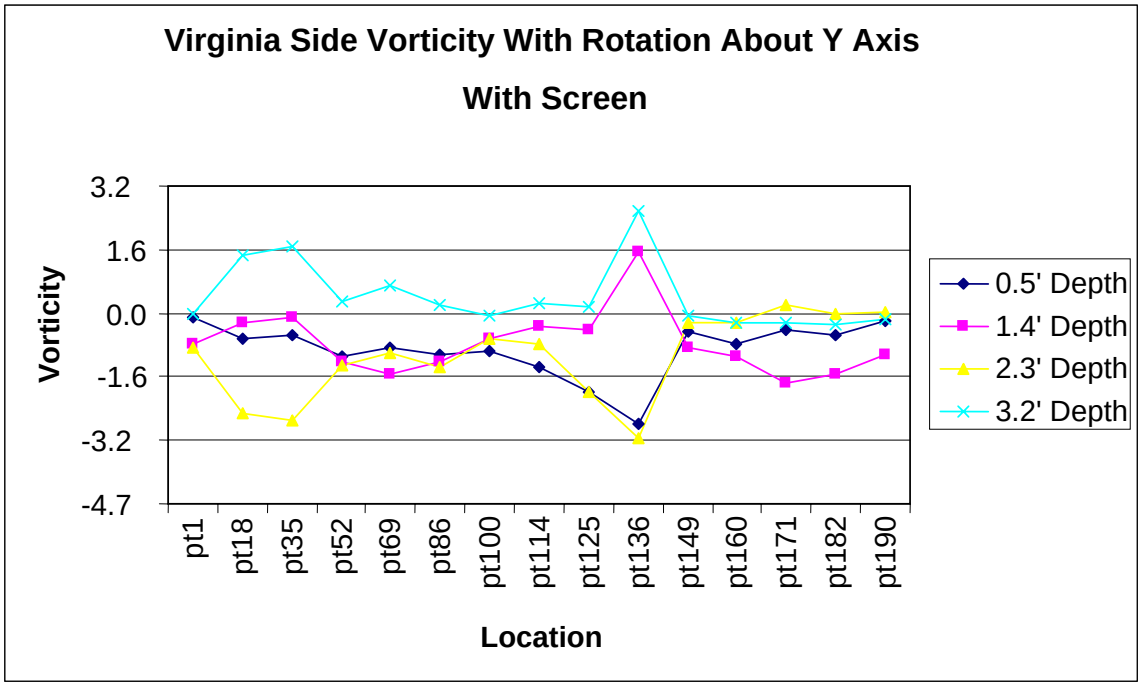

Figure 4.24. Estimated vorticity about the y-axis along the Virginia side of the 11th geometry with a screen (street side at SAFL). Streamflow is from left to right. Location numbers are shown in Figure 2.3.

4.3.2. Sediment Withdrawal

Three tests were conducted on the 11th geometry to measure the sediment withdrawal. The first test, May 12, 2008, resulted in a large increase in the sediment withdrawal with a value of 5937 grams. This result did not appear reasonable and after close inspection a new seepage point through the membrane was identified. To avoid any more seepage the sediments around the structure were removed, the membrane was cut and only extended to the wooden base of the structure and the basin was refilled with the original mix again. With this modification, seepage from underneath the membrane could not impact the sediment withdrawal because the membrane was far away from the capture zone of the intake.

Subsequently, one test was conducted on June 6, 2008 and a repeat test was conducted on June 18. The results are summarized in Table 4.3. The bed scan (Figure 4.25) does not show any significant difference from the 10th geometry (Figure 4.15). The average withdrawal of Tests 10 and 11 was estimated to be 3864 grams. Using the particle size distribution given in Figure 1.3 for the original geometry, i.e. 8,802×0.6=5,281 grams, and the 11th geometry, i.e. 3,864×0.45=1,739 grams, the sediment withdrawal was reduced by 67%. By incorporating the effect of a smaller depth and therefore, a more turbulent condition at the model scale, the 11the geometry with a screen reduced the sediment withdrawal by about 70%. Given a slight change in water temperature in June, the sediment withdrawal through the 11th geometry is most likely less than 70%. Nevertheless, the added screen showed an improvement over the sixth geometry.

Table 4.3. Summary of the tests with 4-hour duration and 8-hour pre-runs on the 11th geometry.

11th Geometry (nose wall and wingwalls with a crown and screen)	Settling Tank (grams)	Date
Test no. 9	5937	5/12/2008
Test no. 10	3819	6/6/2008
Test no. 11	3910	6/18/2008

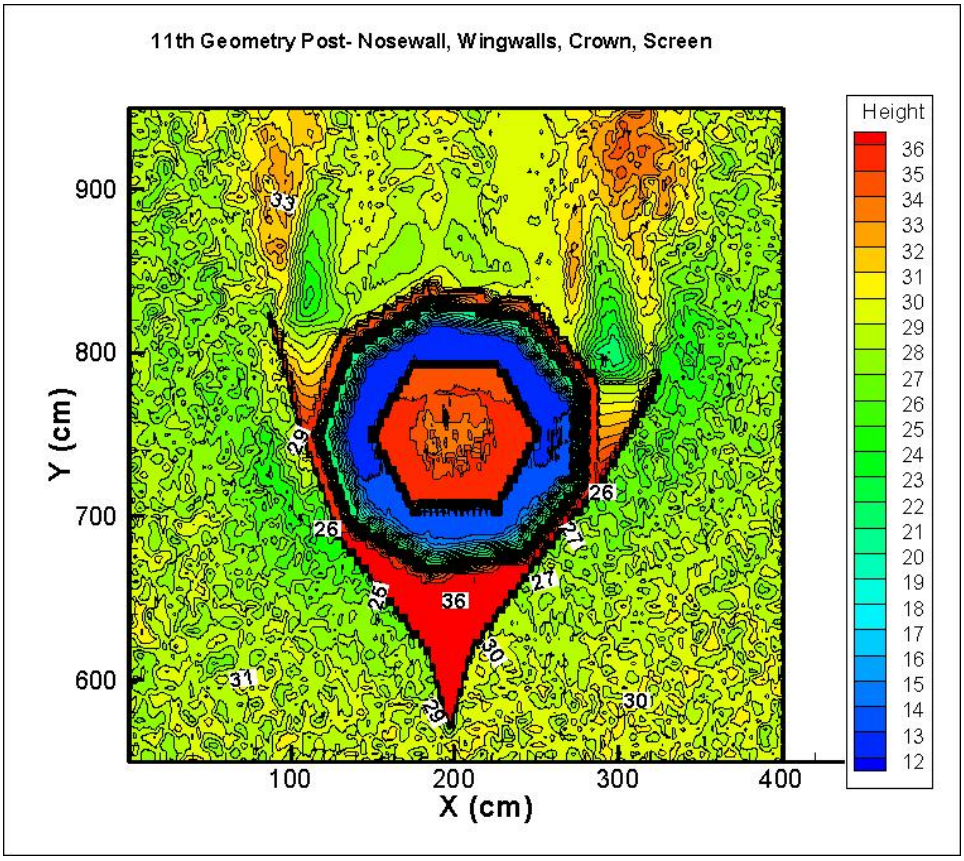

Figure 4.25. Results of the topographical scan of the bed after the test was conducted on the 11th geometry on 06/06/08. The intake flow rate was 300 MGPD (1.47 cfs). It was a 4-hour duration test with an 8-hour pre-run.

5. Summary

Fairfax Water constructed an off-shore intake in 2004 to withdraw water with a better quality when the flow is less than 20,000 cfs in the river. The intake started operating in late 2004. During the two year period of operation, the intake withdrew a significant amount of sand during flow conditions near 20,000 cfs. To study the causes of sand withdrawal by the intake and to provide design modifications to minimize the sand withdrawal, a physical model study was conducted at the St. Anthony Falls Laboratory in 2006 and 2007. The model was built at a scale of 1:10 simulating 390×180 feet of the river with the intake and its sand barrier near the downstream end of the model basin. The physical model study showed that the sixth geometry, which was comprised of a broken nose wall at the upstream end, two wingwalls at the downstream end and a crown over the entire perimeter of the structure, had the best impact among all geometries tested. The tests conducted on the sixth geometry showed a 60% reduction in the bedload withdrawal. However, Fairfax Water asked for further modification of the sand barrier for further reduction in sediment withdrawal. Therefore, more testing was conducted using the same model in the winter of 2007 and spring of 2008.

A total of three modifications and 11 tests were conducted on the modified design as well as on the original geometry. All tests started with the same initial conditions by flattening the bed, and an 8-hour pre-run. Each test had a duration of four hours.

The first two modifications were only made to the crown of the structure and did not show any improvement over the sixth geometry. Therefore, three sets of velocities were measured around the structure using a 3-dimnsional Acoustic Doppler Velocimeter to assess the flow patterns, turbulence intensity and vorticity around the structure. The measured velocity data provided information on general characteristics of the flow. From the analysis of the velocity data, it was decided to add a screen at the mid height of the wall around the sixth geometry. The screen was intended to keep the eddies near the bed to prevent any dispersion of the resuspended materials along the walls of the structure. Subsequently, the velocities around the final geometry (the 11^{th} geometry) were measured which showed a decrease in turbulence intensity near the bed. Two more withdrawal tests were conducted on the 11^{th} geometry which showed about 70% reduction in sediment withdrawal which was an improvement over the sixth geometry.

6. References

Clunie, T. M., Nikora, V. I., Coleman, S. E., Freidrich, H., and Melville, B. W. 2007. Flow Measurement Using Flying ADV Probes. *Journal of Hydraulic Engineering* 133:1345-1355.

Goring, D. G., and Nikora, V. I. 2002 . Despiking Acoustic Doppler Velocimeter Data. *J. Hydraulic Engineering*, 128 (1):117–126.

Nortek. 2004. *Vectrino Velocimeter User Guide*. Rev. C. 17.

Wahl, T. L. 2003. Discussion of 'Despiking Acoustic Doppler Velocimeter Data'. *J. Hydraulic Engineering*, 129(6): 484–488.

Sontek. 2008. 1*0-Mhz ADV Principles of Operation*. <http://www.sontek.com/princop/adv/advpo.htm>.

Mohseni, O., and Lueker, M. 2007. A Physical Model Study of the Fairfax Off-Shore Intake in the Potomac River. *St. Anthony Falls Laboratory Project Report no. 500*. Minneapolis, MN.

Appendix A: Velocity Measurements along the Sixth Geometry without the Crown (First Set)

All dimensions and values are at the model scale.

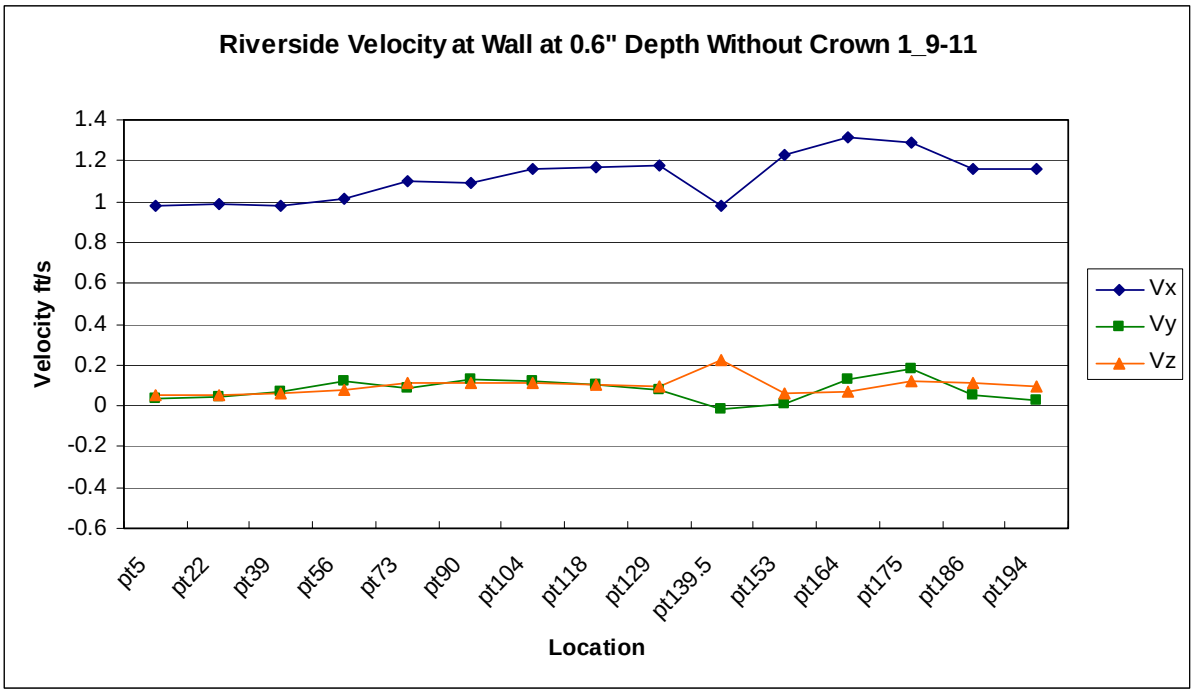

Figure A.1. Average velocity components along the Virginia side of the structure (riverside at SAFL) without the crown at a depth of 0.6 inches from the surface. Streamflow is from left to right. Location numbers are shown in Figure 2.3.

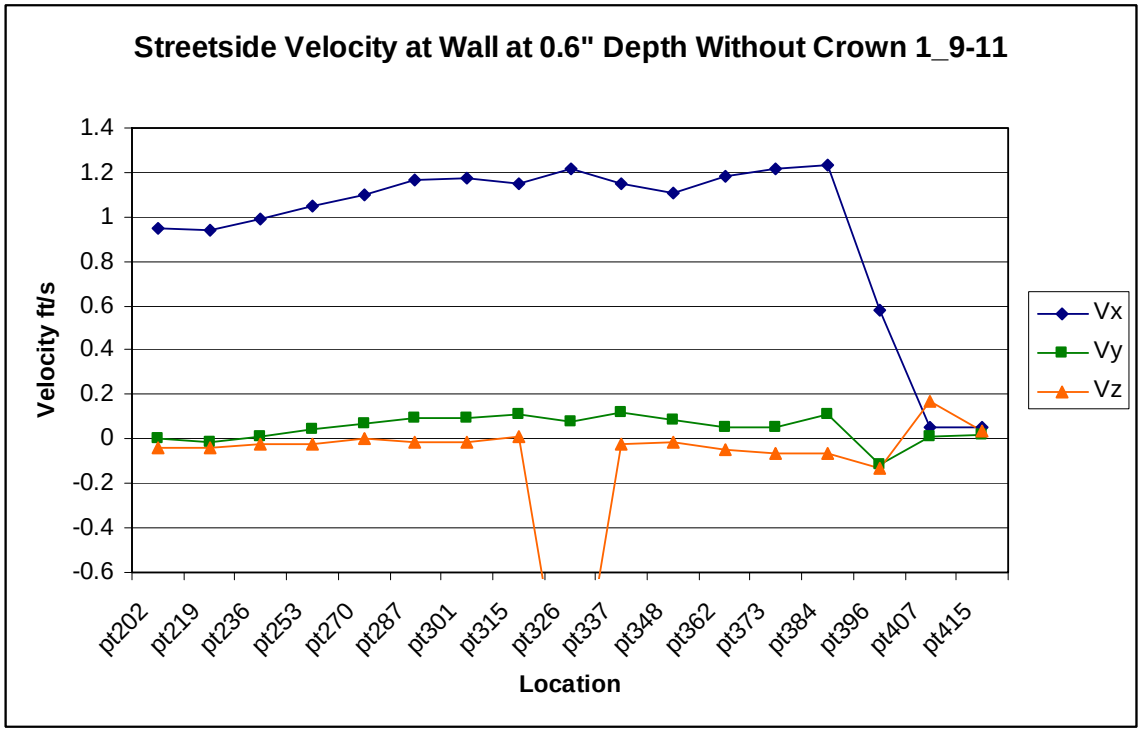

Figure A.2. Average velocity components along the Maryland side of the structure (street side at SAFL) without the crown at a depth of 0.6 inches from the surface. Streamflow is from left to right. Location numbers are shown in Figure 2.3.

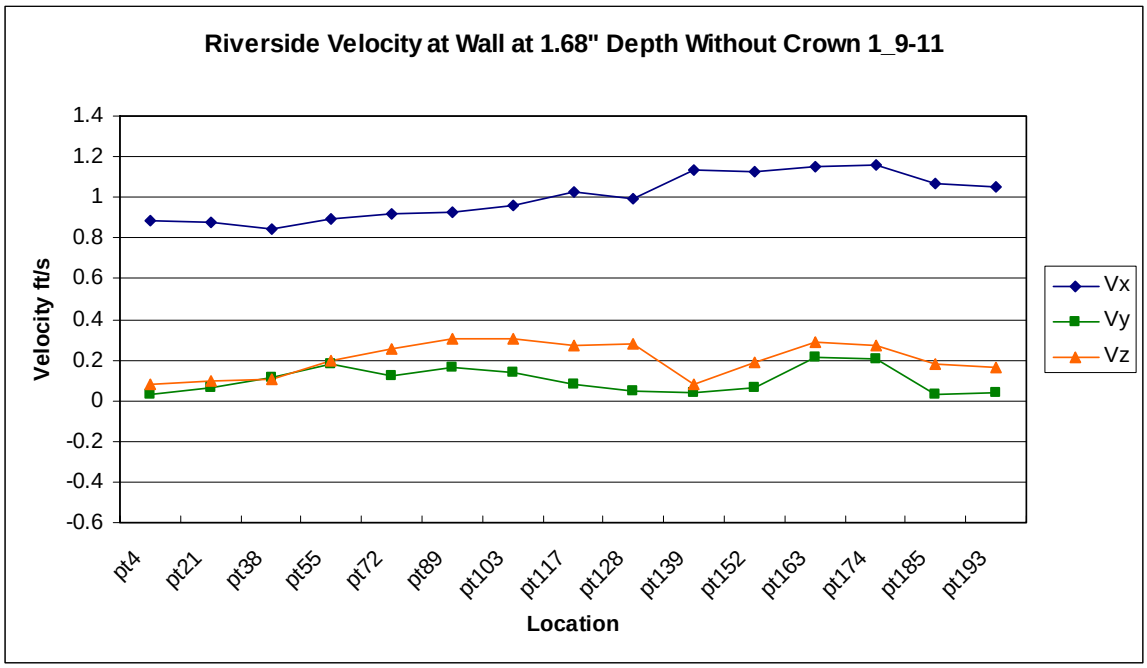

Figure A.3. Average velocity components along the Virginia side of the structure (riverside at SAFL) without the crown at a depth of 1.68 inches from the surface. Streamflow is from left to right. Location numbers are shown in Figure 2.3.

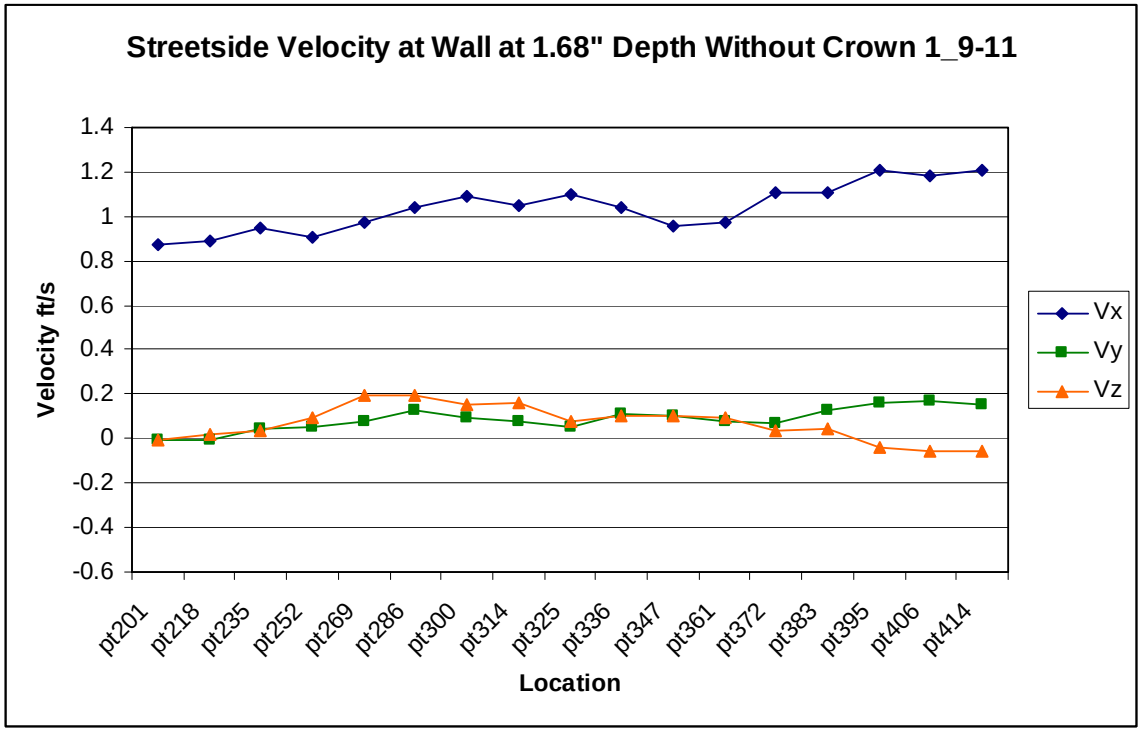

Figure A.4. Average velocity components along the Maryland side of the structure (street side at SAFL) without the crown at a depth of 1.68 inches from the surface. Streamflow is from left to right. Location numbers are shown in Figure 2.3.

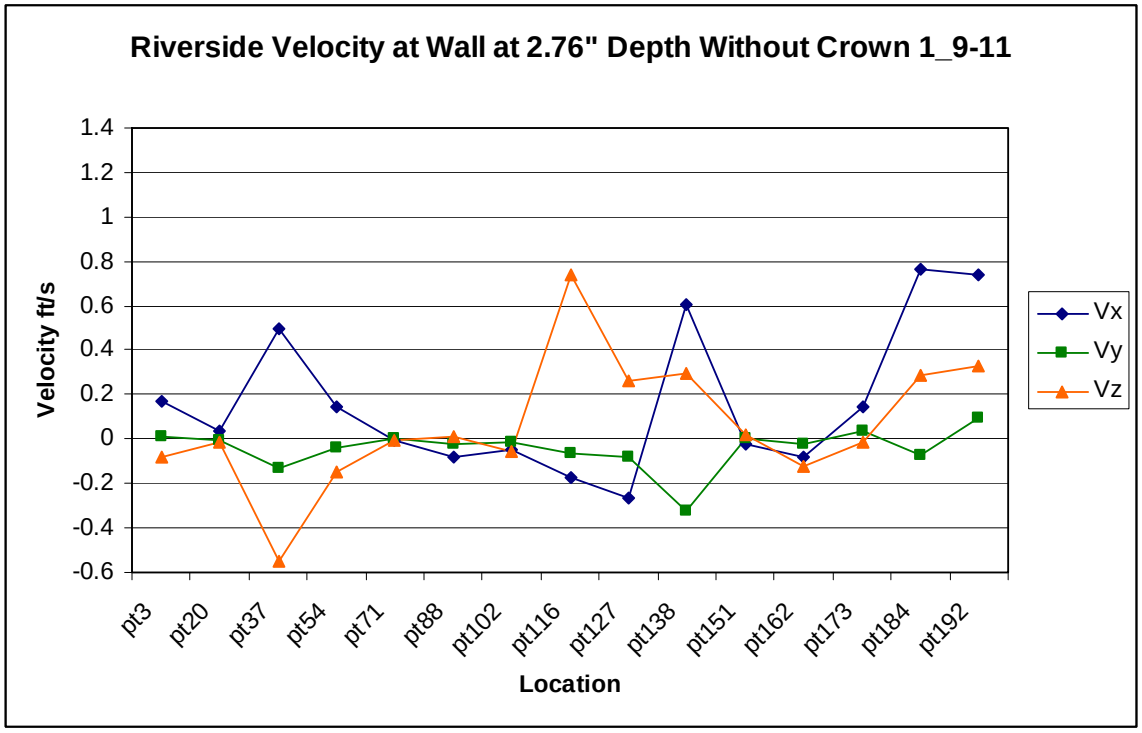

Figure A.5. Average velocity components along the Virginia side of the structure (river side at SAFL) without the crown at a depth of 2.76 inches from the surface. Streamflow is from left to right. Location numbers are shown in Figure 2.3.

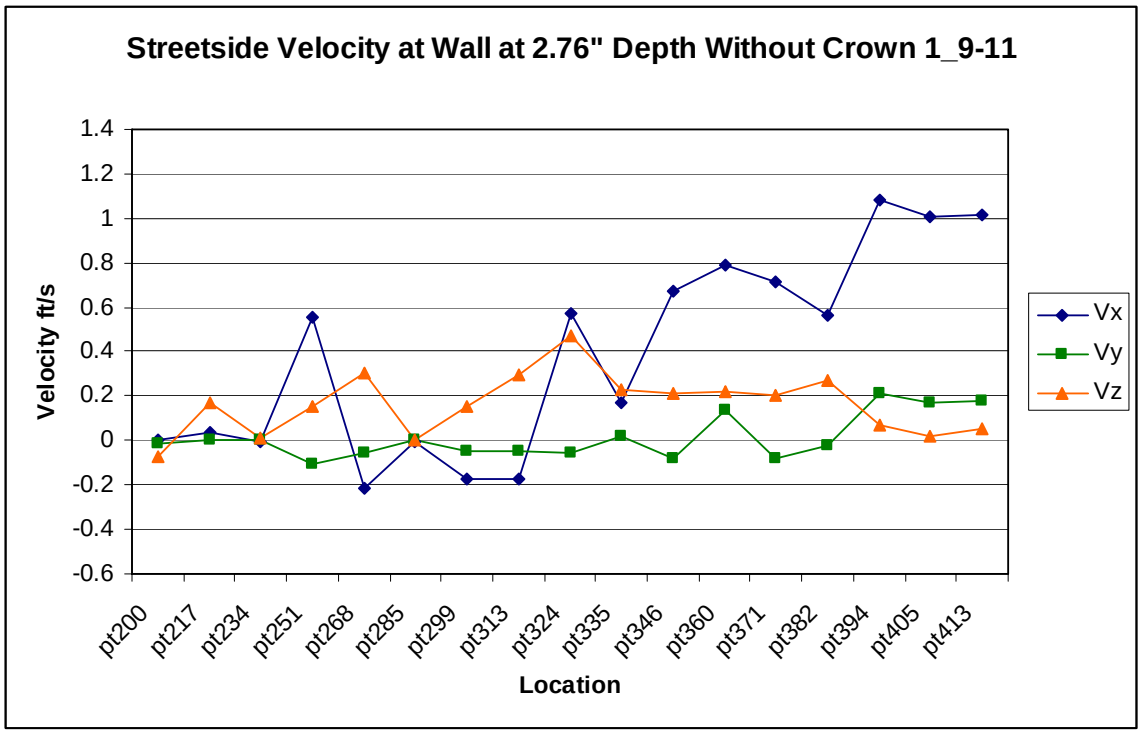

Figure A.6. Average velocity components along the Maryland side of the structure (street side at SAFL) without the crown at a depth of 2.76 inches from the surface. Streamflow is from left to right. Location numbers are shown in Figure 2.3.

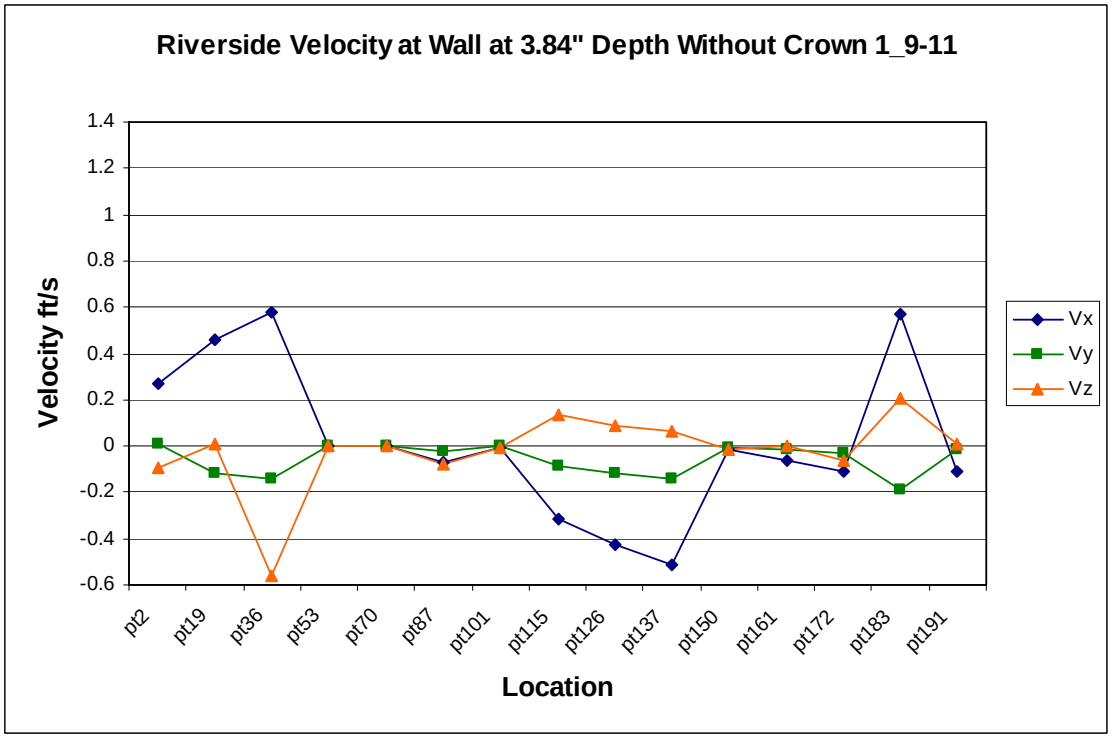

Figure A.7. Average velocity components along the Virginia side of the structure (river side at SAFL) without the crown at a depth of 3.84 inches from the surface. Streamflow is from left to right. Location numbers are shown in Figure 2.3.

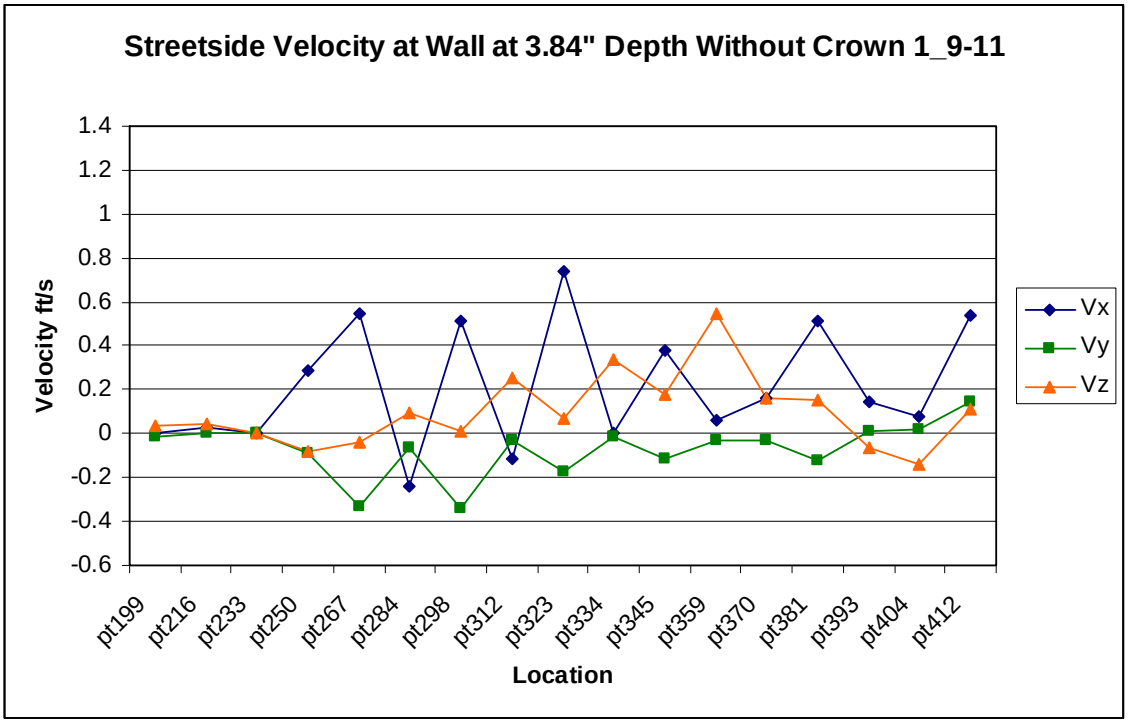

Figure A.8. Average velocity components along the Maryland side of the structure (street side at SAFL) without the crown at a depth of 3.84 inches from the surface. Streamflow is from left to right. Location numbers are shown in Figure 2.3.

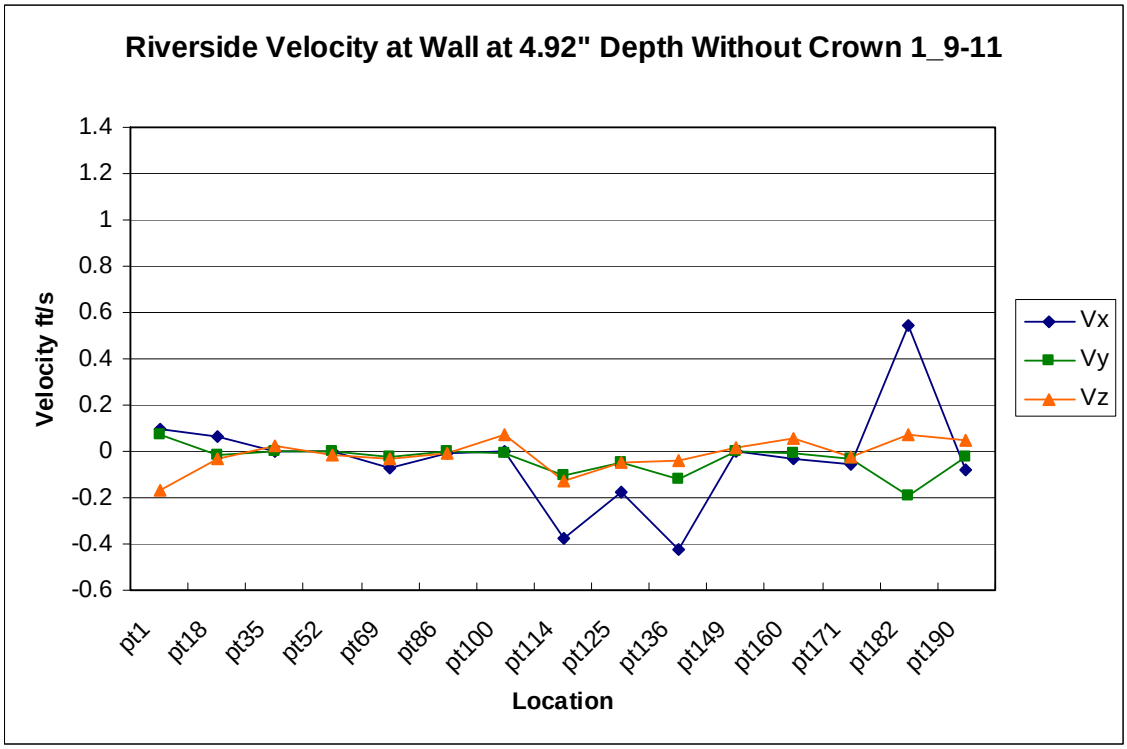

Figure A.9. Average velocity components along the Virginia side of the structure (river side at SAFL) without the crown at a depth of 4.92 inches from the surface. Streamflow is from left to right. Location numbers are shown in Figure 2.3.

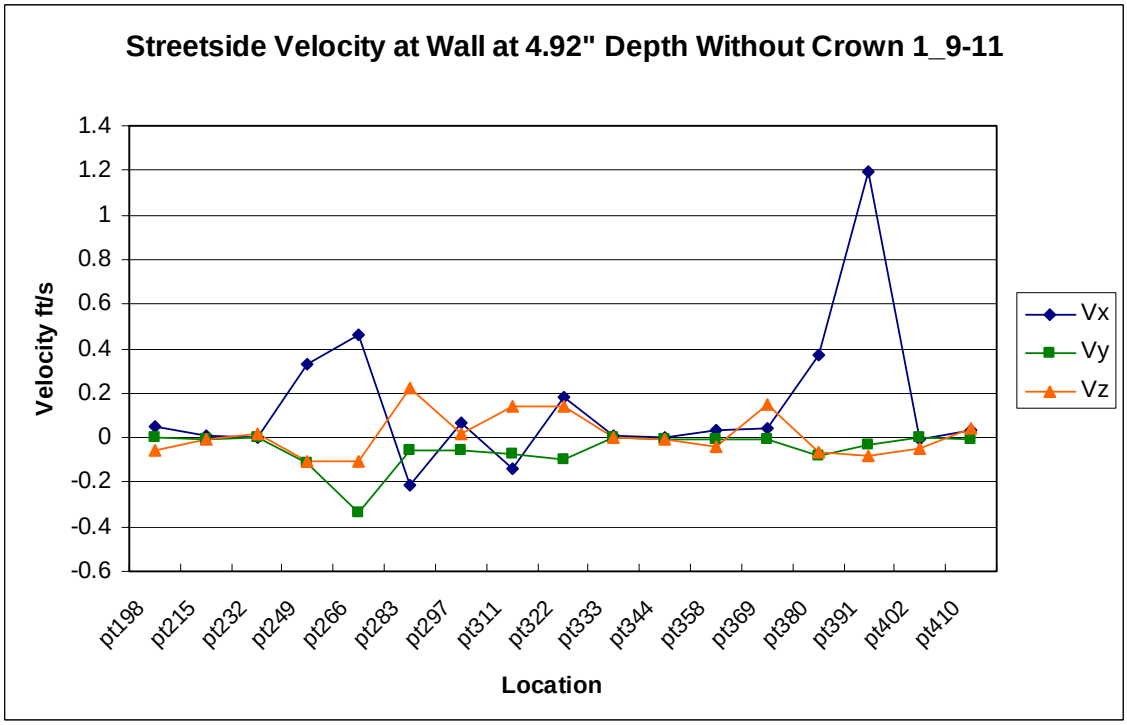

Figure A.10. Average velocity components along the Maryland side of the structure (street side at SAFL) without the crown at a depth of 4.92 inches from the surface. Streamflow is from left to right. Location numbers are shown in Figure 2.3.

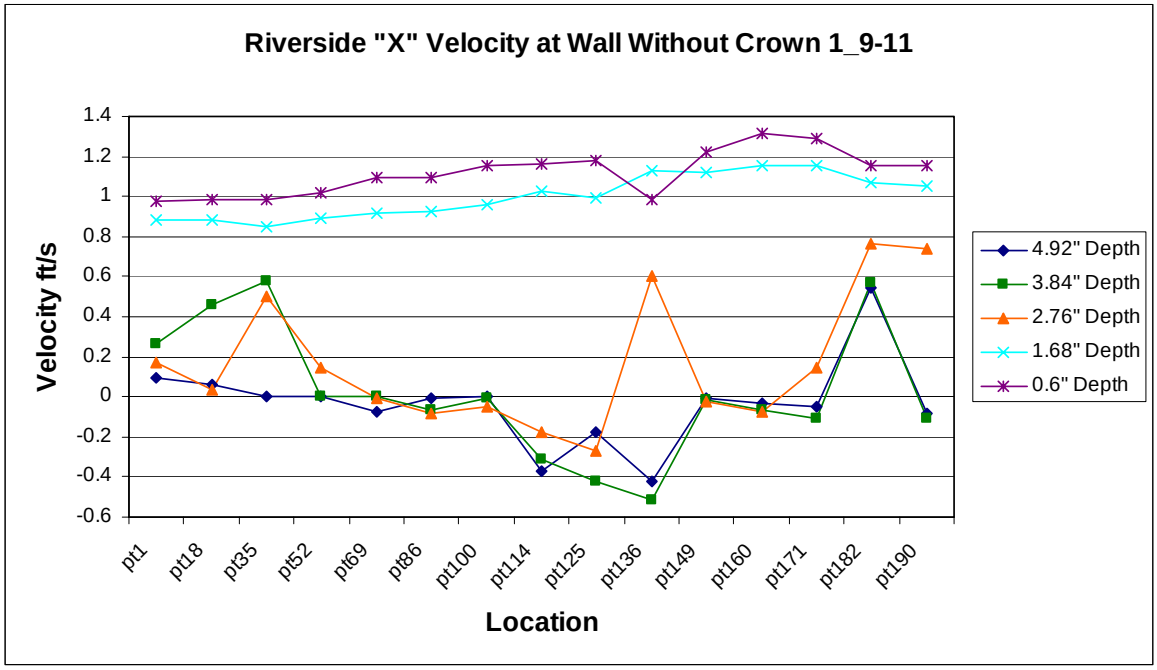

Figure A.11. X-components of velocities measured at all depths along the Virginia side of the structure (river side at SAFL) without the crown. Streamflow is from left to right. Location numbers are shown in Figure 2.3.

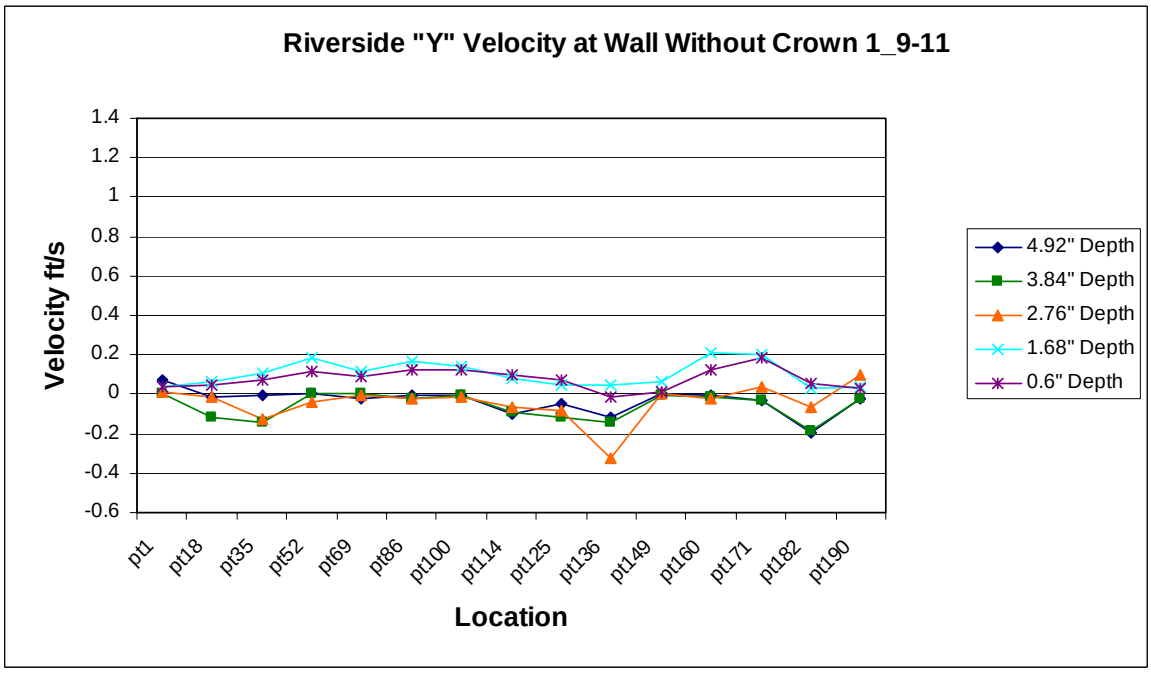

Figure A.12. Y-components of velocities measured at all depths along the Virginia side of the structure (river side at SAFL) without the crown. Streamflow is from left to right. Location numbers are shown in Figure 2.3.

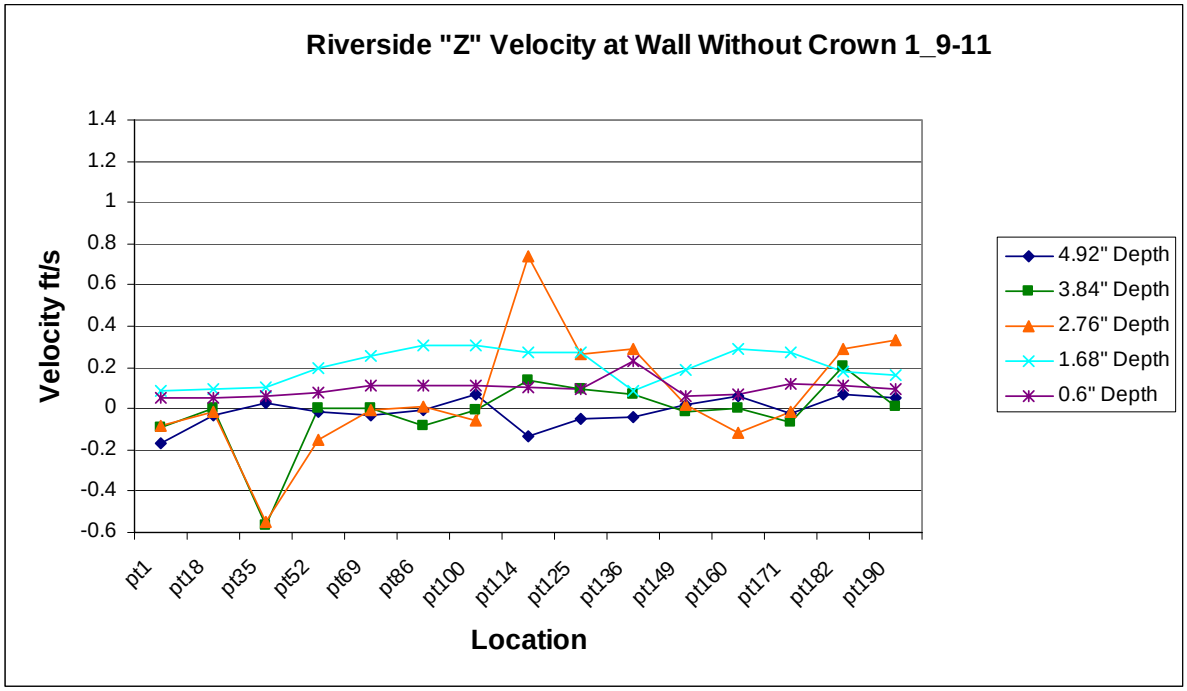

Figure A.13. Z-components of velocities measured at all depths along the Virginia side of the structure (river side at SAFL) without the crown. Streamflow is from left to right. Location numbers are shown in Figure 2.3.

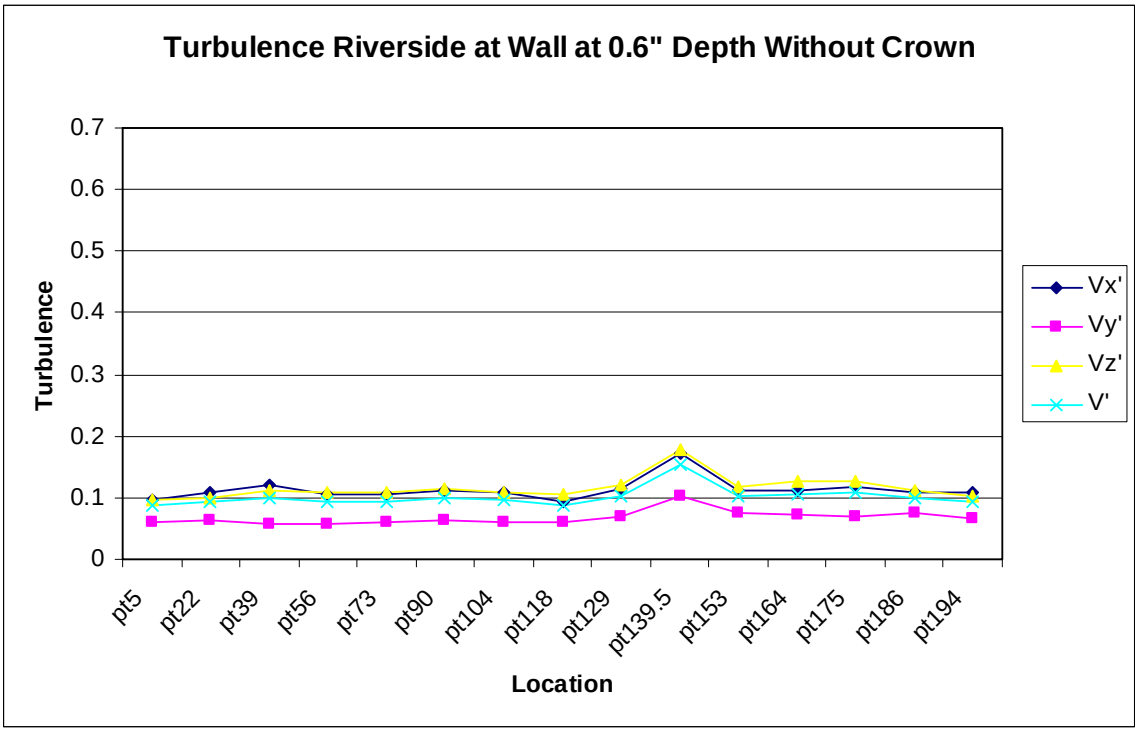

Figure A.14. Turbulence intensity along the Virginia side of the structure (river side at SAFL) without the crown at a depth of 0.6 inches from the surface. Streamflow is from left to right. Location numbers are shown in Figure 2.3.

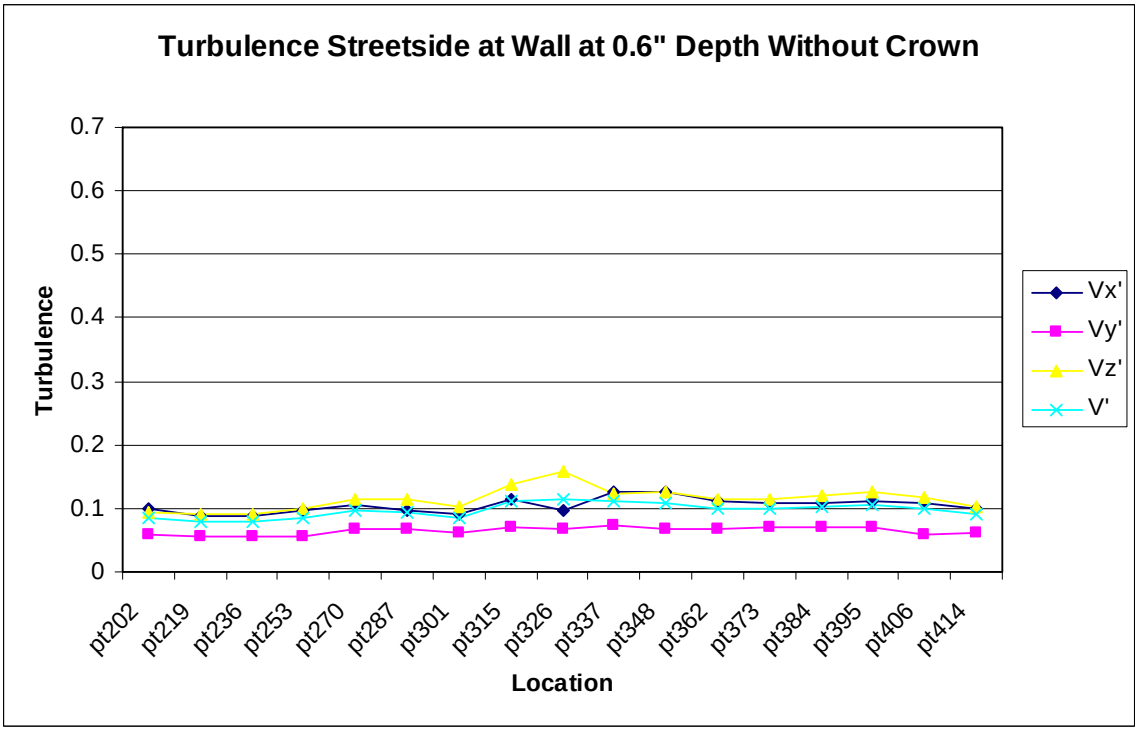

Figure A.15. Turbulence along the Maryland side of the structure (street side at SAFL) without the crown at a depth of 0.6 inches from the surface. Streamflow is from left to right. Location numbers are shown in Figure 2.3.

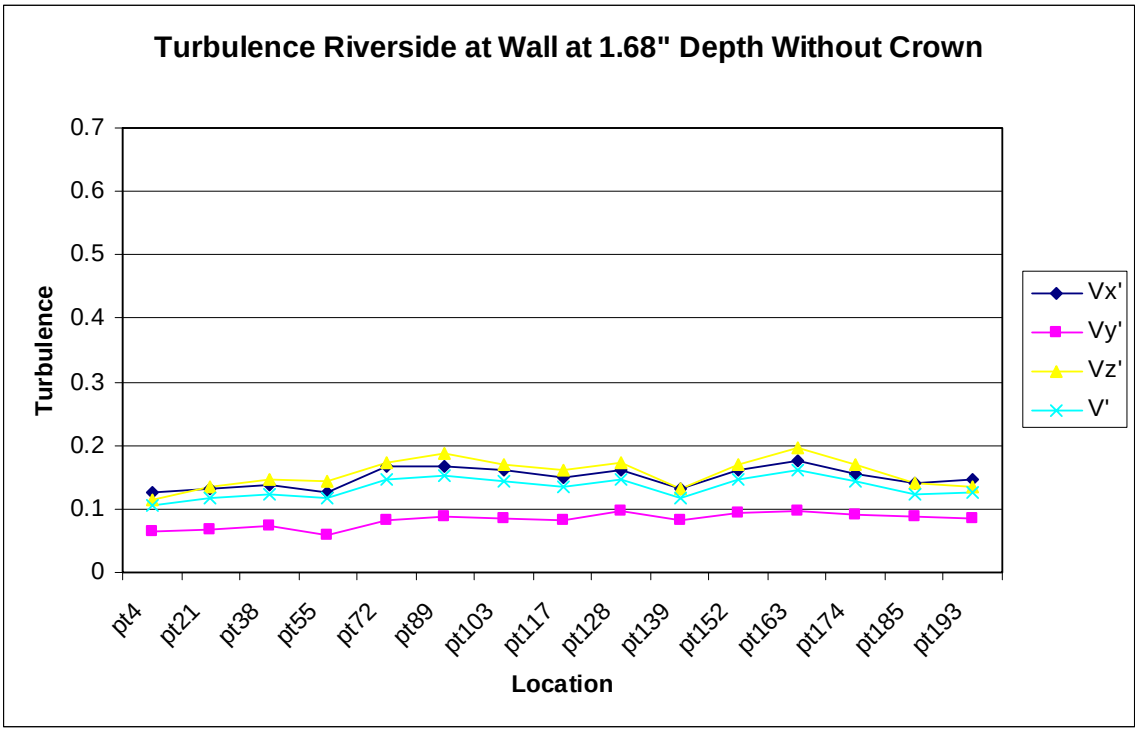

Figure A.16. Turbulence intensity along the Virginia side of the structure (river side at SAFL) without the crown at a depth of 1.68 inches from the surface. Streamflow is from left to right. Location numbers are shown in Figure 2.3.

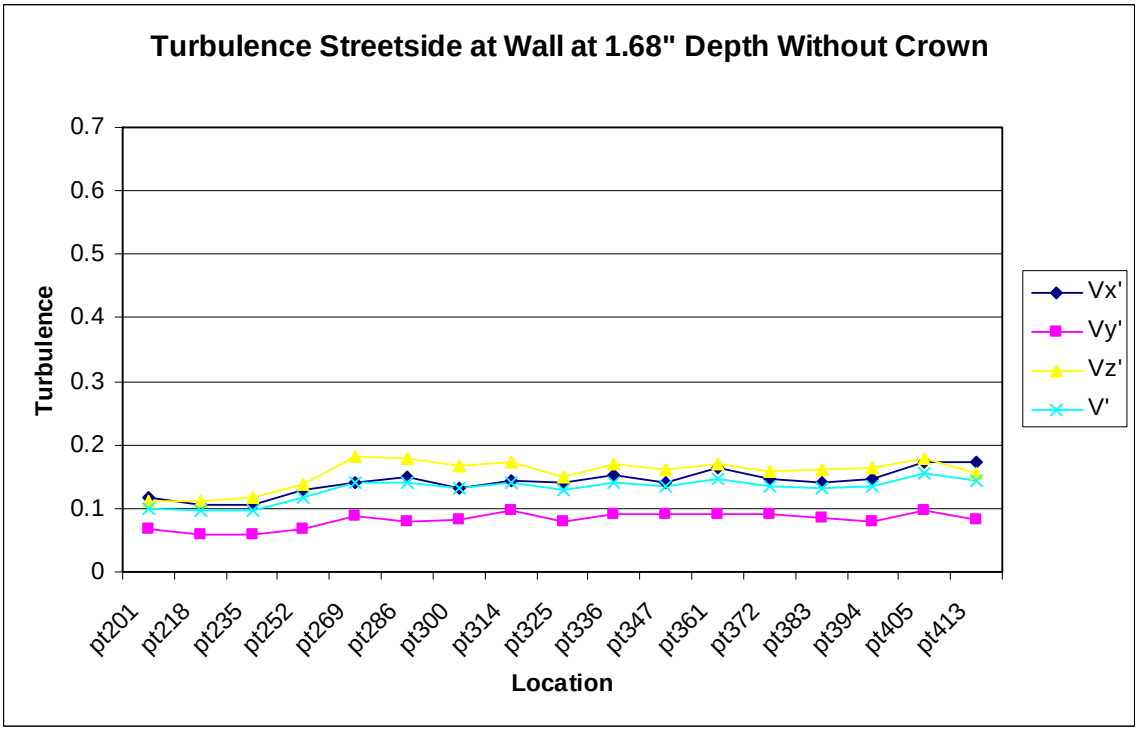

Figure A.17. Turbulence intensity along the Maryland side of the structure (street side at SAFL) without the crown at a depth of 1.68 inches from the surface. Streamflow is from left to right. Location numbers are shown in Figure 2.3.

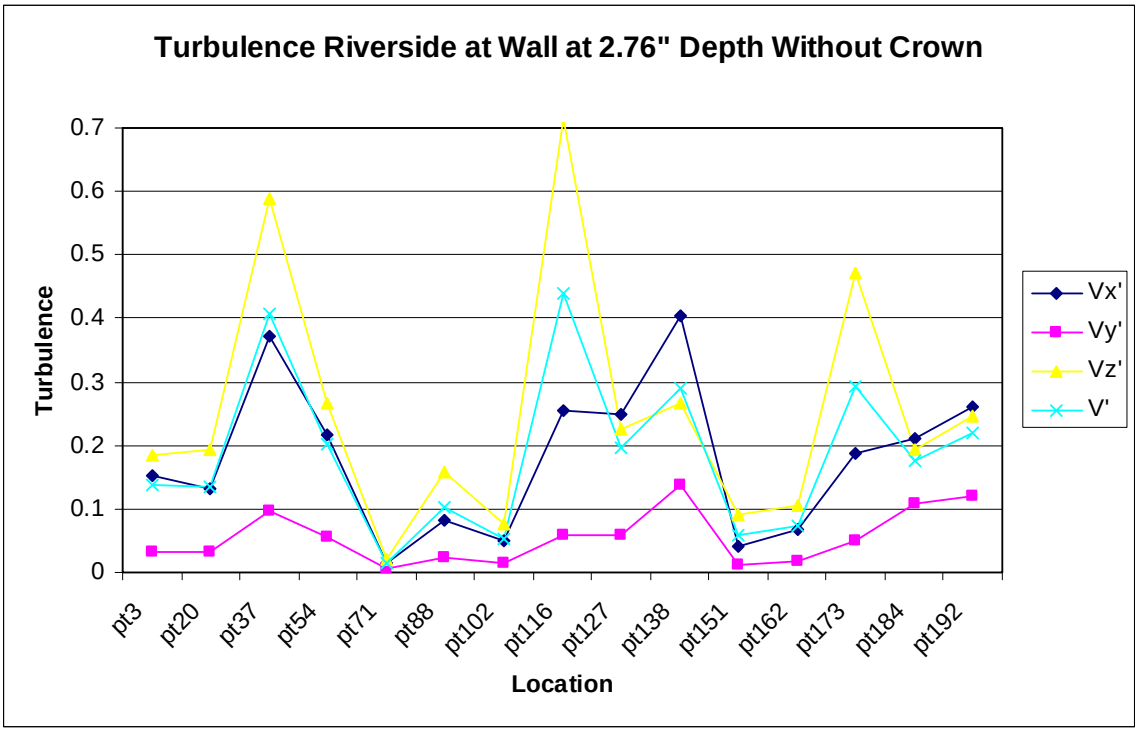

Figure A.18. Turbulence intensity along the Virginia side of the structure (river side at SAFL) without the crown at a depth of 2.76 inches from the surface. Streamflow is from left to right. Location numbers are shown in Figure 2.3.

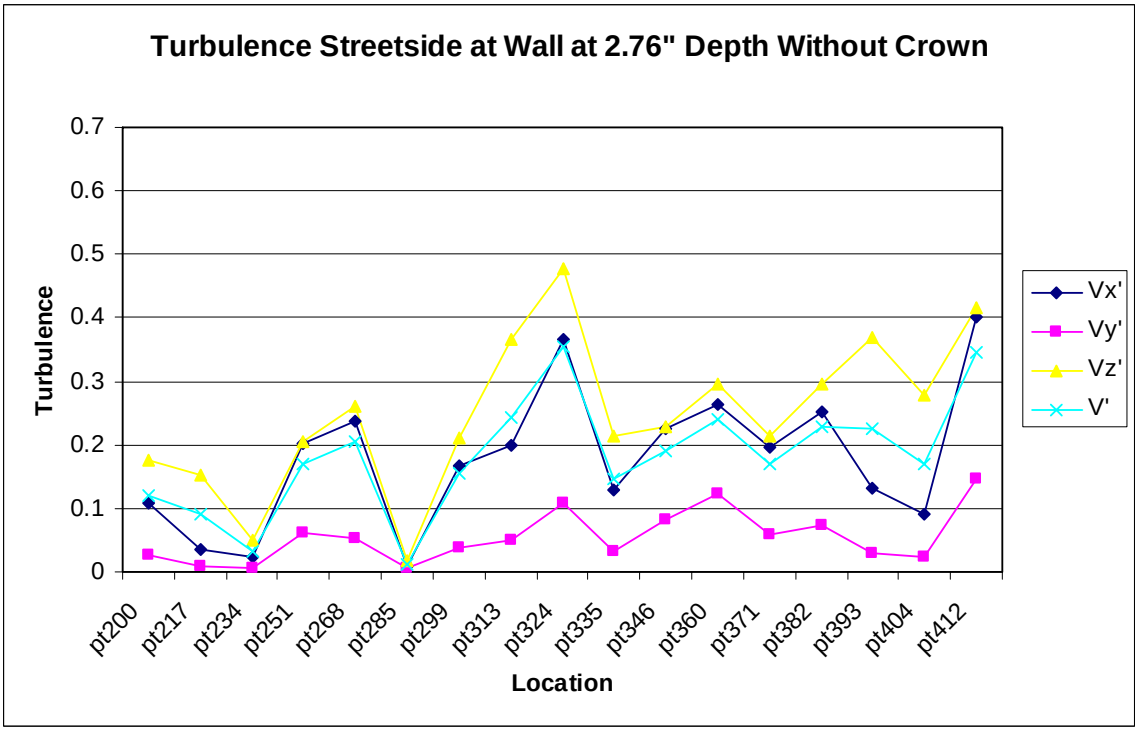

Figure A.19. Turbulence intensity along the Maryland side of the structure (street side at SAFL) without the crown at a depth of 2.76 inches from the surface. Streamflow is from left to right. Location numbers are shown in Figure 2.3.

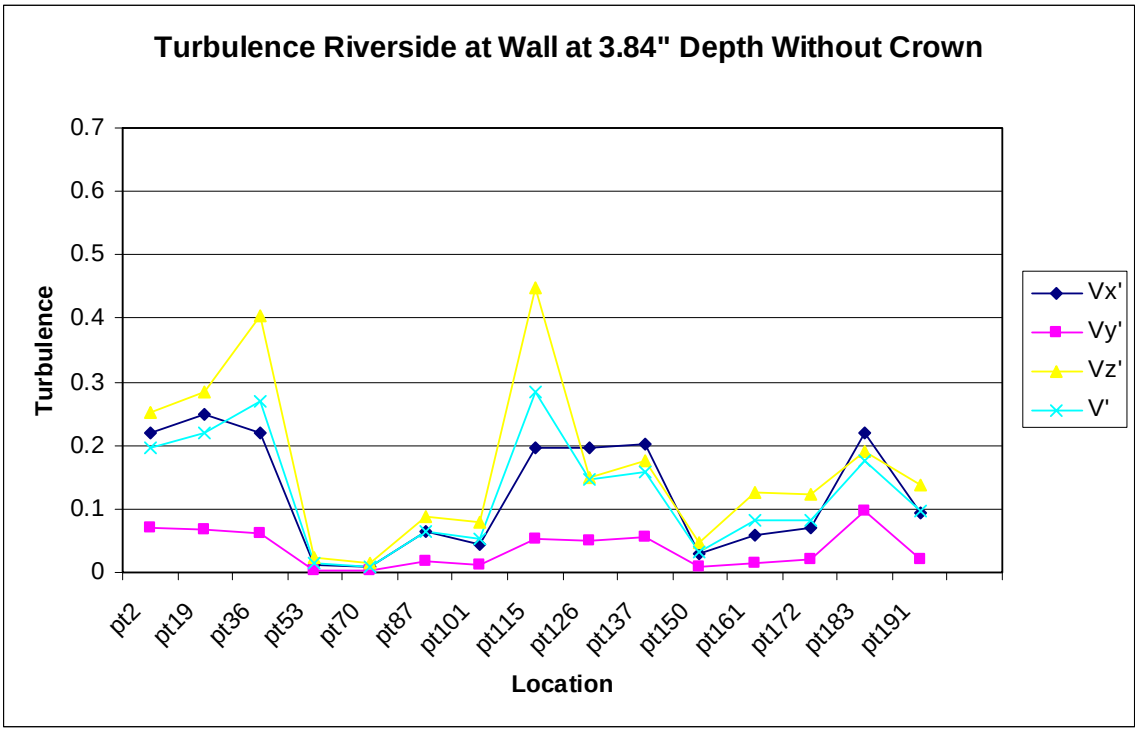

Figure A.20. Turbulence intensity along the Virginia side of the structure (river side at SAFL) without the crown at a depth of 3.84 inches from the surface. Streamflow is from left to right. Location numbers are shown in Figure 2.3.

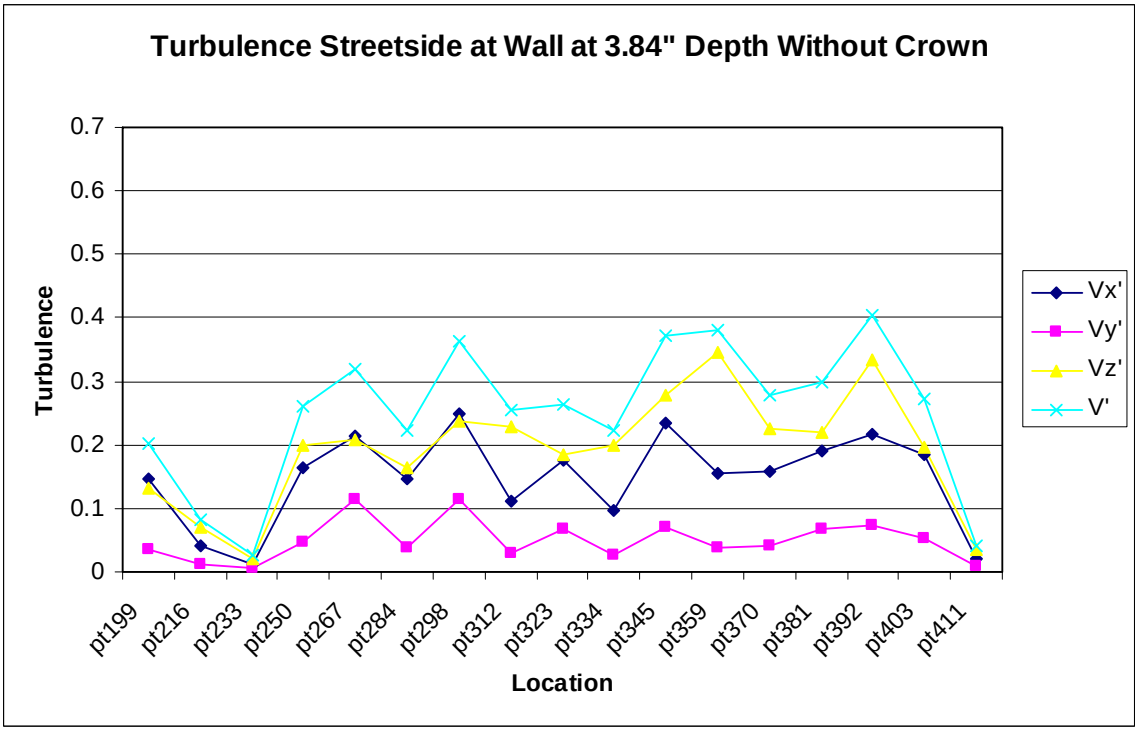

Figure A.21. Turbulence intensity along the Maryland side of the structure (street side at SAFL) without the crown at a depth of 3.84 inches from the surface. Streamflow is from left to right. Location numbers are shown in Figure 2.3.

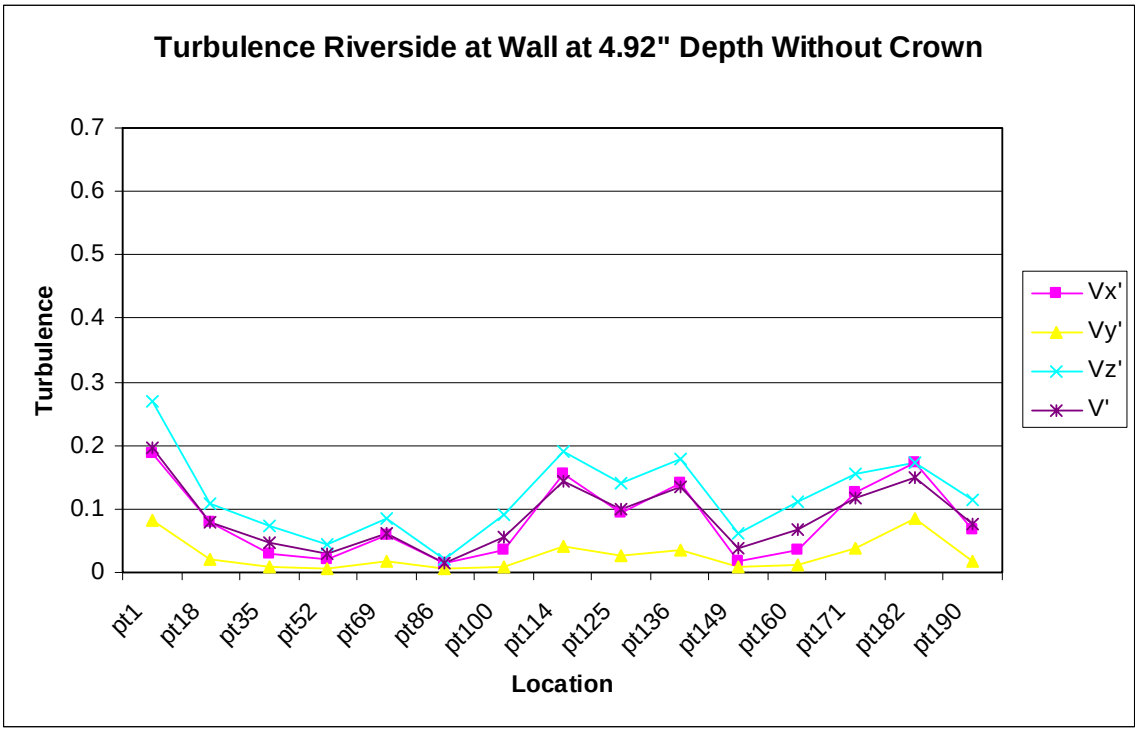

Figure A.22. Turbulence intensity along the Virginia side of the structure (river side at SAFL) without the crown at a depth of 4.92 inches from the surface. Streamflow is from left to right. Location numbers are shown in Figure 2.3.

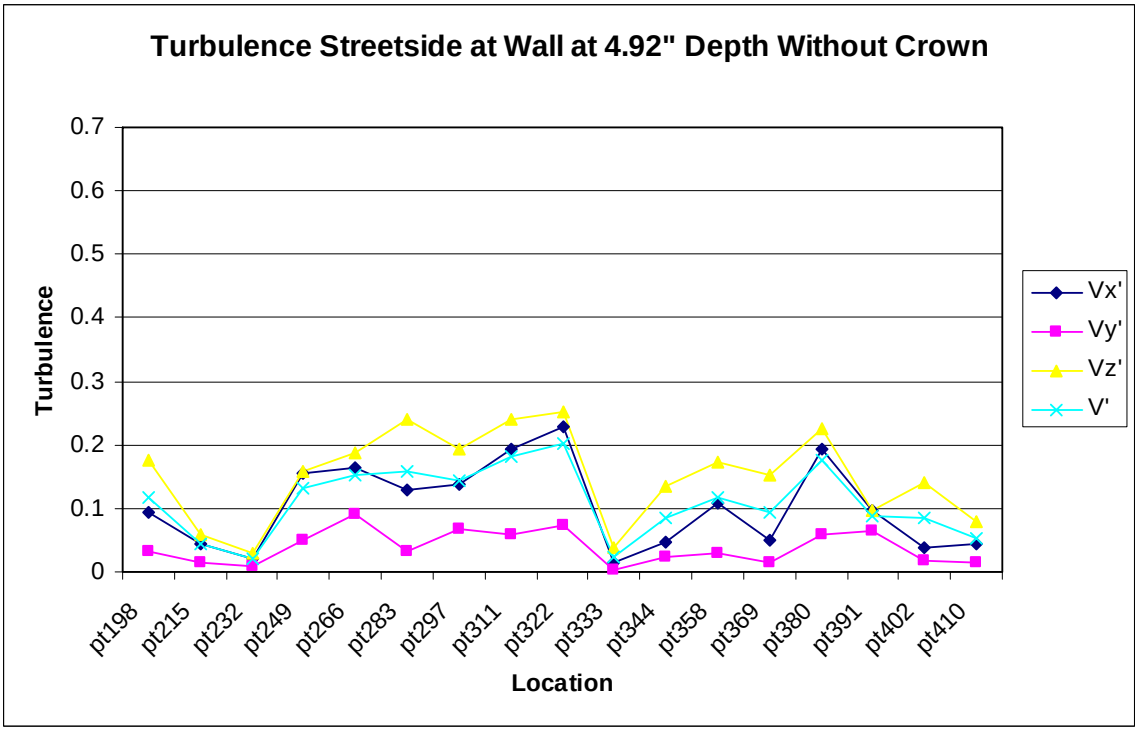

Figure A.23. Turbulence intensity along the Maryland side of the structure (street side at SAFL) without the crown at a depth of 4.92 inches from the surface. Streamflow is from left to right. Location numbers are shown in Figure 2.3.

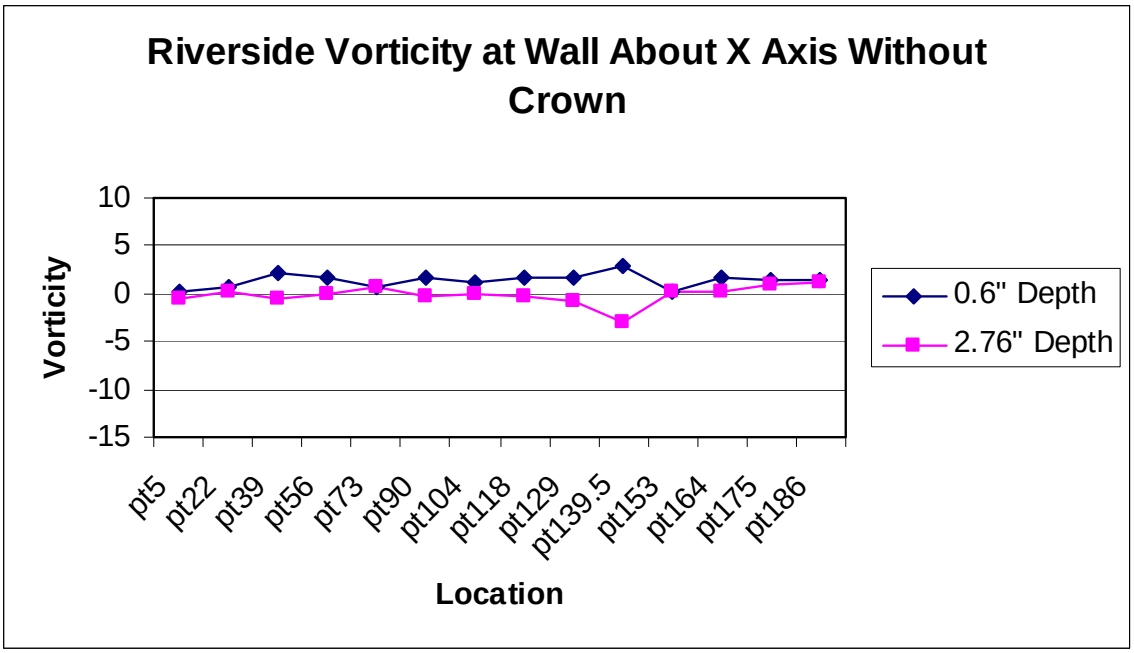

Figure A.24. Estimated vorticity about the x-axis along the Virginia side of the structure (river side at SAFL) without the crown at depths of 0.6 and 2.76 inches from the surface. Streamflow is from left to right. Location numbers are shown in Figure 2.3.

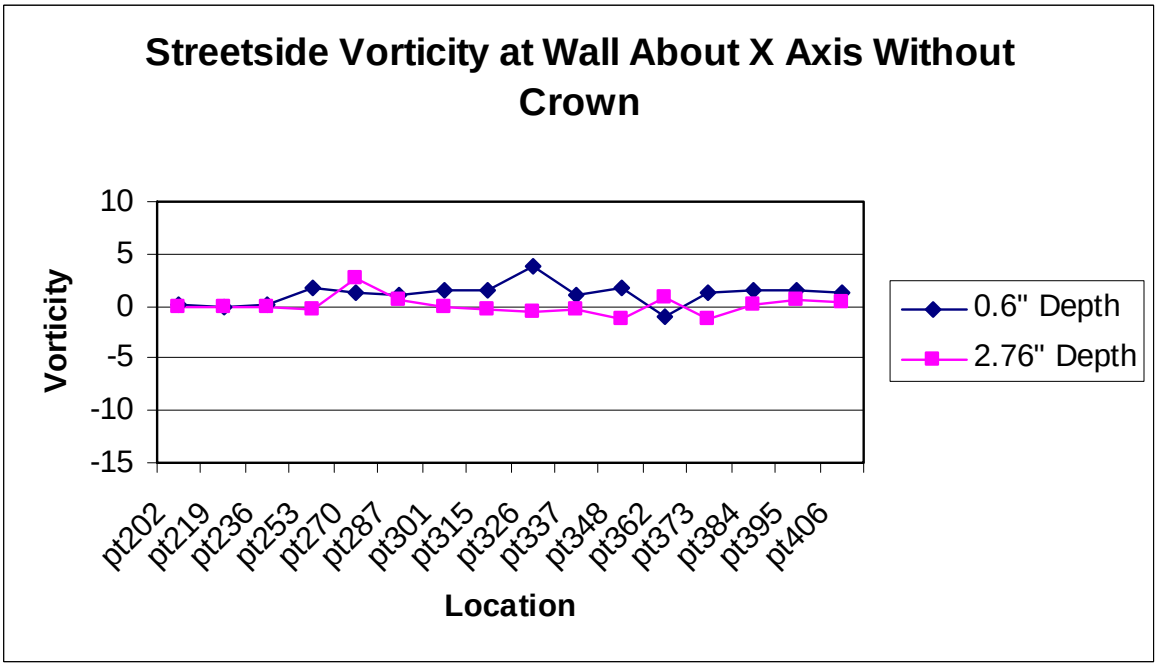

Figure A.25. Estimated vorticity about the x-axis along the Maryland side of the structure (street side at SAFL) without the crown at depths of 0.6 and 2.76 inches from the surface. Streamflow is from left to right. Location numbers are shown in Figure 2.3.

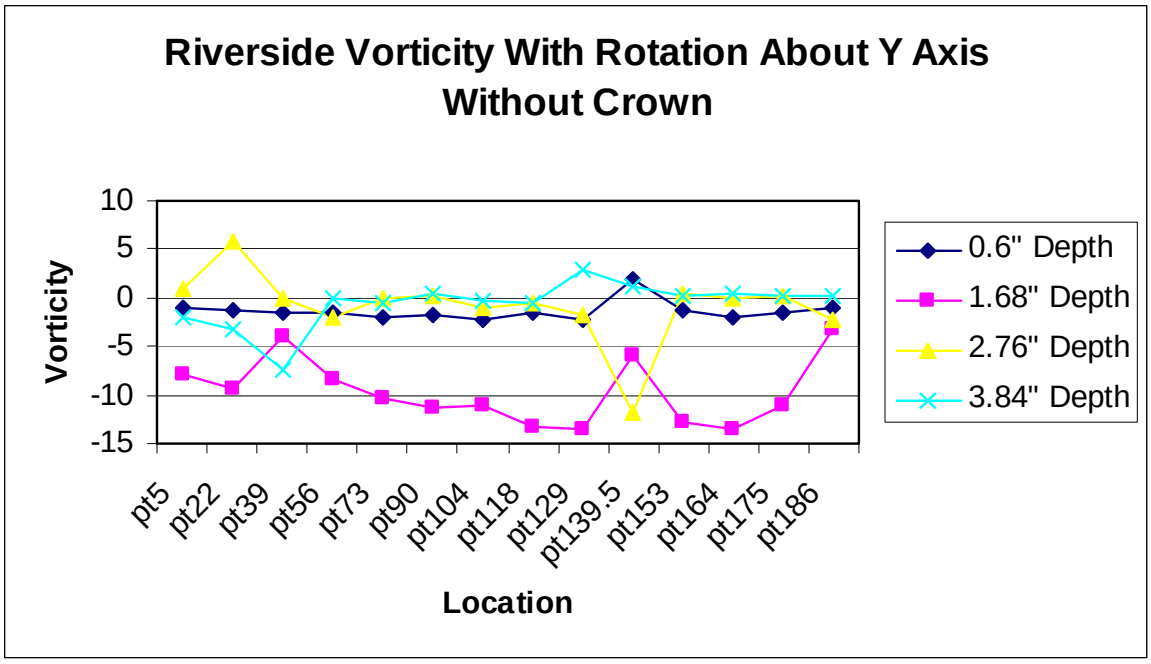

Figure A.26. Estimated vorticity about the y-axis along the Virginia side of the structure (river side at SAFL) without the crown. Streamflow is from left to right. Location numbers are shown in Figure 2.3.

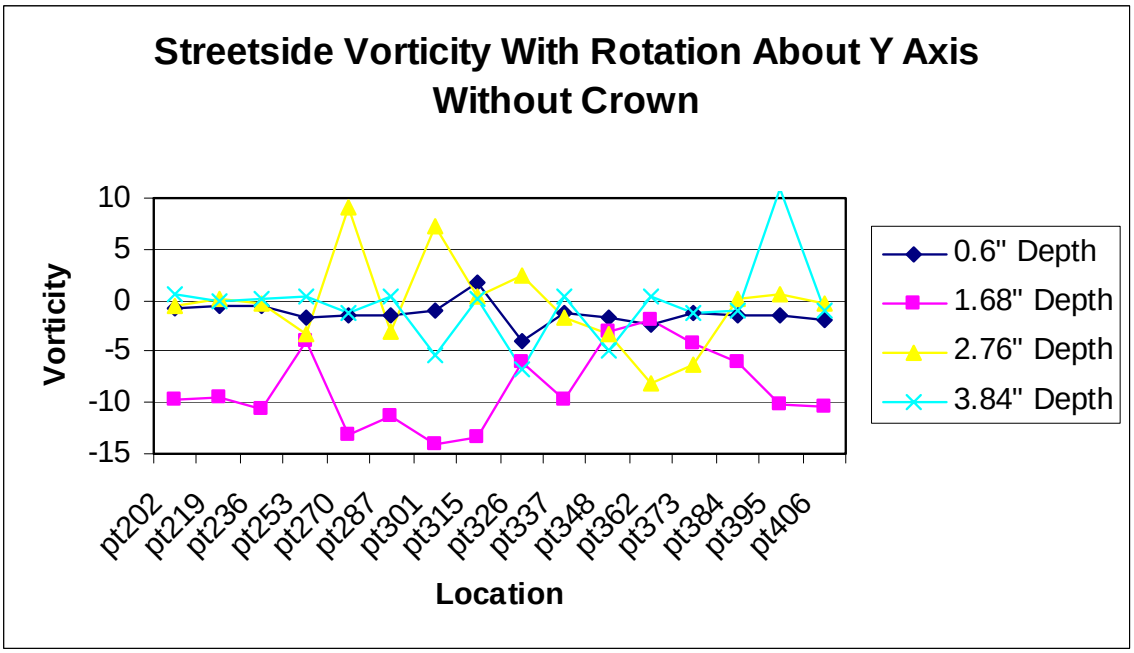

Figure A.27. Estimated vorticity about the y-axis along the Maryland side of the structure (street side at SAFL) without the crown. Streamflow is from left to right. Location numbers are shown in Figure 2.3.

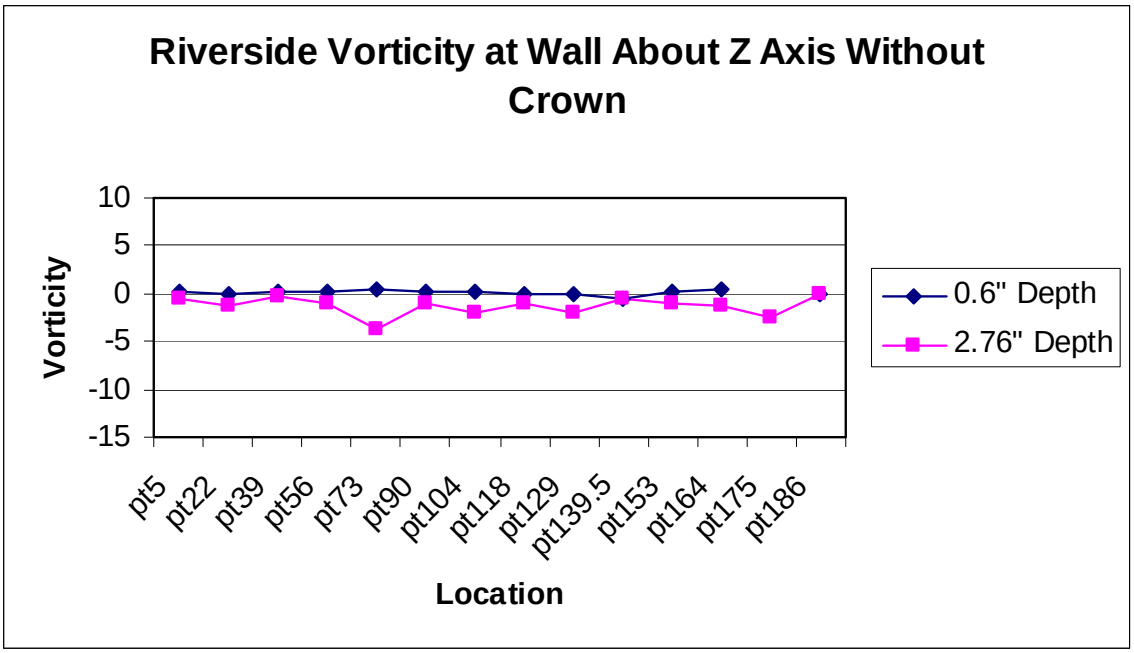

Figure A.28. Estimated vorticity about the z-axis along the Virginia side of the structure (street side at SAFL) without the crown at depths of 0.6 and 2.76 inches from the surface. Streamflow is from left to right. Location numbers are shown in Figure 2.3.

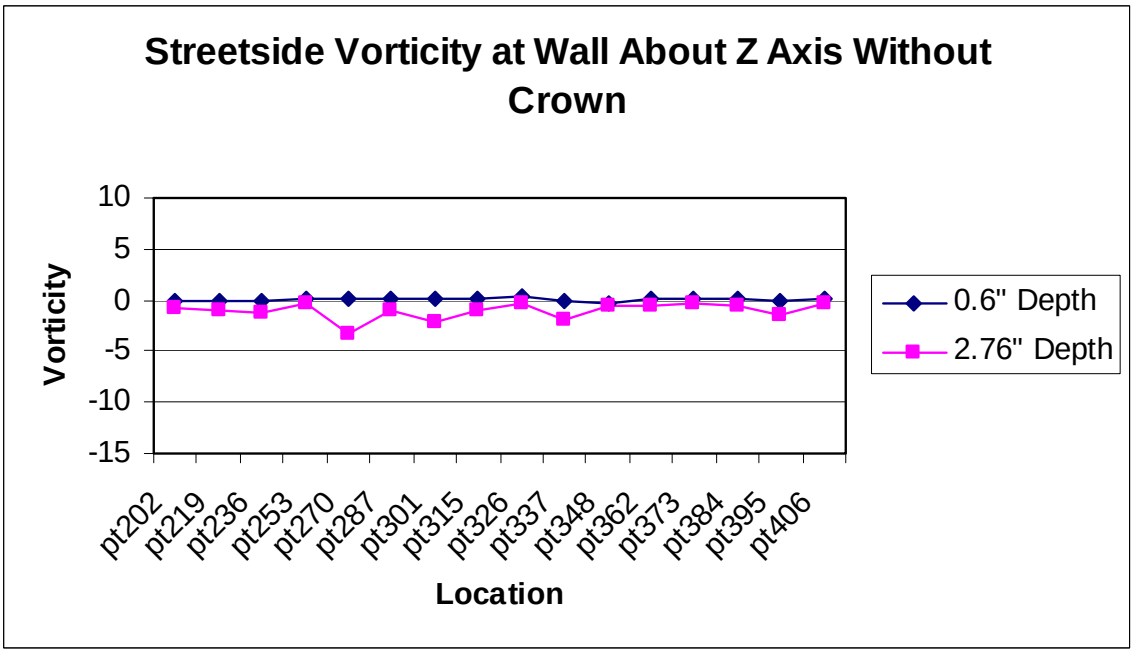

Figure A.29. Estimated vorticity about the z-axis along the Maryland side of the structure (street side at SAFL) without the crown at depths of 0.6 and 2.76 inches from the surface. Streamflow is from left to right. Location numbers are shown in Figure 2.3.

Appendix B: Velocity Measurements along the 10th Geometry with the Crown (Third Set)

All dimensions and values are at the model scale.

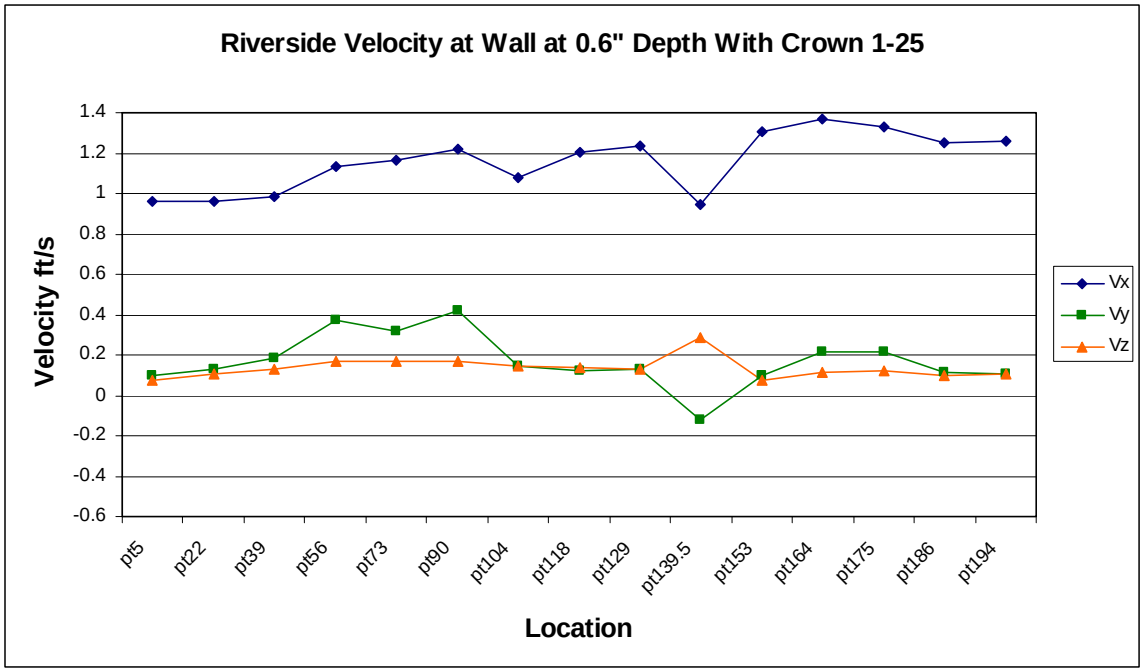

Figure B.1. Average velocity components along the Virginia side of the 10th geometry (riverside at SAFL) at a depth of 0.6 inches from the surface. Streamflow is from left to right. Location numbers are shown in Figure 2.3.

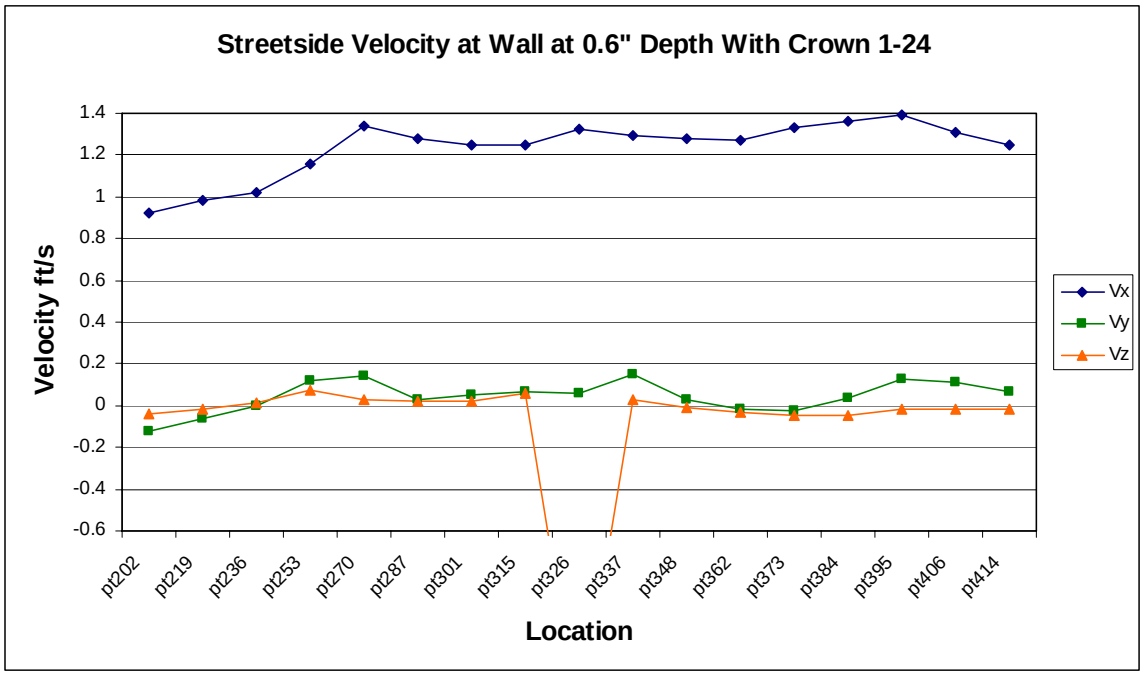

Figure B.2. Average velocity components along the Maryland side of the 10th geometry (street side at SAFL) at a depth of 0.6 inches from the surface. Streamflow is from left to right. Location numbers are shown in Figure 2.3.

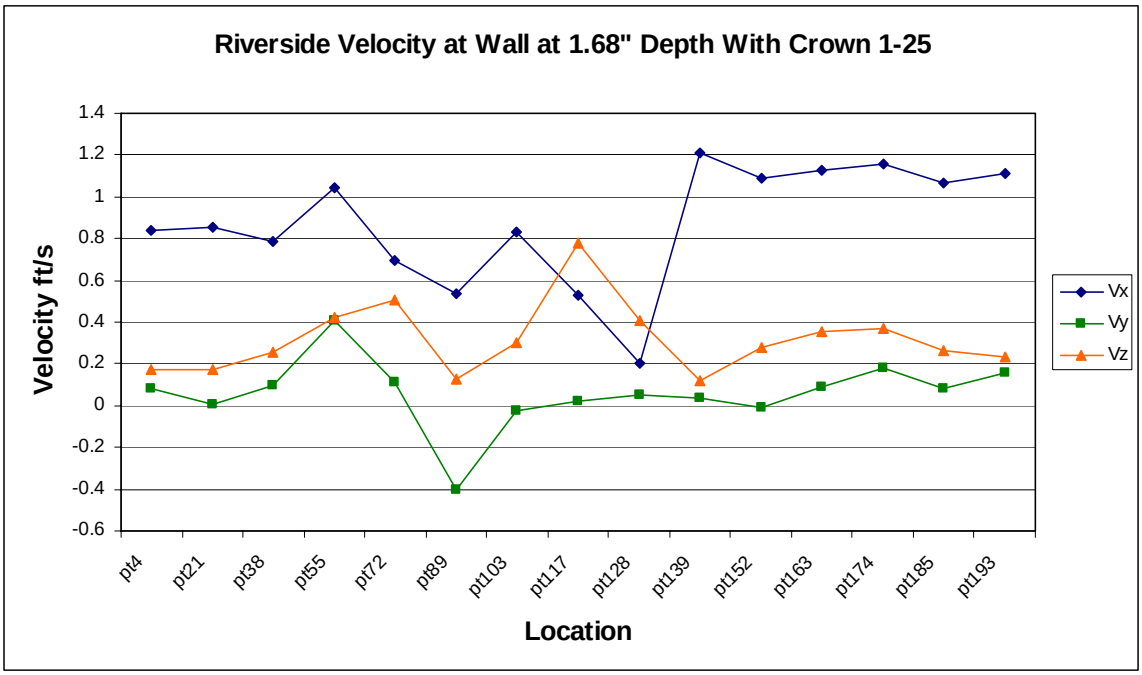

Figure B.3. Average velocity components along the Virginia side of the 10th geometry (riverside at SAFL) at a depth of 1.68 inches from the surface. Streamflow is from left to right. Location numbers are shown in Figure 2.3.

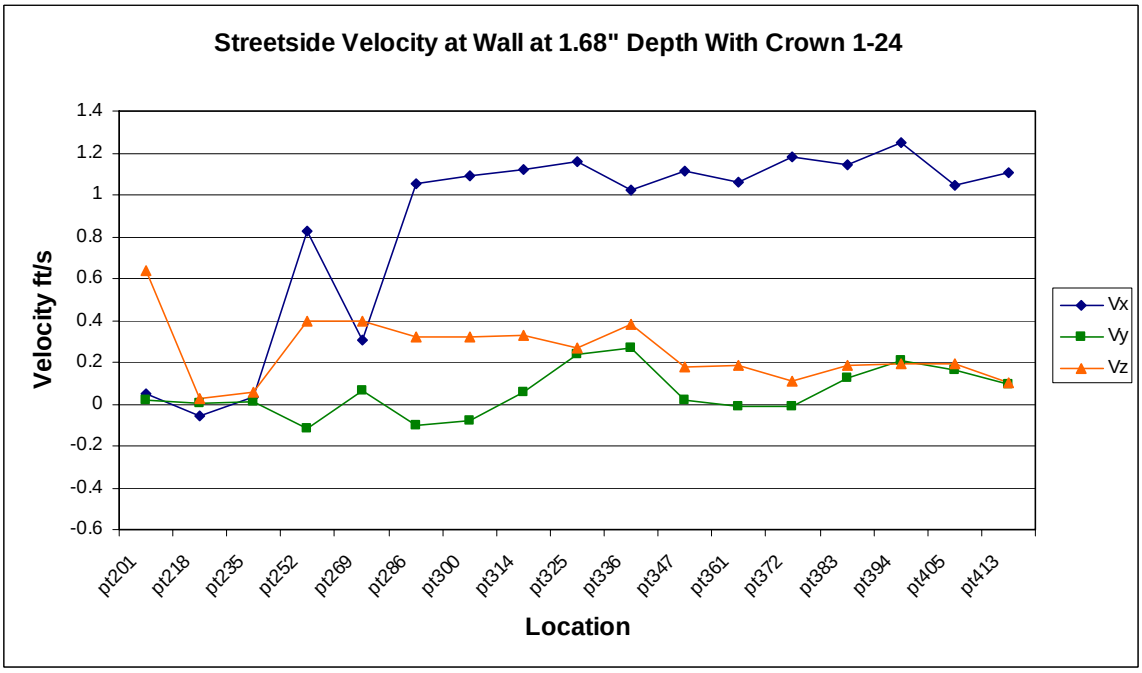

Figure B.4. Average velocity components along the Maryland side of the 10th geometry (street side at SAFL) at a depth of 1.68 inches from the surface. Streamflow is from left to right. Location numbers are shown in Figure 2.3.

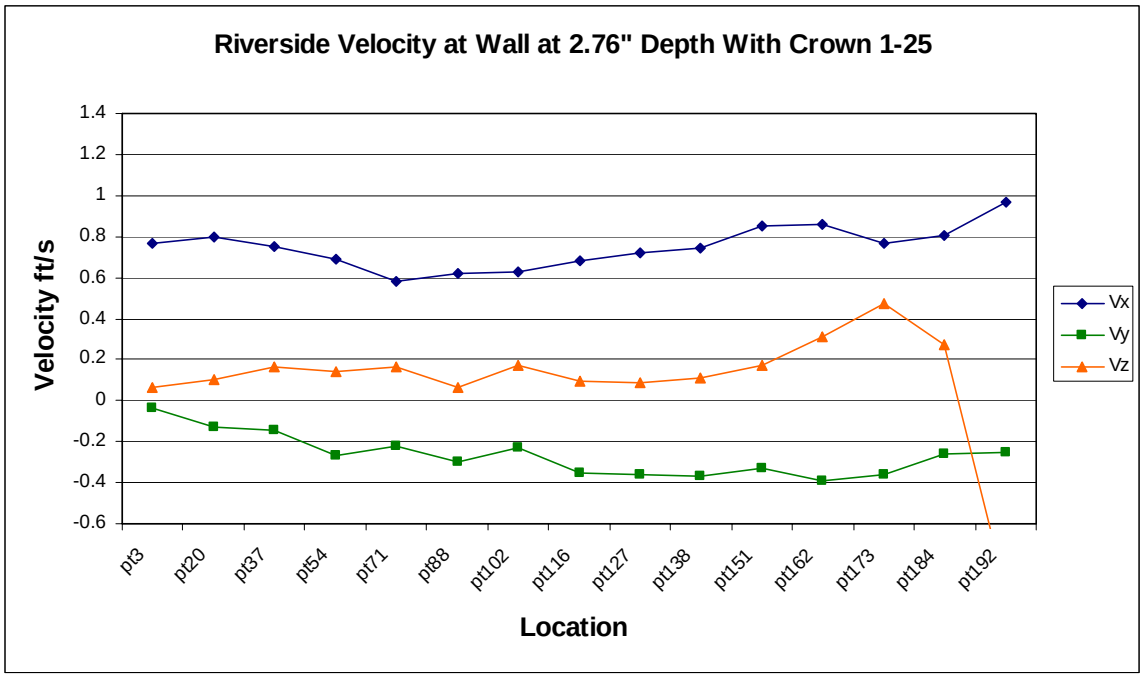

Figure B.5. Average velocity components along the Virginia side of the 10th geometry (riverside at SAFL) at a depth of 2.76 inches from the surface. Streamflow is from left to right. Location numbers are shown in Figure 2.3.

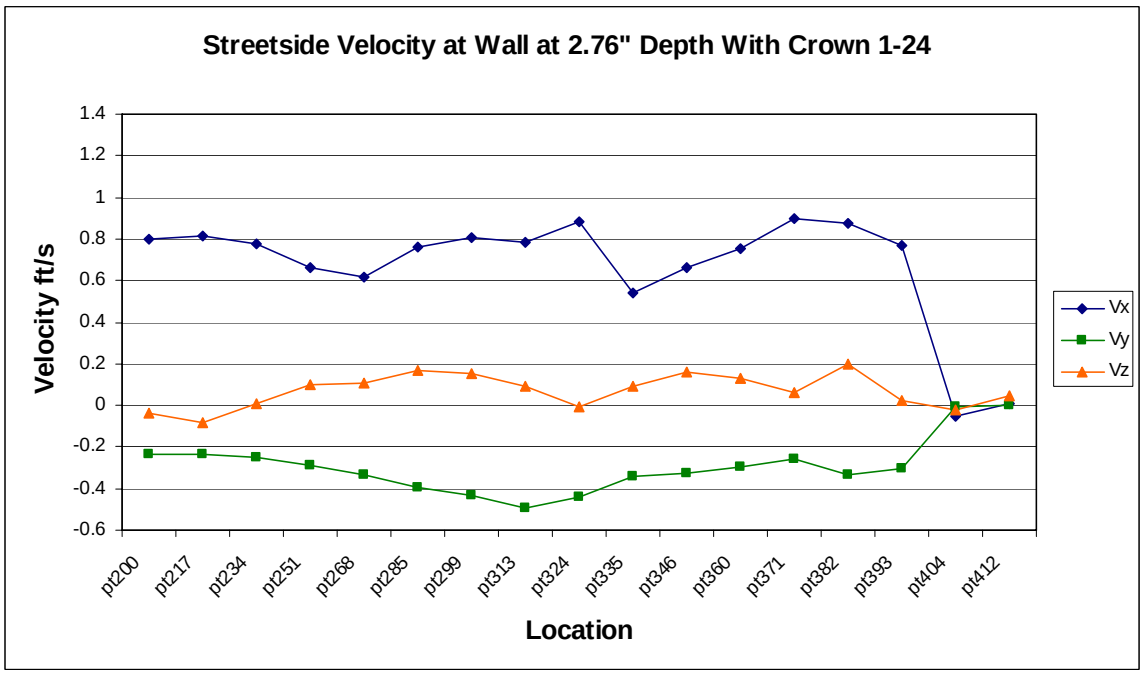

Figure B.6. Average velocity components along the Maryland side of the 10th geometry (street side at SAFL) at a depth of 2.76 inches from the surface. Streamflow is from left to right. Location numbers are shown in Figure 2.3.

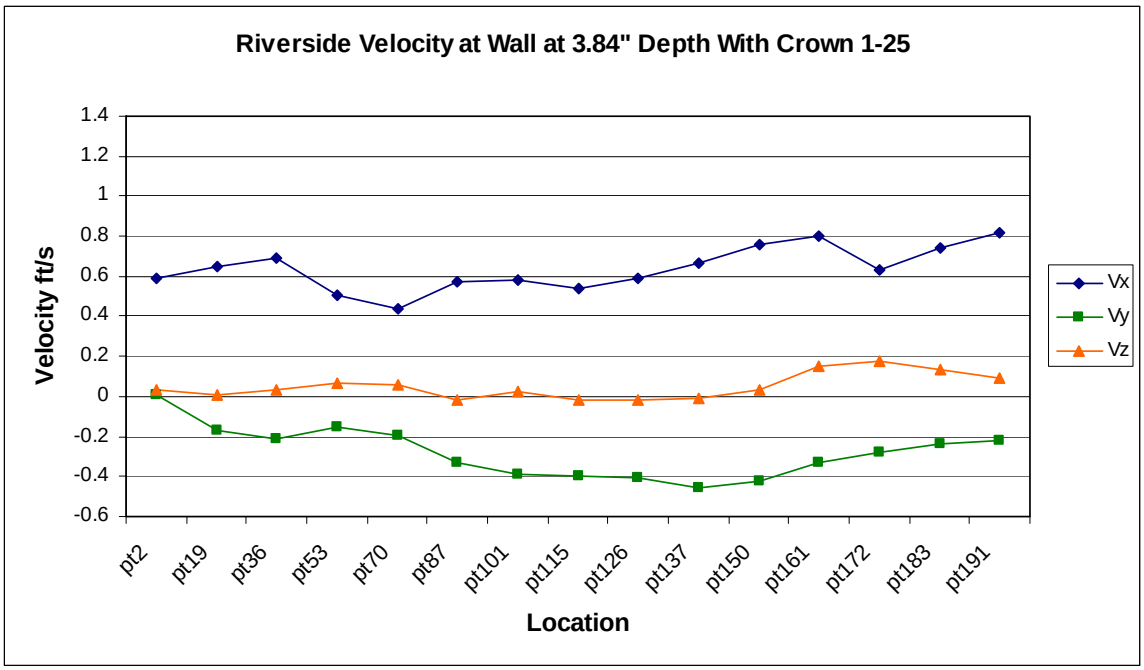

Figure B.7. Average velocity components along the Virginia side of the 10th geometry (riverside at SAFL) at a depth of 3.84 inches from the surface. Streamflow is from left to right. Location numbers are shown in Figure 2.3.

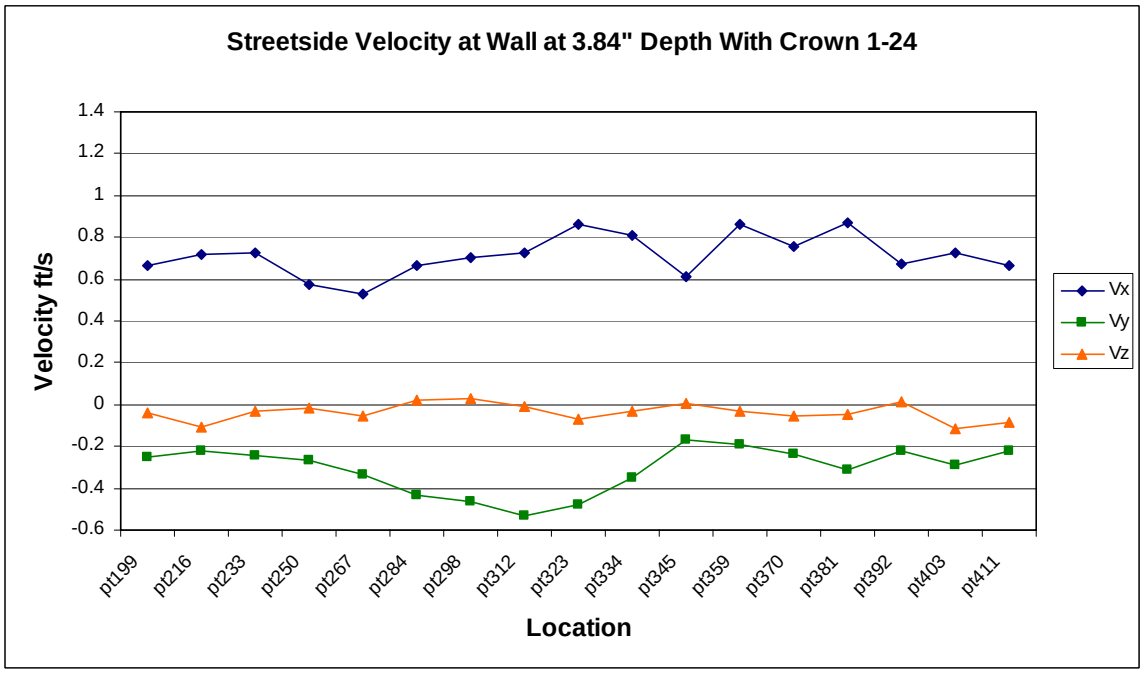

Figure B.8. Average velocity components along the Maryland side of the 10th geometry (street side at SAFL) at a depth of 3.84 inches from the surface. Streamflow is from left to right. Location numbers are shown in Figure 2.3.

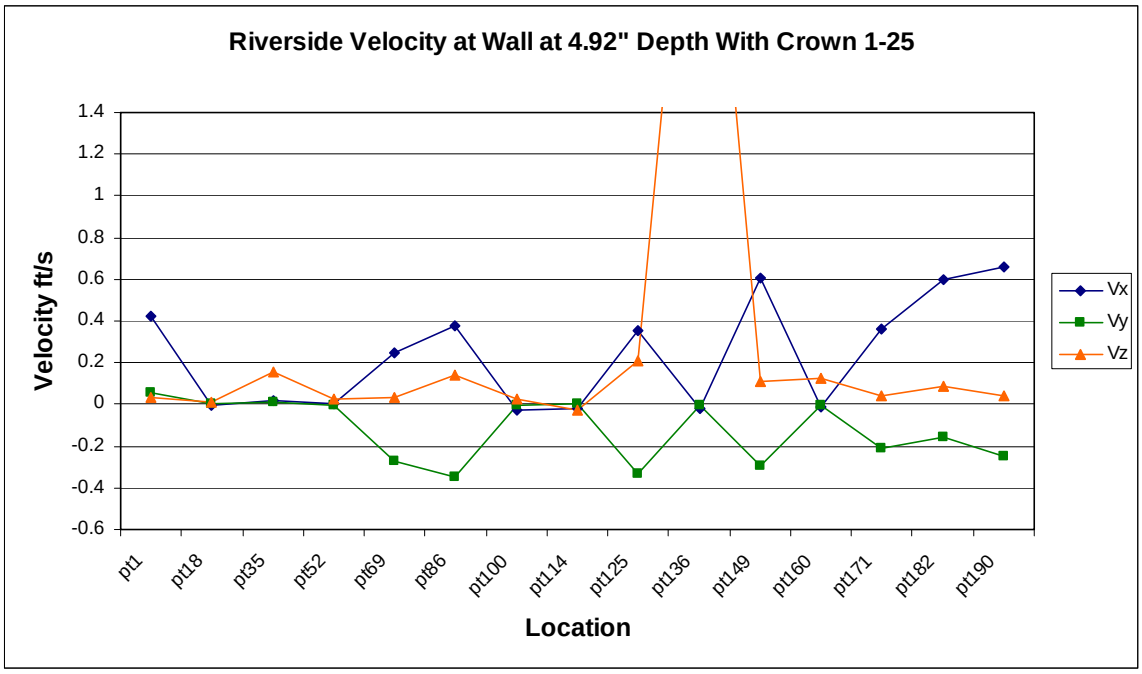

Figure B.9. Average velocity components along the Virginia side of the 10th geometry (riverside at SAFL) at a depth of 4.92 inches from the surface. Streamflow is from left to right. Location numbers are shown in Figure 2.3.

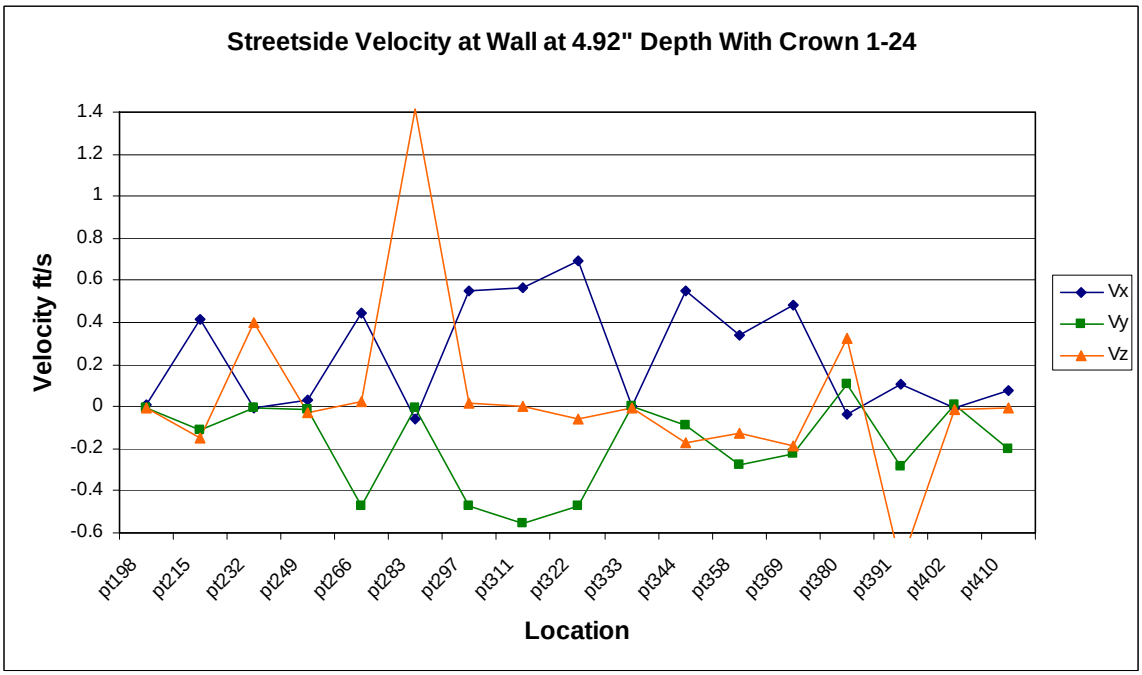

Figure B.10. Average velocity components along the Maryland side of the 10th geometry (street side at SAFL) at a depth of 4.92 inches from the surface. Streamflow is from left to right. Location numbers are shown in Figure 2.3.

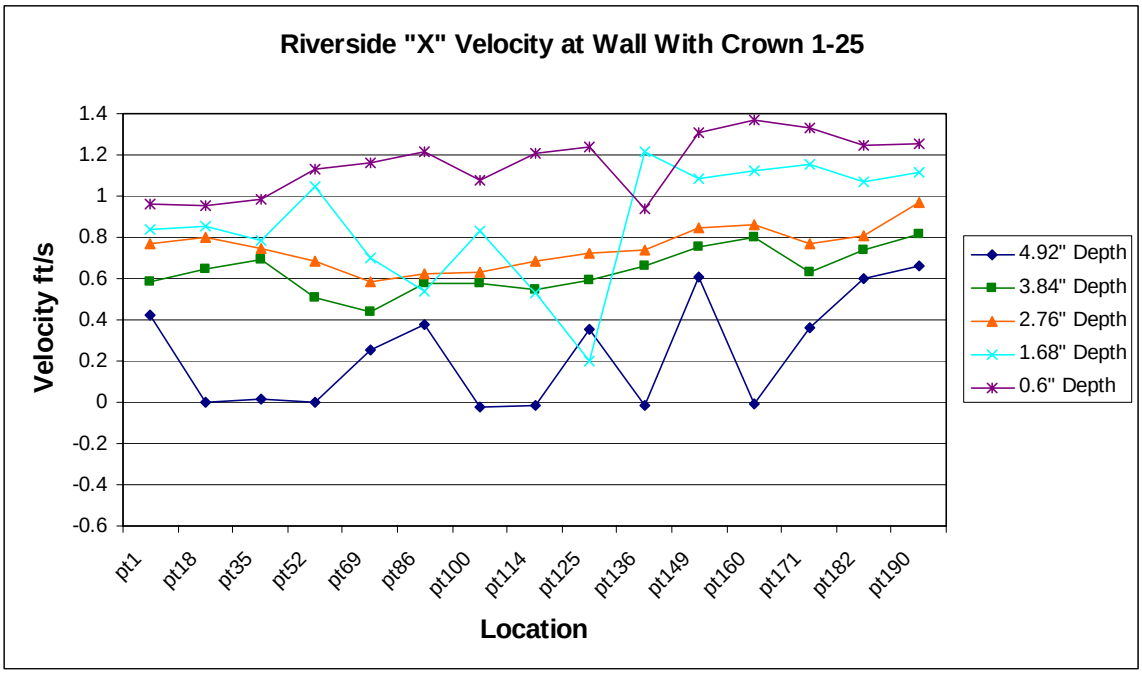

Figure B.11. X-components of velocities along the Virginia side of the 10th geometry (riverside at SAFL). Streamflow is from left to right. Location numbers are shown in Figure 2.3.

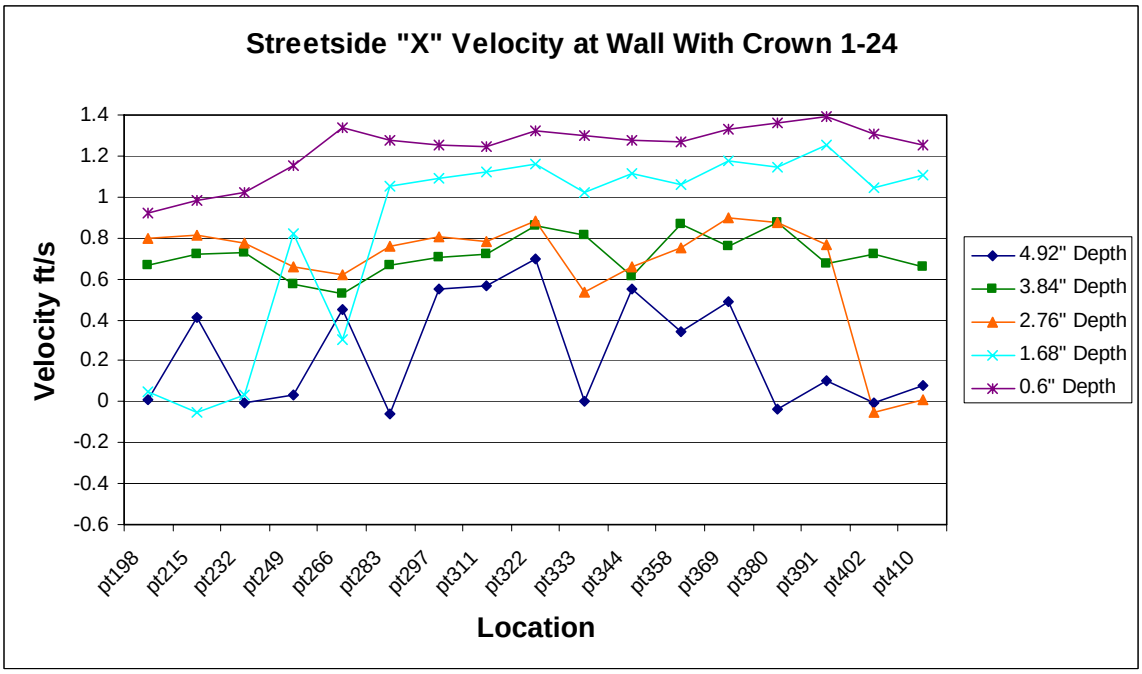

Figure B.12. X-components of velocities along the Maryland side of the 10th geometry (street side at SAFL). Streamflow is from left to right. Location numbers are shown in Figure 2.3.

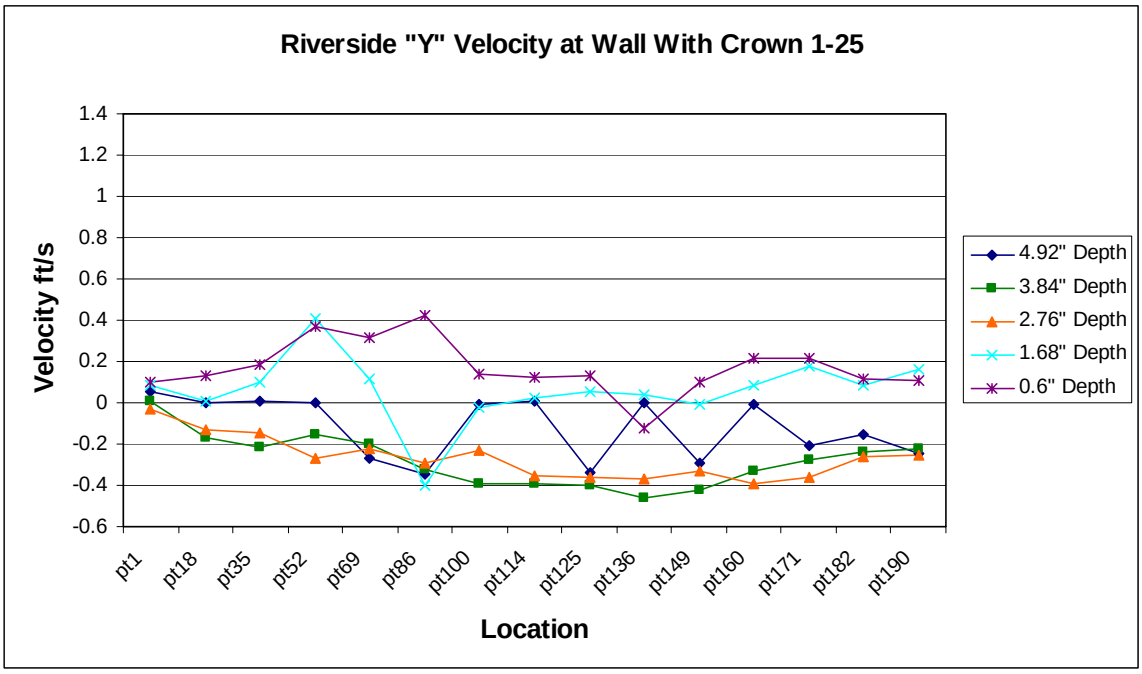

Figure B.13. Y-components of velocities along the Virginia side of the 10th geometry (riverside at SAFL). Streamflow is from left to right. Location numbers are shown in Figure 2.3.

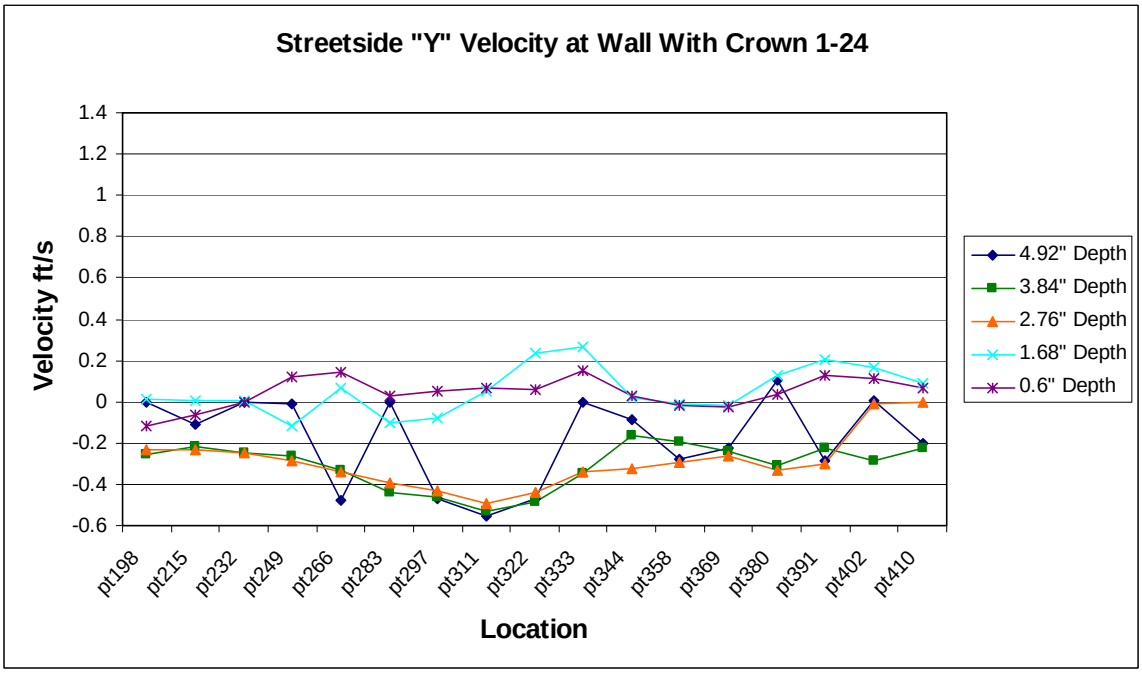

Figure B.14. Y-components of velocities along the Maryland side of the 10th geometry (street side at SAFL). Streamflow is from left to right. Location numbers are shown in Figure 2.3.

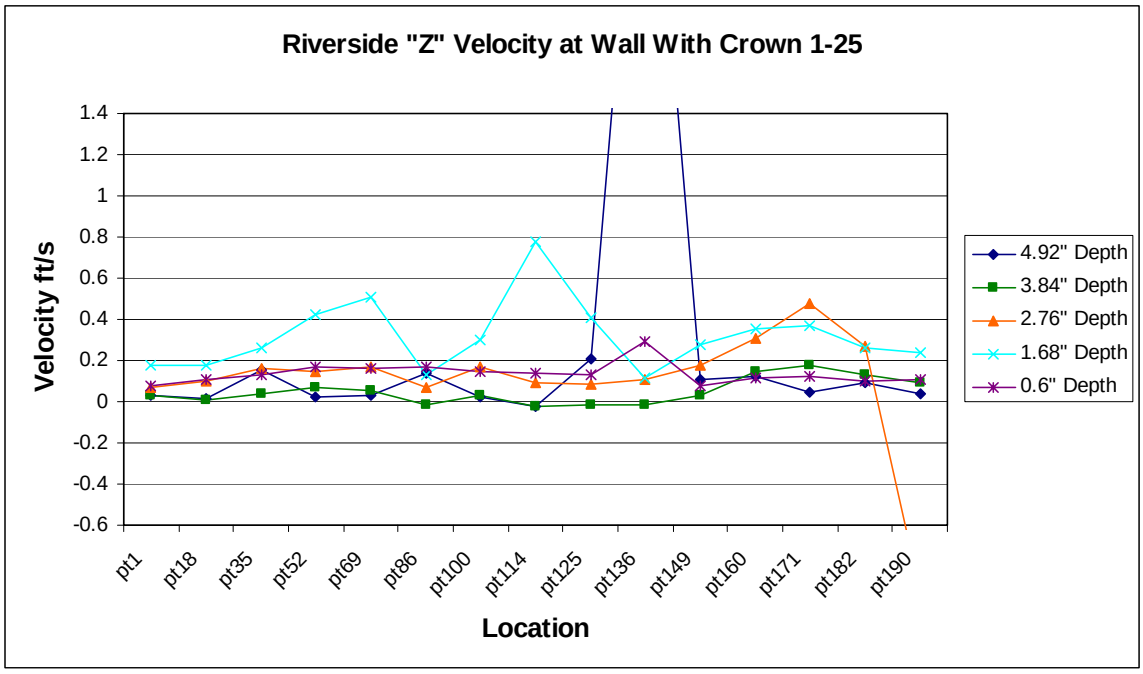

Figure B.15. Z-components of velocities along the Virginia side of the 10th geometry (riverside at SAFL). Streamflow is from left to right. Location numbers are shown in Figure 2.3.

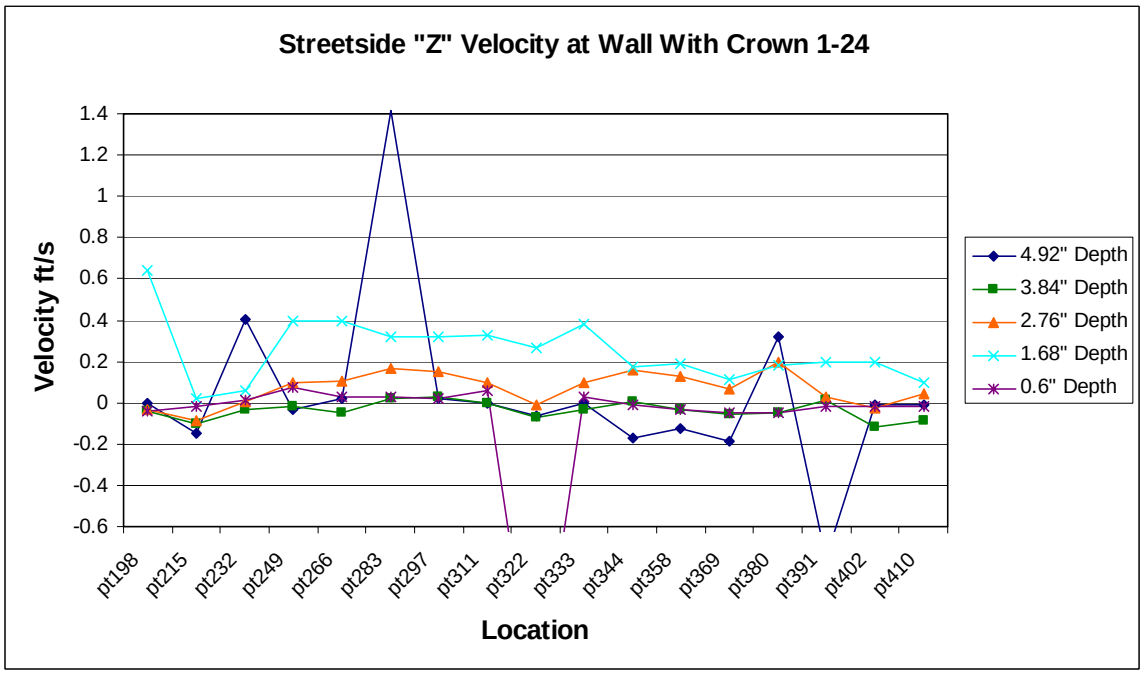

Figure B.16. Z-components of velocities along the Maryland side of the 10th geometry (street side at SAFL). Streamflow is from left to right. Location numbers are shown in Figure 2.3.

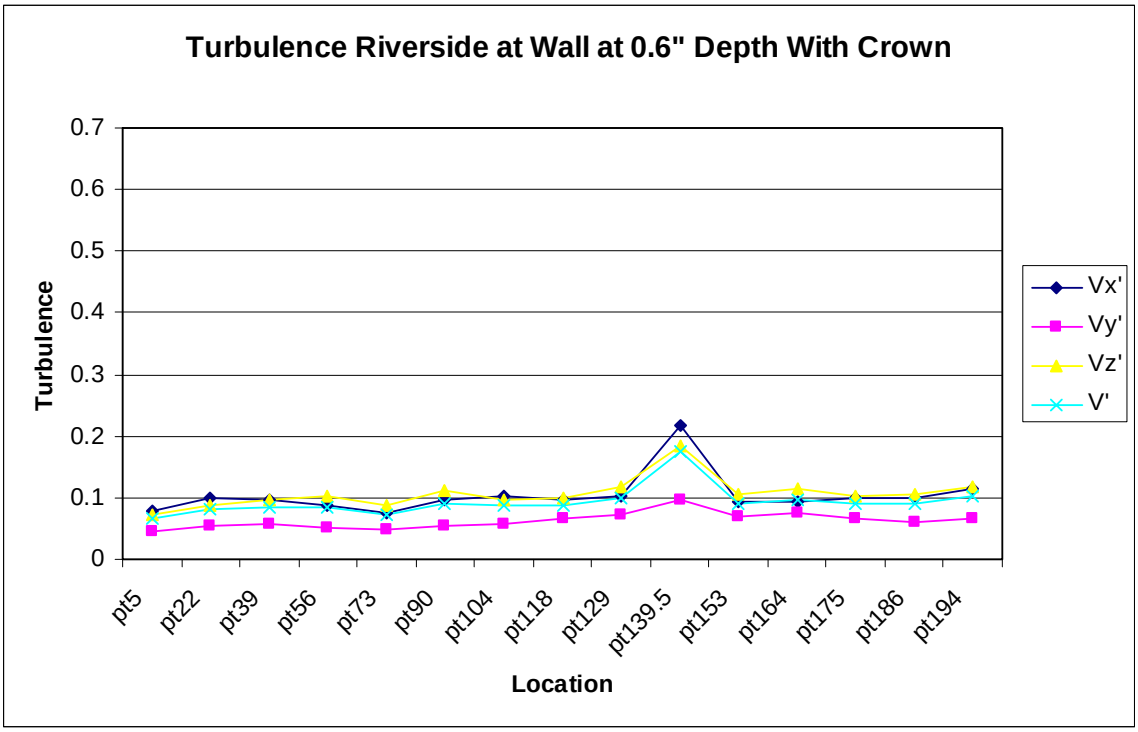

Figure B.17. Turbulence intensity along the Virginia side of the 10th geometry (riverside at SAFL) at a depth of 0.6 inches from the surface. Streamflow is from left to right. Location numbers are shown in Figure 2.3.

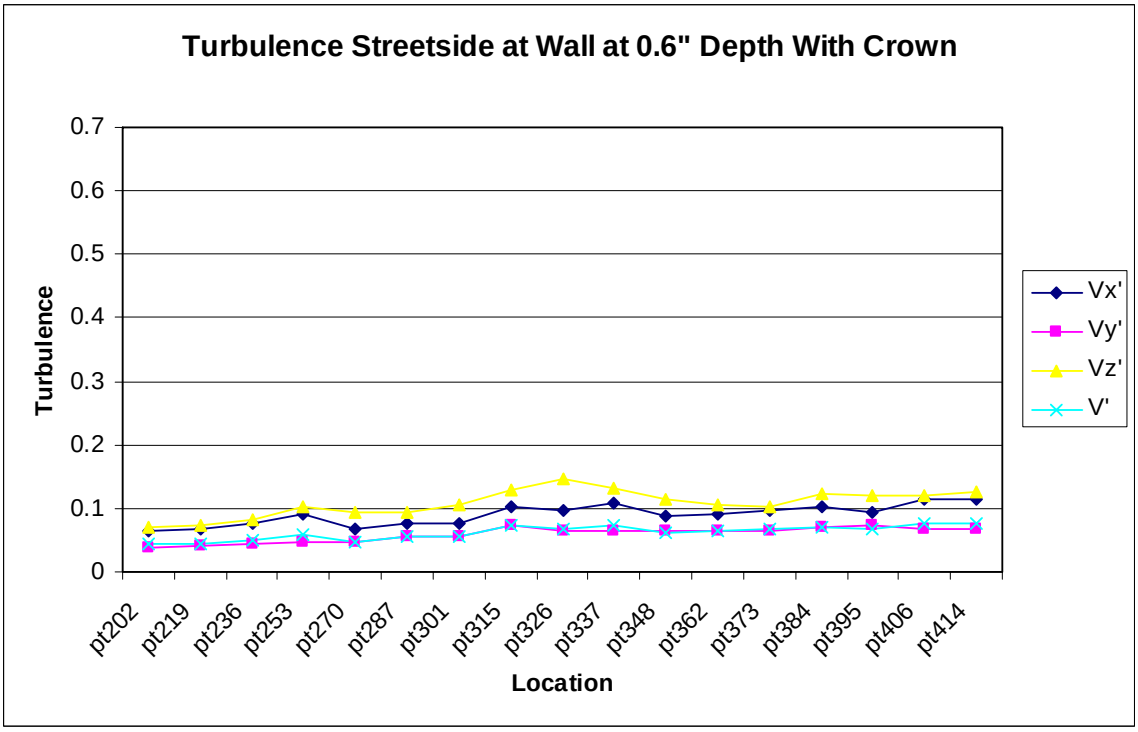

Figure B.18. Turbulence intensity along the Maryland side of the 10th geometry (street side at SAFL) at a depth of 0.6 inches from the surface. Streamflow is from left to right. Location numbers are shown in Figure 2.3.

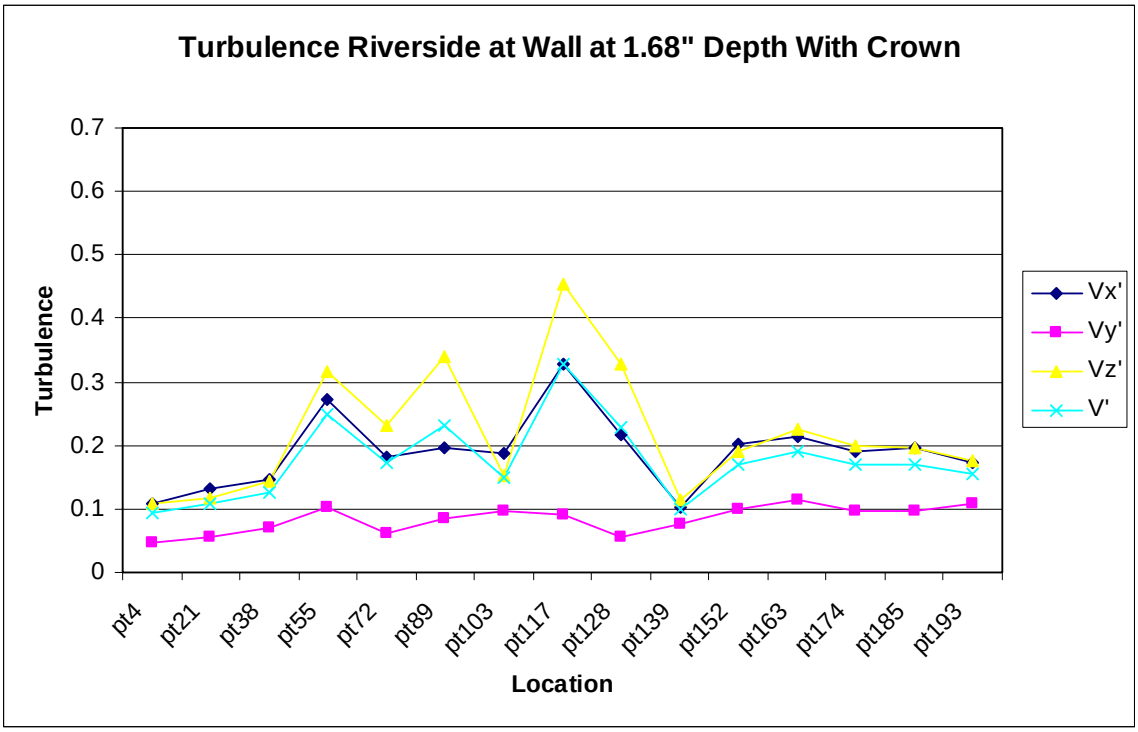

Figure B.19. Turbulence intensity along the Virginia side of the 10th geometry (riverside at SAFL) at a depth of 1.68 inches from the surface. Streamflow is from left to right. Location numbers are shown in Figure 2.3.

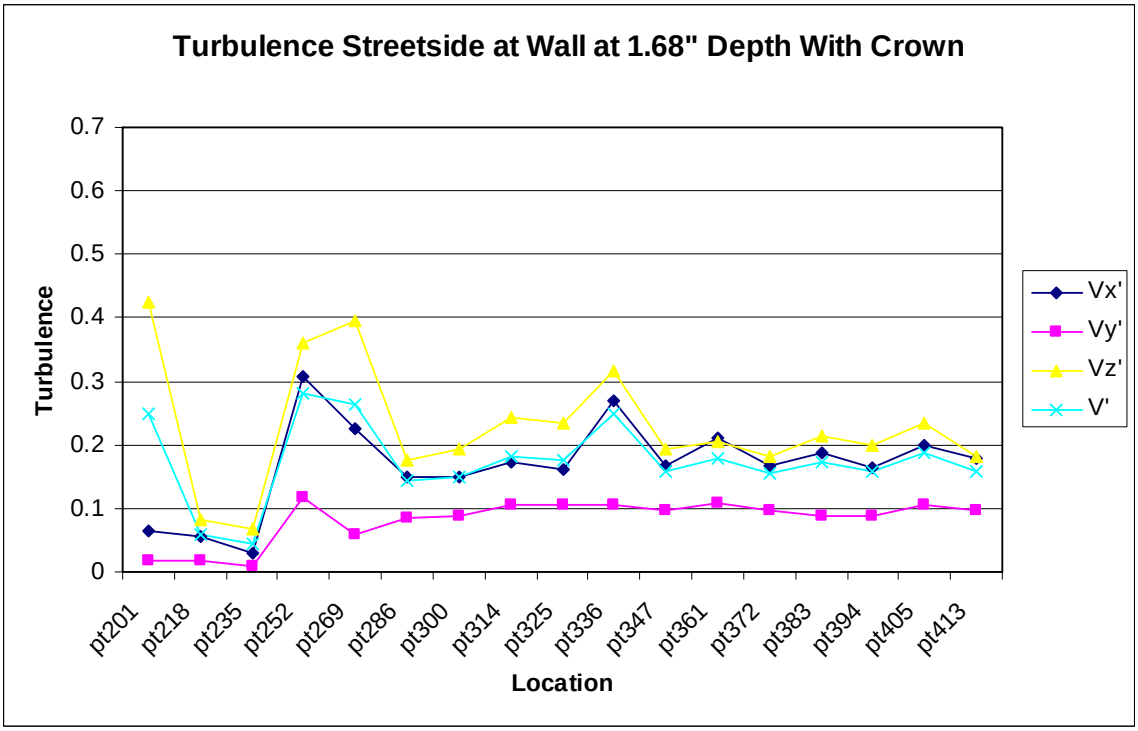

Figure B.20. Turbulence intensity along the Maryland side of the 10th geometry (street side at SAFL) at a depth of 1.68 inches from the surface. Streamflow is from left to right. Location numbers are shown in Figure 2.3.

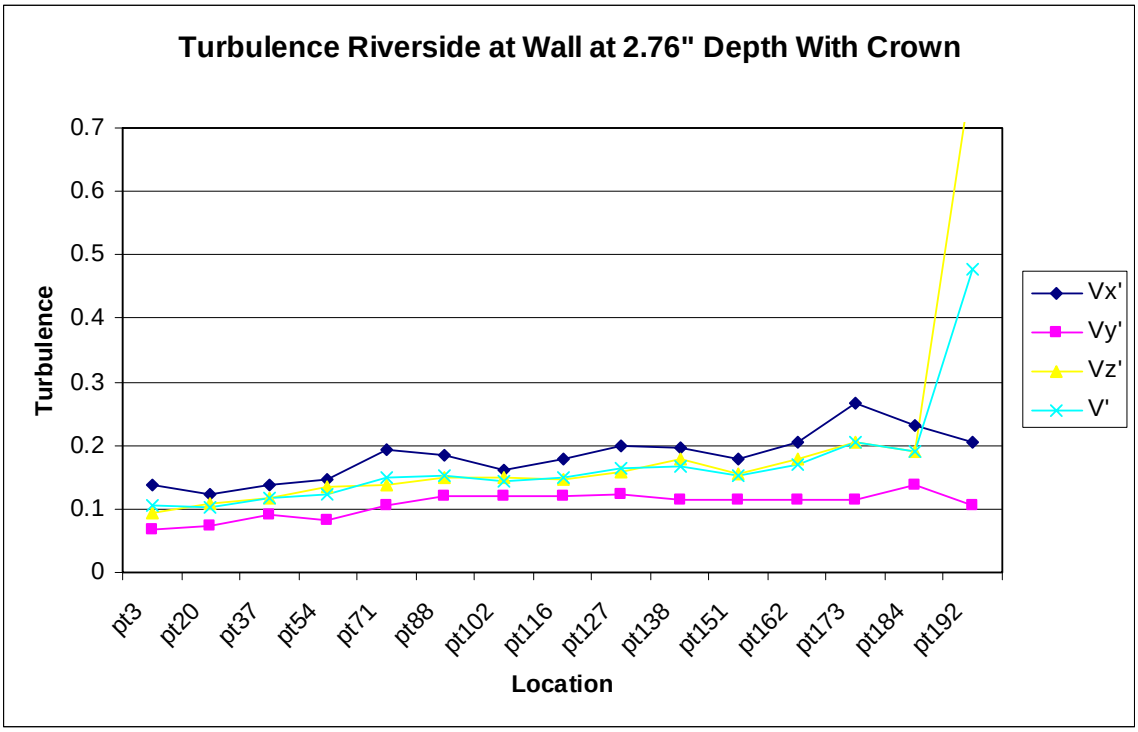

Figure B.21. Turbulence intensity along the Virginia side of the 10th geometry (riverside at SAFL) at a depth of 2.76 inches from the surface. Streamflow is from left to right. Location numbers are shown in Figure 2.3.

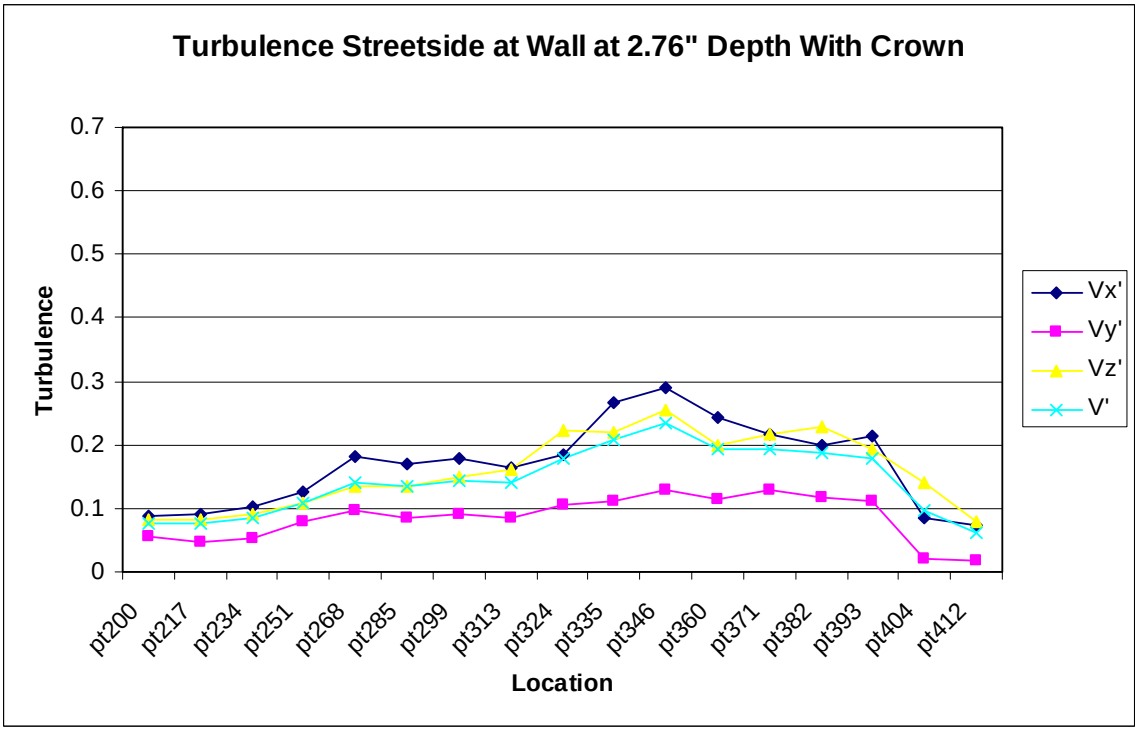

Figure B.22. Turbulence intensity along the Maryland side of the 10th geometry (street side at SAFL) at a depth of 2.76 inches from the surface. Streamflow is from left to right. Location numbers are shown in Figure 2.3.

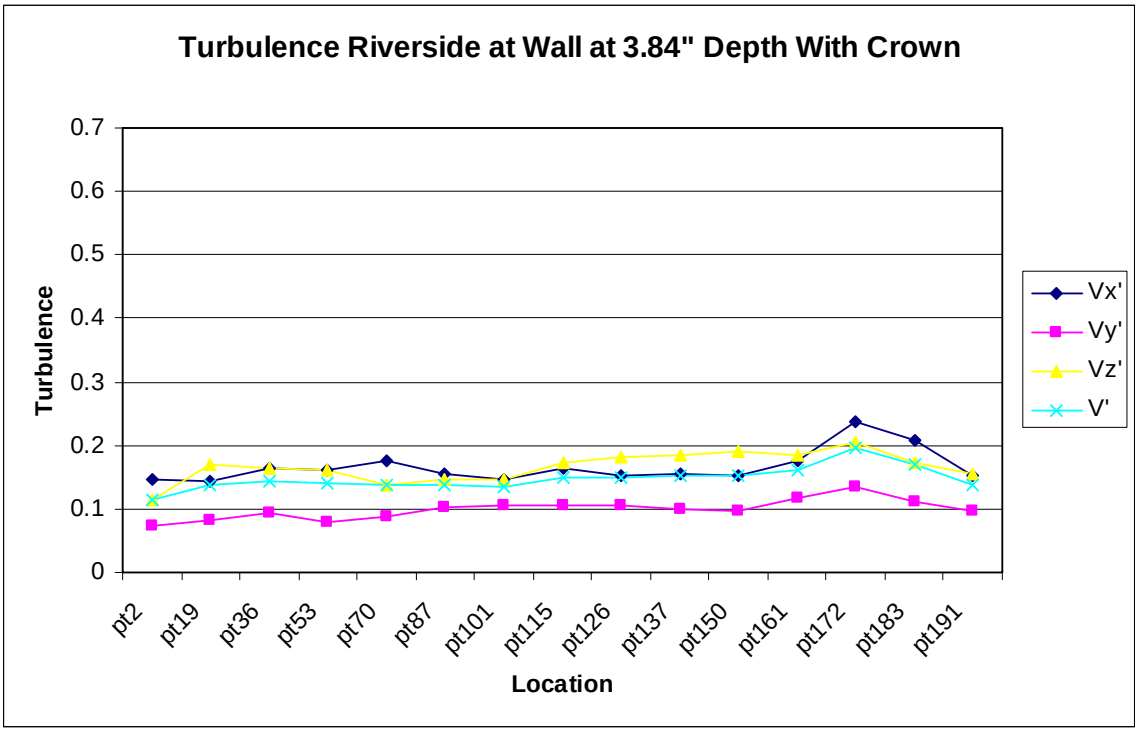

Figure B.23. Turbulence intensity along the Virginia side of the 10th geometry (riverside at SAFL) at a depth of 3.84 inches from the surface. Streamflow is from left to right. Location numbers are shown in Figure 2.3.

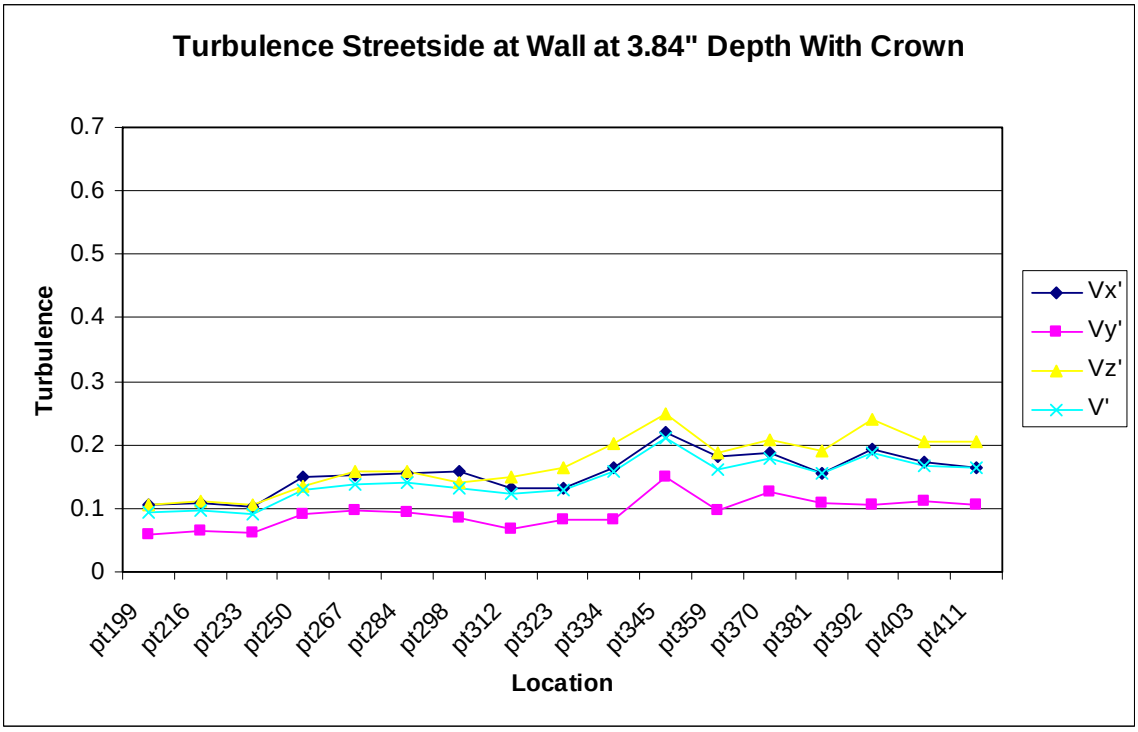

Figure B.24. Turbulence intensity along the Maryland side of the 10th geometry (street side at SAFL) at a depth of 3.84 inches from the surface. Streamflow is from left to right. Location numbers are shown in Figure 2.3.

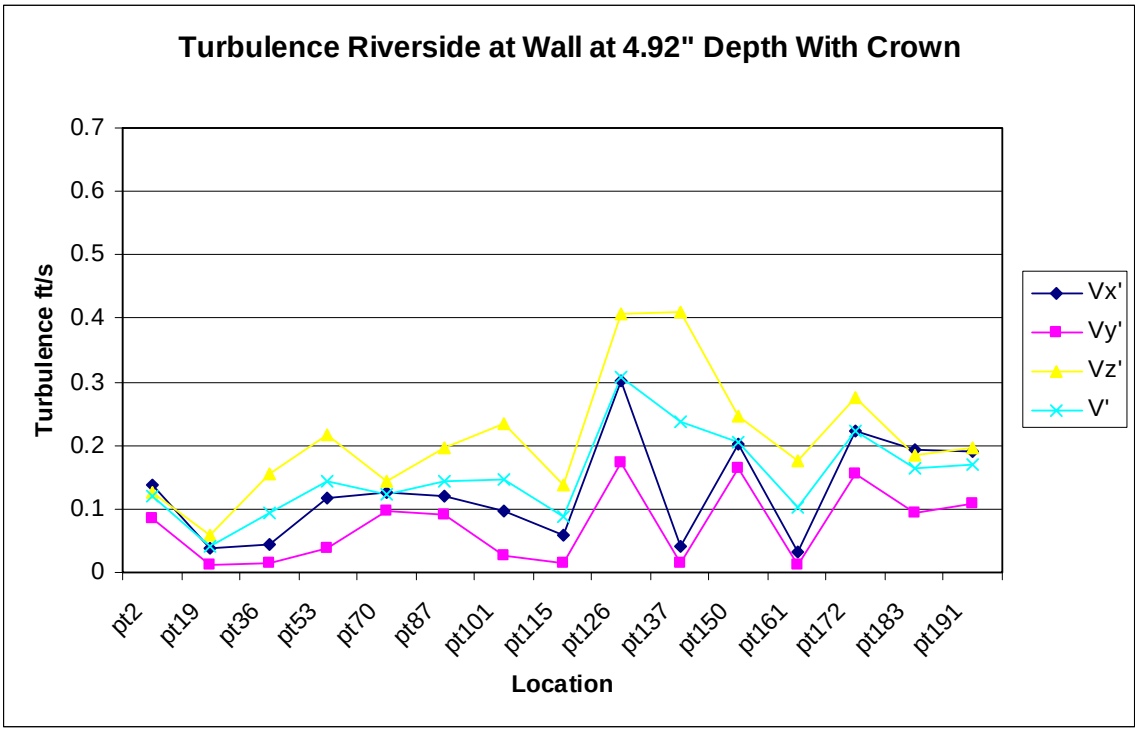

Figure B.25. Turbulence intensity along the Virginia side of the 10th geometry (riverside at SAFL) at a depth of 4.92 inches from the surface. Streamflow is from left to right. Location numbers are shown in Figure 2.3.

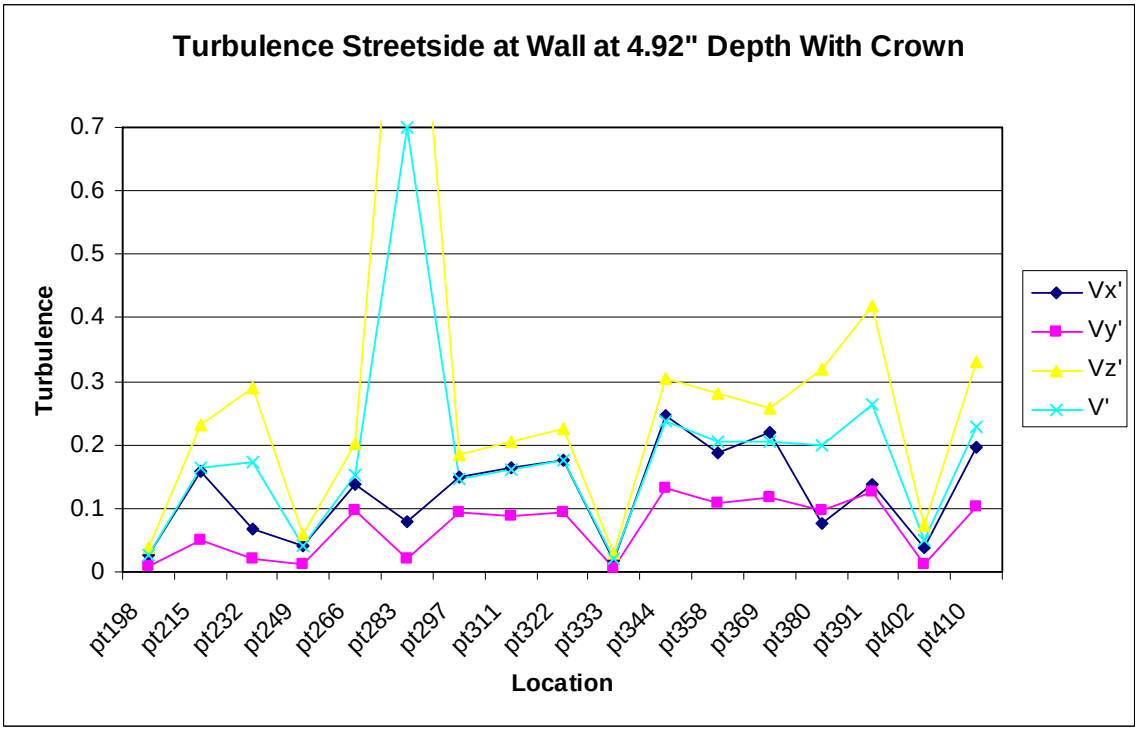

Figure B.26. Turbulence intensity along the Maryland side of the 10th geometry (street side at SAFL) at a depth of 4.92 inches from the surface. Streamflow is from left to right. Location numbers are shown in Figure 2.3.

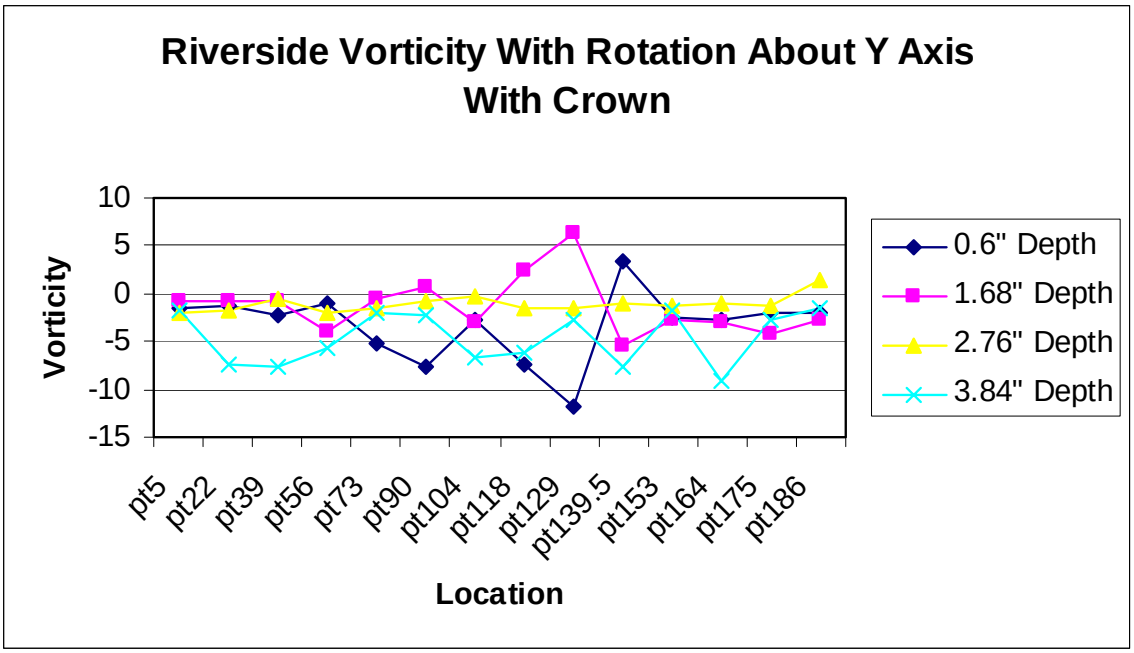

Figure B.27. Estimated vorticity about the y-axis along the Virginia side of the 10th geometry (riverside at SAFL). Streamflow is from left to right. Location numbers are shown in Figure 2.3.

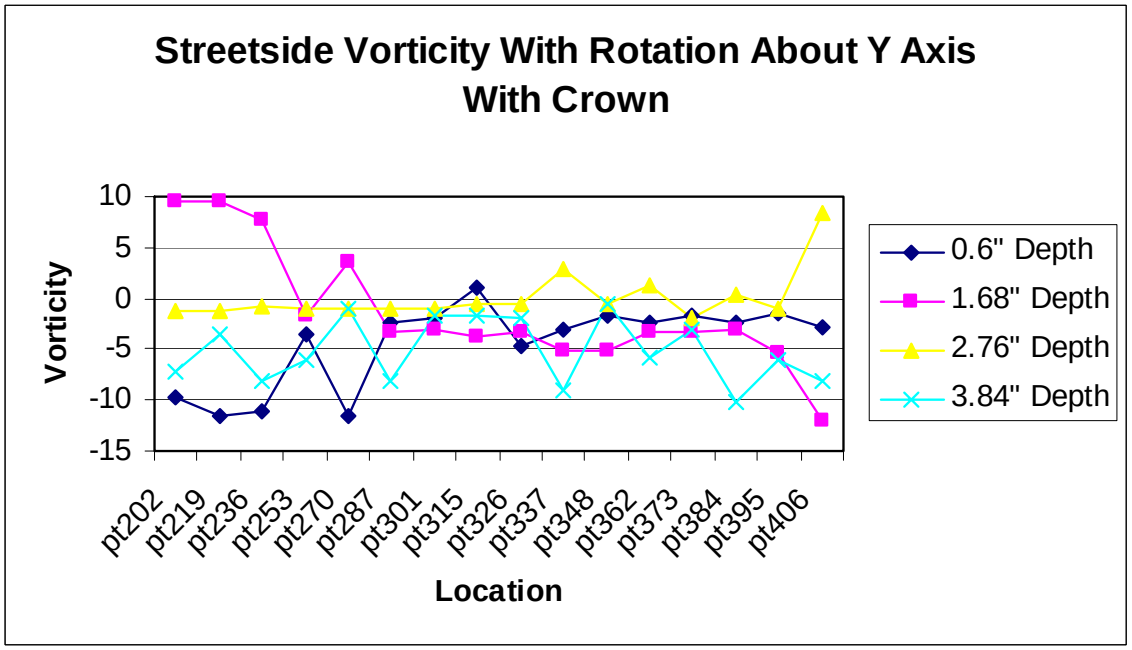

Figure B.28. Estimated vorticity about the y-axis along the Maryland side of the 10th geometry (street side at SAFL). Streamflow is from left to right. Location numbers are shown in Figure 2.3.

Appendix C: Velocity Measurements along the 11th Geometry with the Crown and Screen (Fourth Set)

All dimensions and values are at the model scale.

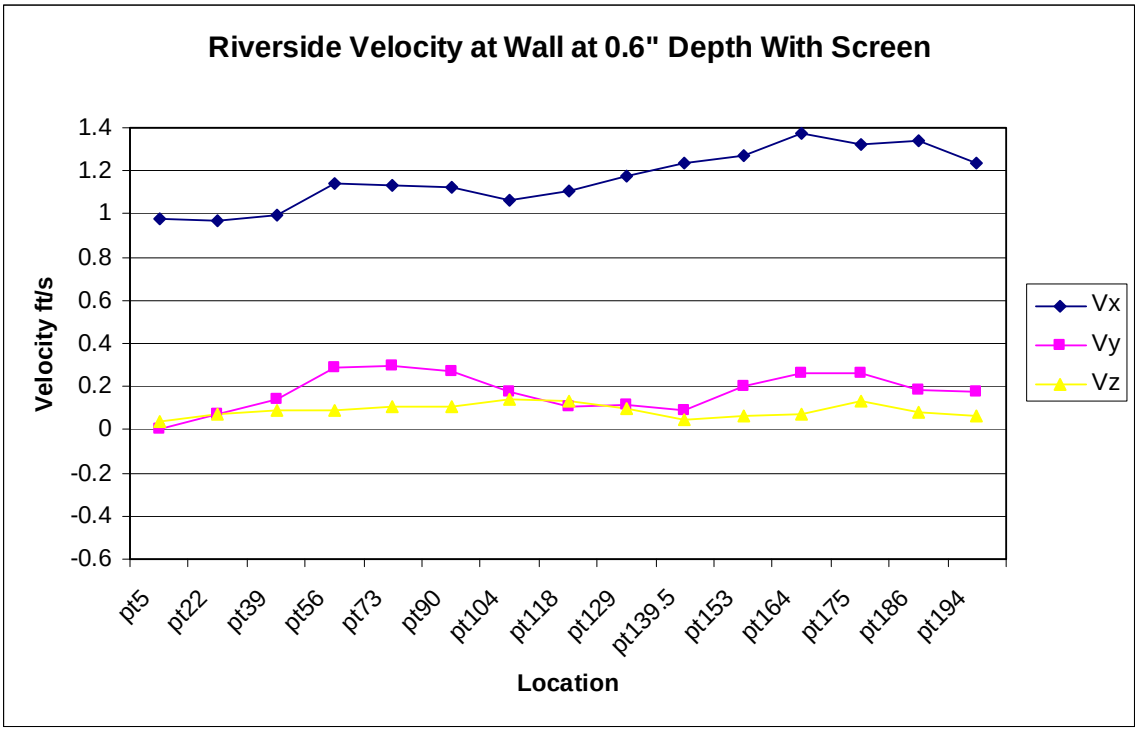

Figure C.1. Average velocity components along the Virginia side of the 11th geometry (riverside at SAFL) at a depth of 0.6 inches from the surface. Streamflow is from left to right. Location numbers are shown in Figure 2.3.

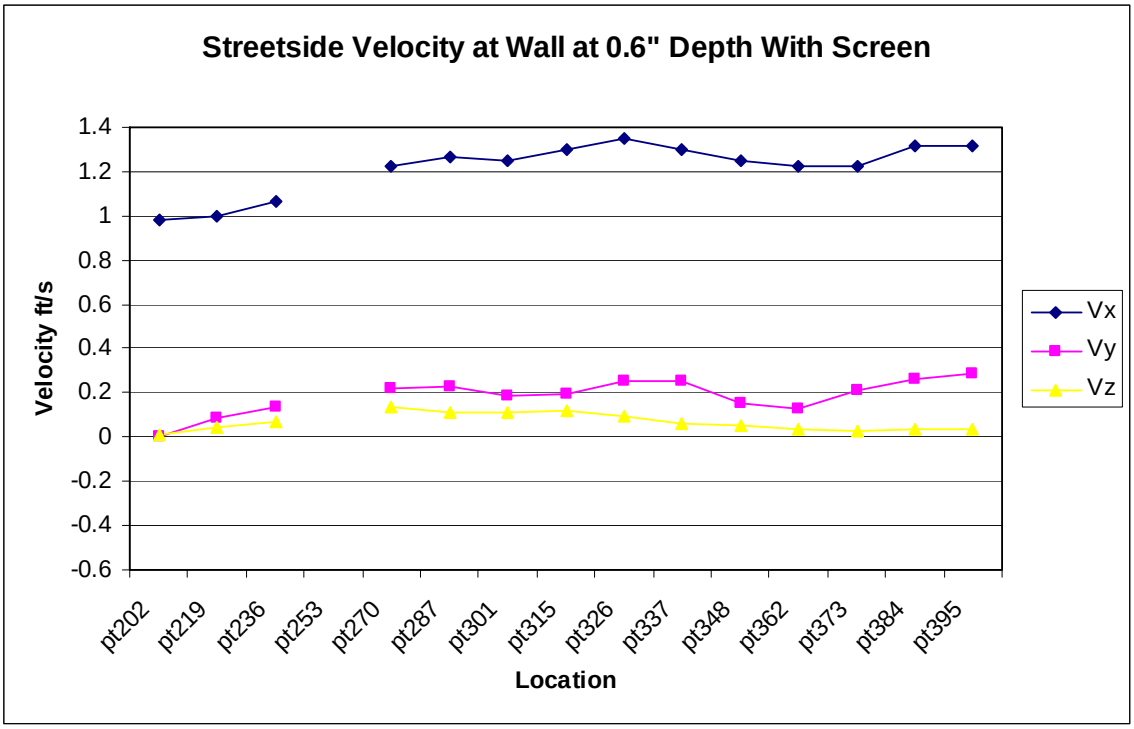

Figure C.2. Average velocity components along the Maryland side of the 11th geometry (street side at SAFL) at a depth of 0.6 inches from the surface. Streamflow is from left to right. Location numbers are shown in Figure 2.3.

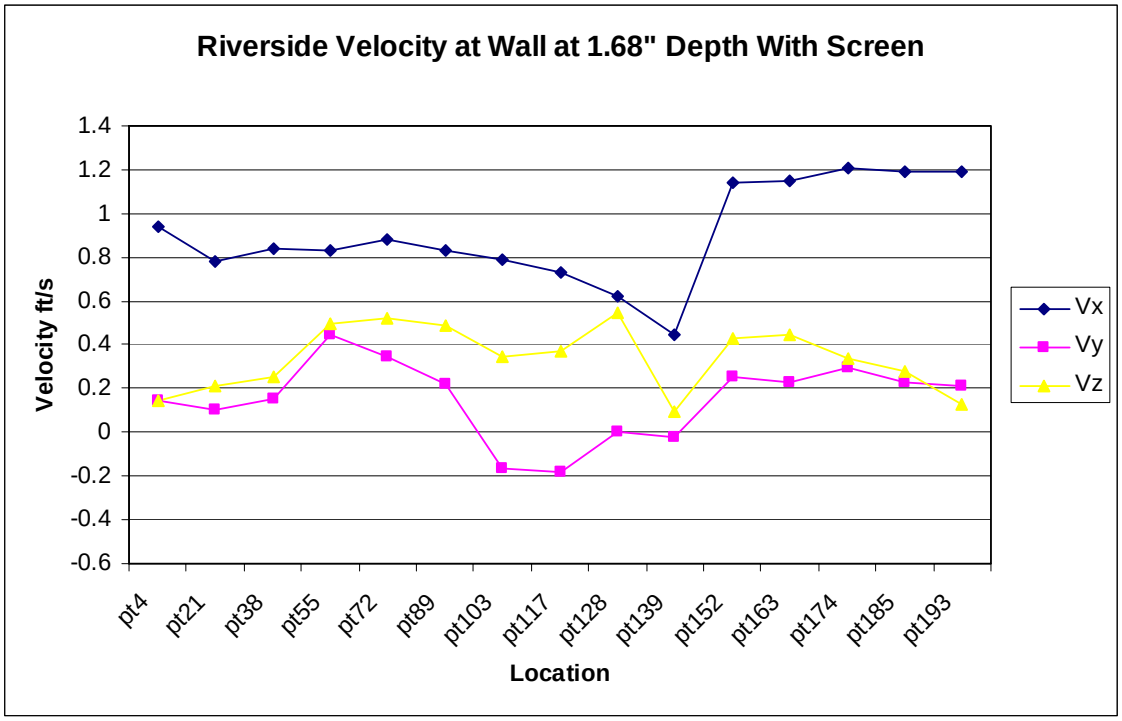

Figure C.3. Average velocity components along the Virginia side of the 11th geometry (riverside at SAFL) at a depth of 1.68 inches from the surface. Streamflow is from left to right. Location numbers are shown in Figure 2.3.

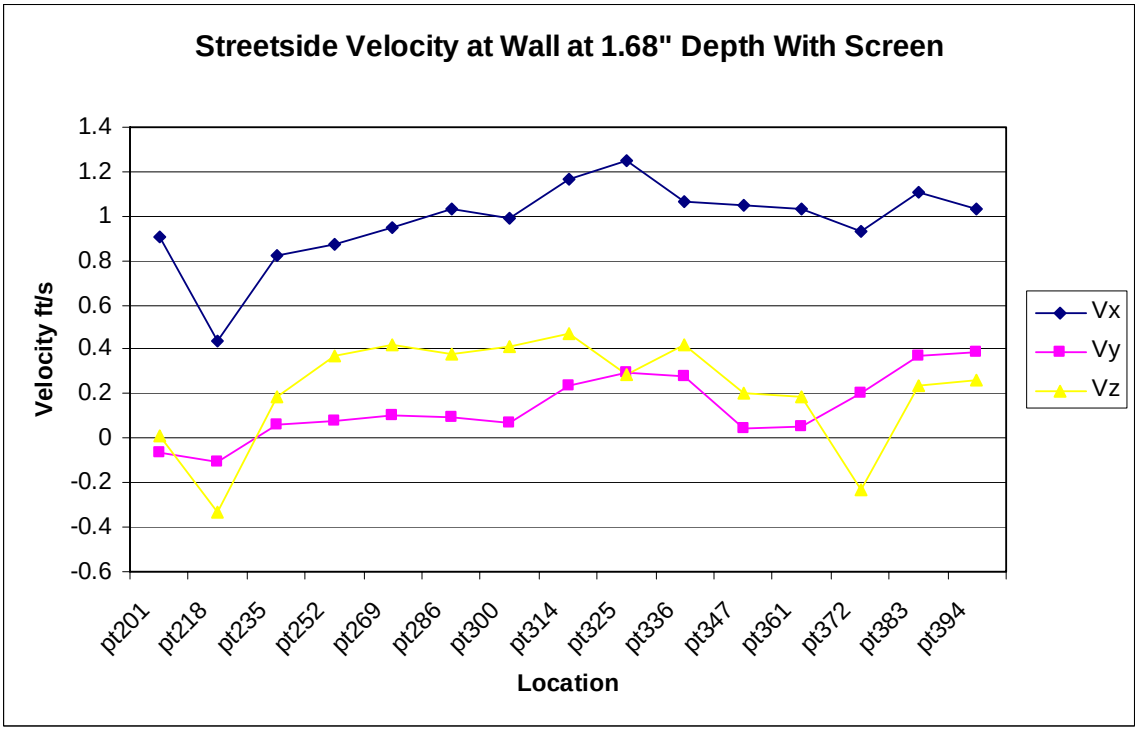

Figure C.4. Average velocity components along the Maryland side of the 11th geometry (street side at SAFL) at a depth of 1.68 inches from the surface. Streamflow is from left to right. Location numbers are shown in Figure 2.3.

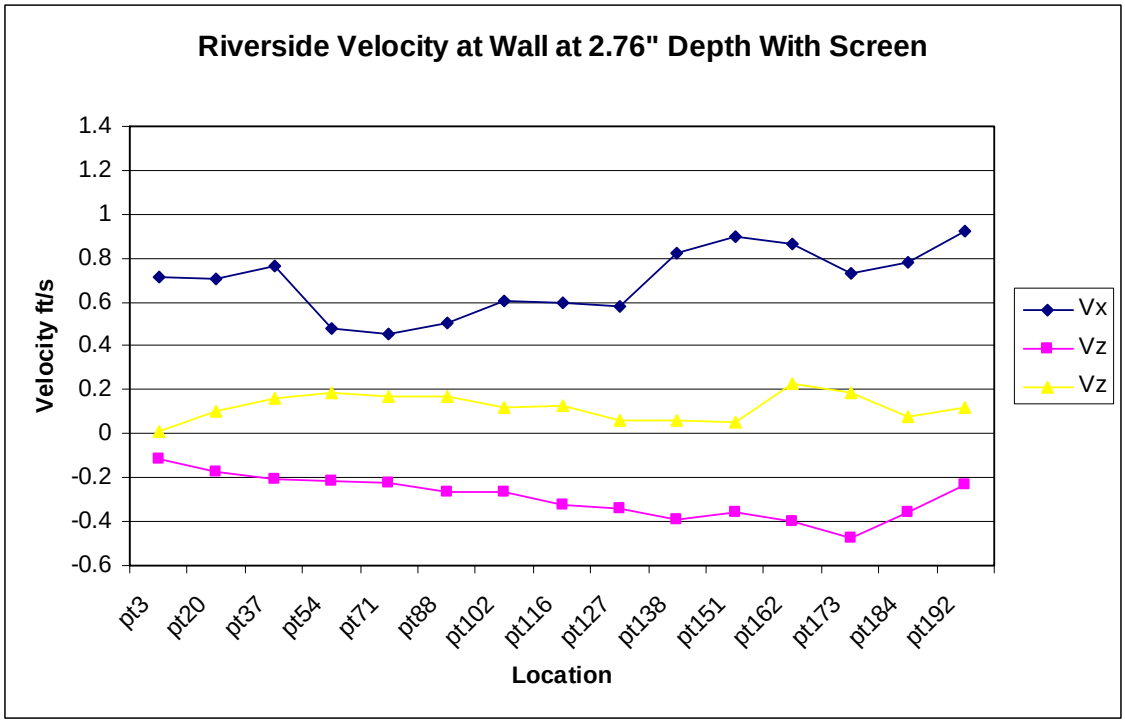

Figure C.5. Average velocity components along the Virginia side of the 11th geometry (riverside at SAFL) at a depth of 2.76 inches from the surface. Streamflow is from left to right. Location numbers are shown in Figure 2.3.

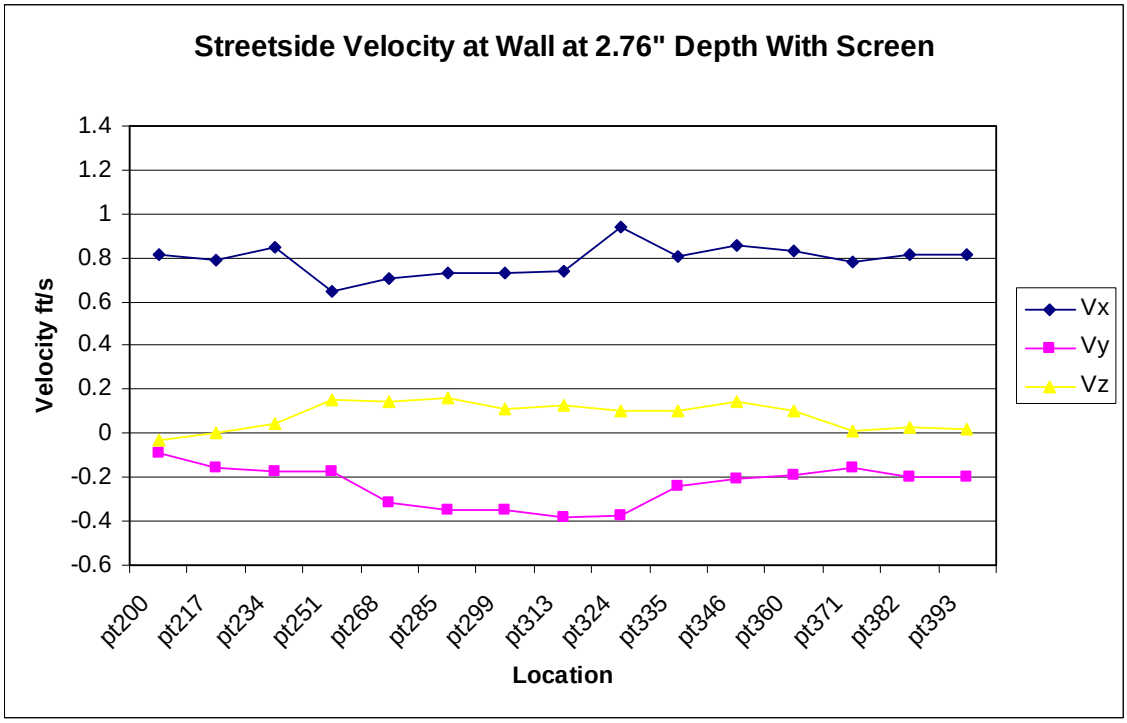

Figure C.6. Average velocity components along the Maryland side of the 11th geometry (street side at SAFL) at a depth of 2.76 inches from the surface. Streamflow is from left to right. Location numbers are shown in Figure 2.3.

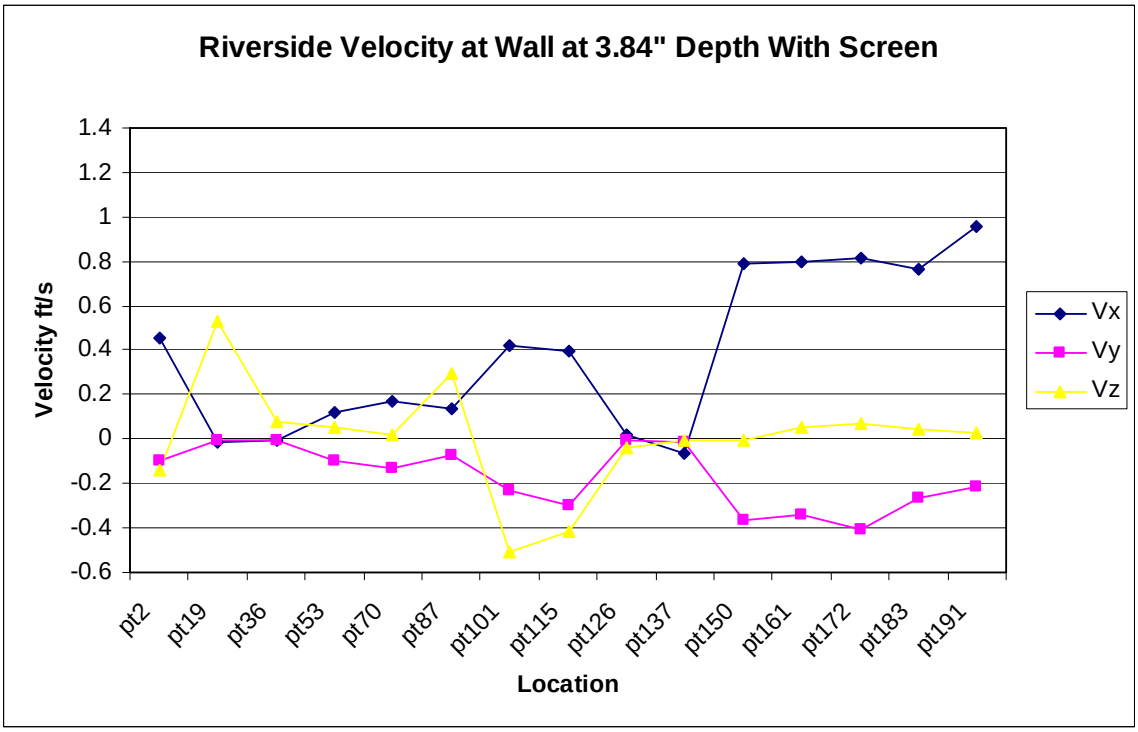

Figure C.7. Average velocity components along the Virginia side of the 11th geometry (riverside at SAFL) at a depth of 3.84 inches from the surface. Streamflow is from left to right. Location numbers are shown in Figure 2.3.

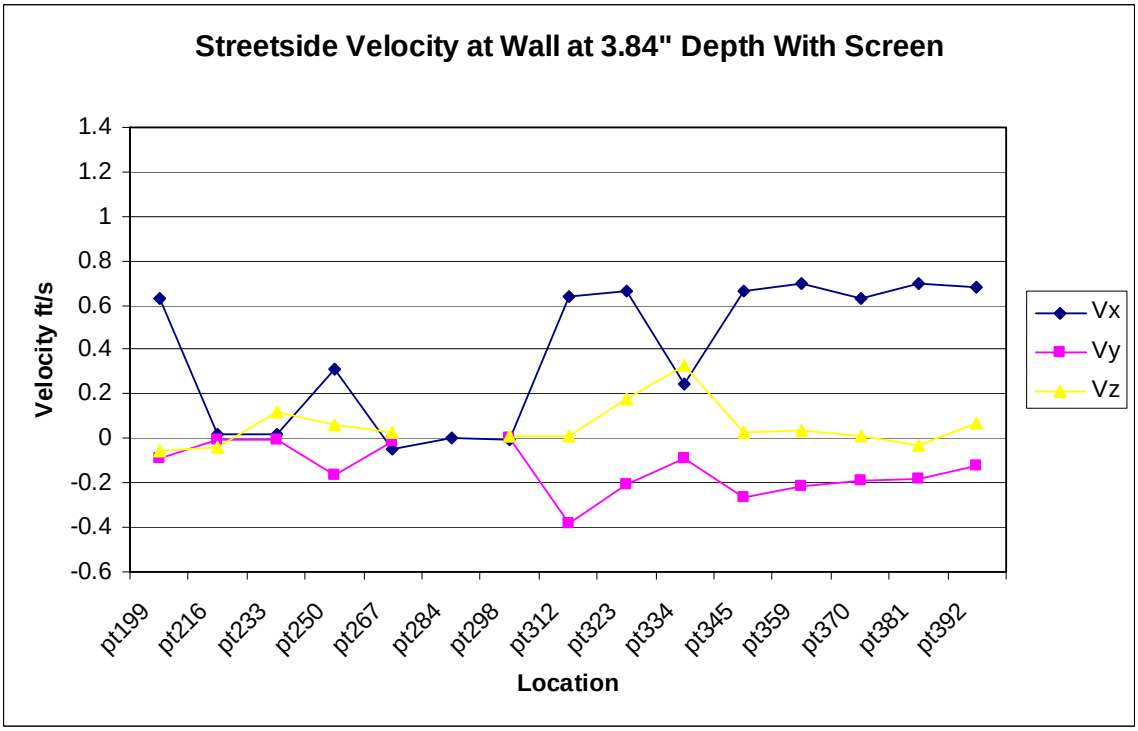

Figure C.8. Average velocity components along the Maryland side of the 11th geometry (street side at SAFL) at a depth of 3.84 inches from the surface. Streamflow is from left to right. Location numbers are shown in Figure 2.3.

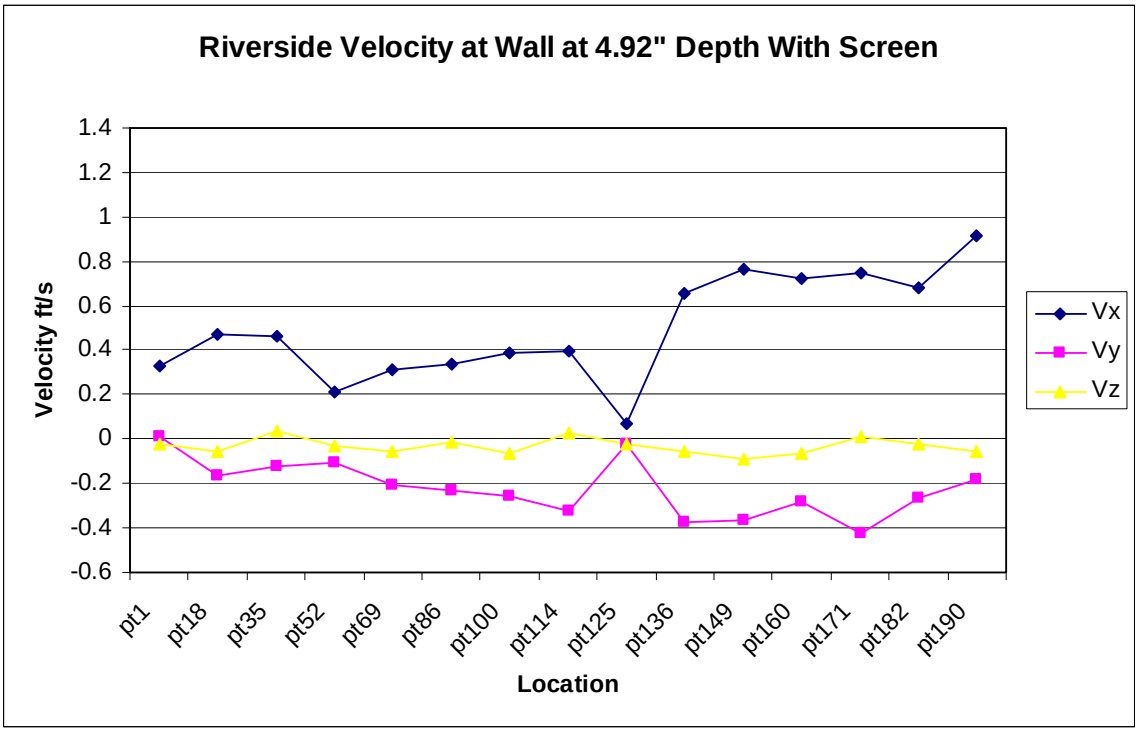

Figure C.9. Average velocity components along the Virginia side of the 11th geometry (riverside at SAFL) at a depth of 4.92 inches from the surface. Streamflow is from left to right. Location numbers are shown in Figure 2.3.

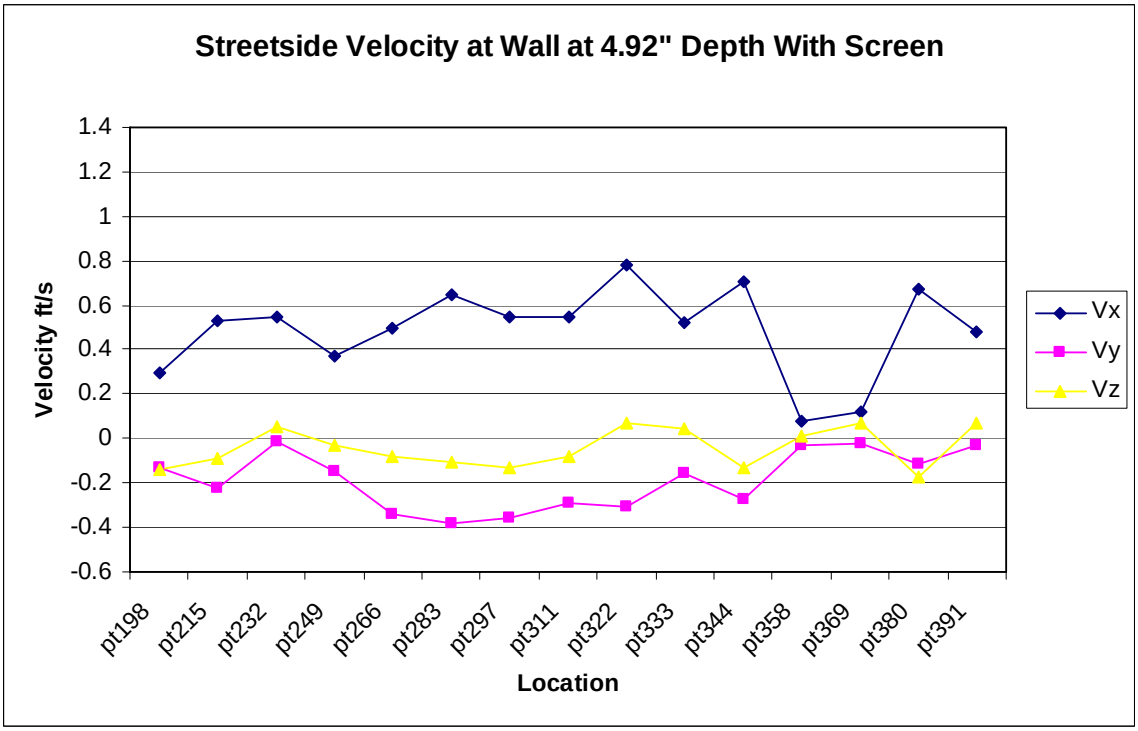

Figure C.10. Average velocity components along the Maryland side of the 11th geometry (street side at SAFL) at a depth of 4.92 inches from the surface. Streamflow is from left to right. Location numbers are shown in Figure 2.3.

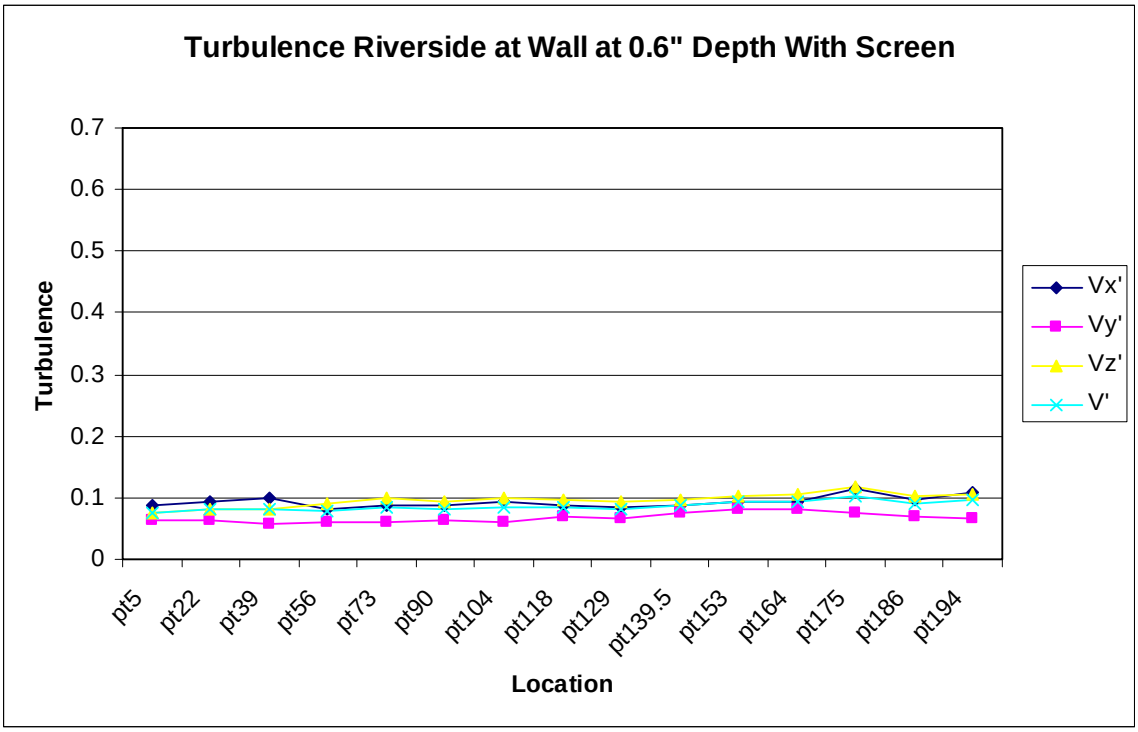

Figure C.11. Turbulence intensity along the Virginia side of the 11th geometry (river side at SAFL) at a depth of 0.6 inches from the surface. Streamflow is from left to right. Location numbers are shown in Figure 2.3.

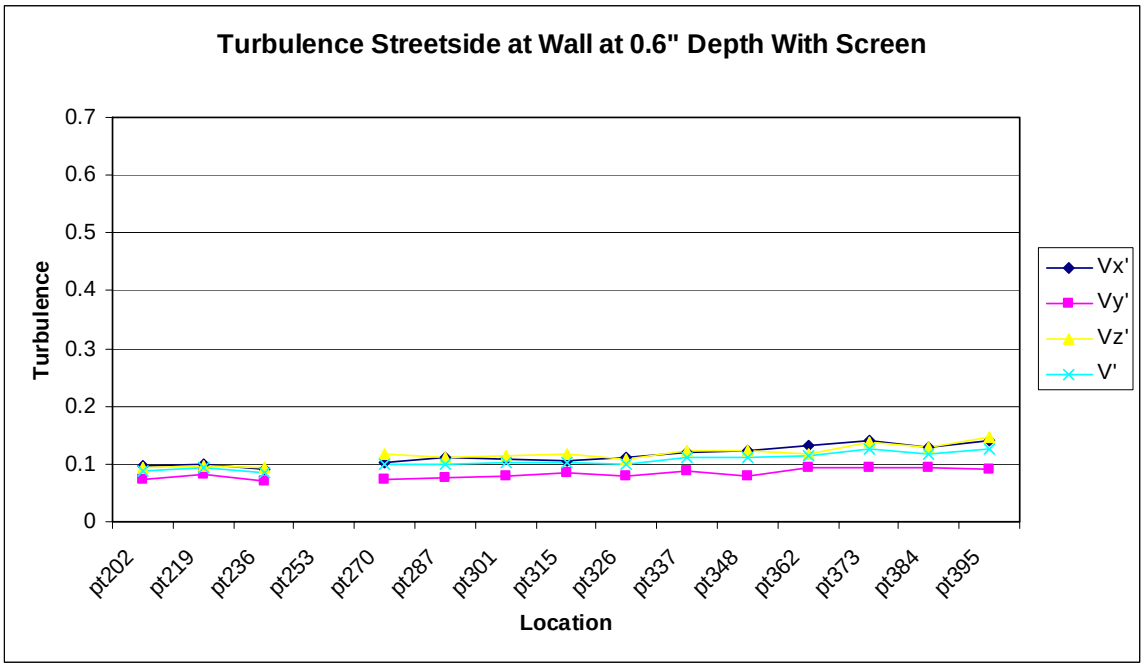

Figure C.12. Turbulence intensity along the Maryland side of the 11th geometry (street side at SAFL) at a depth of 0.6 inches from the surface. Streamflow is from left to right. Location numbers are shown in Figure 2.3.

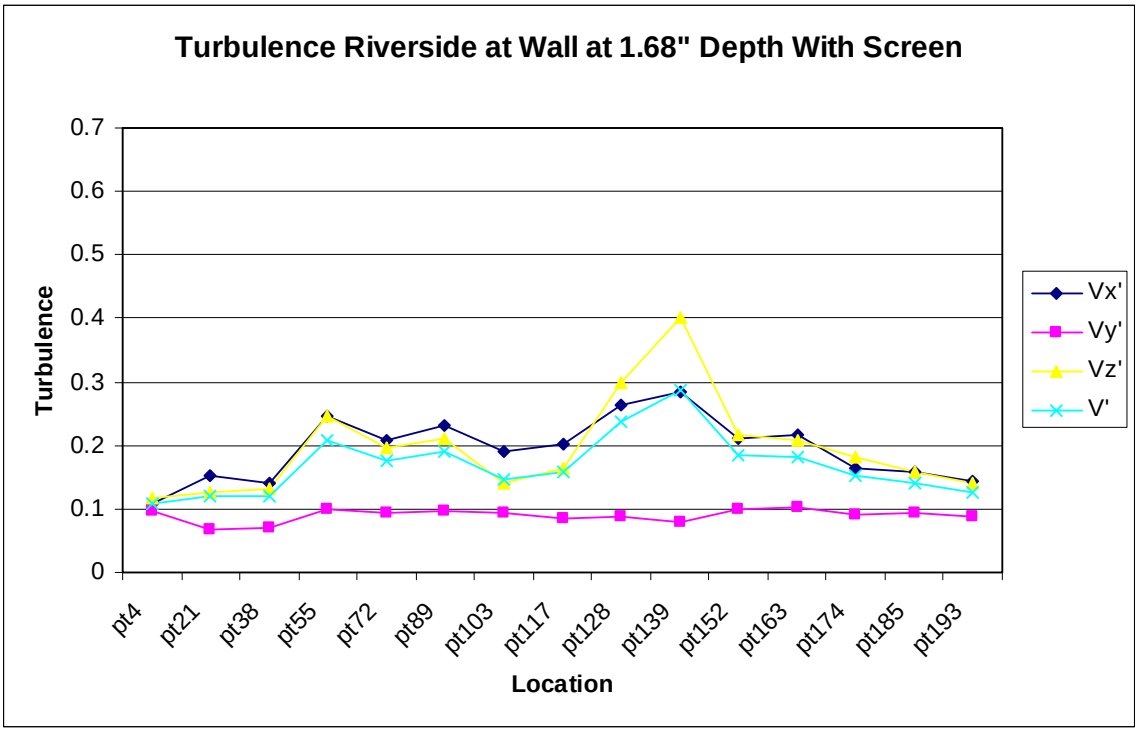

Figure C.13. Turbulence intensity along the Virginia side of the 11th geometry (river side at SAFL) at a depth of 1.68 inches from the surface. Streamflow is from left to right. Location numbers are shown in Figure 2.3.

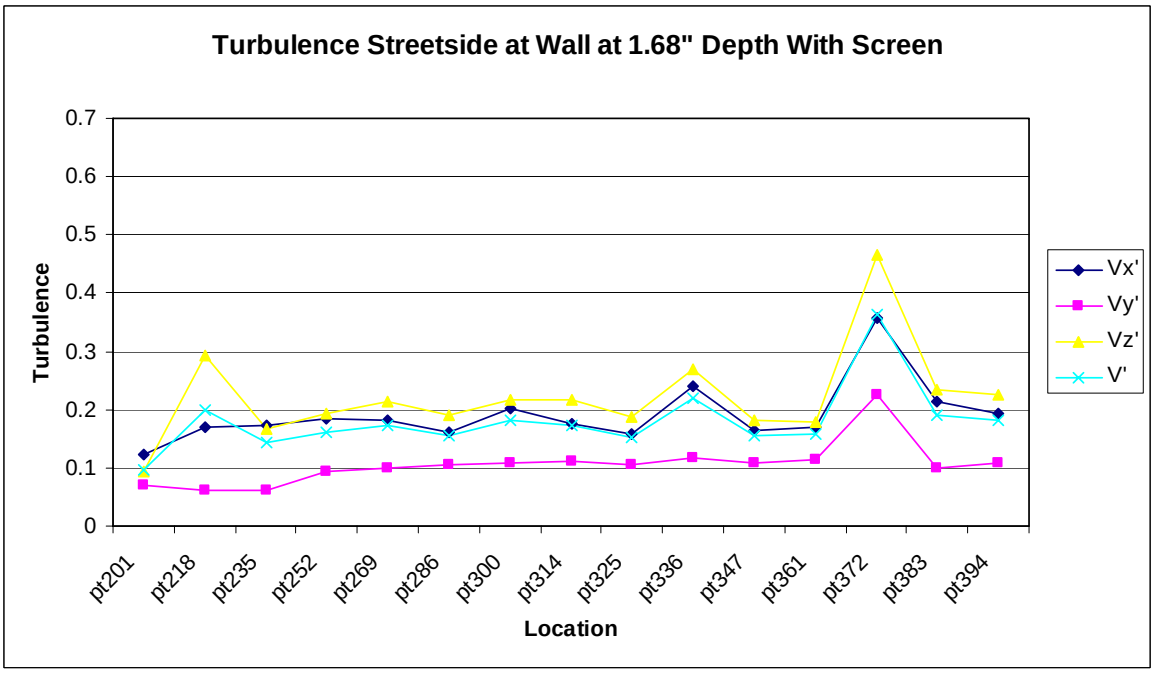

Figure C.14. Turbulence intensity along the Maryland side of the 11th geometry (street side at SAFL) at a depth of 1.68 inches from the surface. Streamflow is from left to right. Location numbers are shown in Figure 2.3.

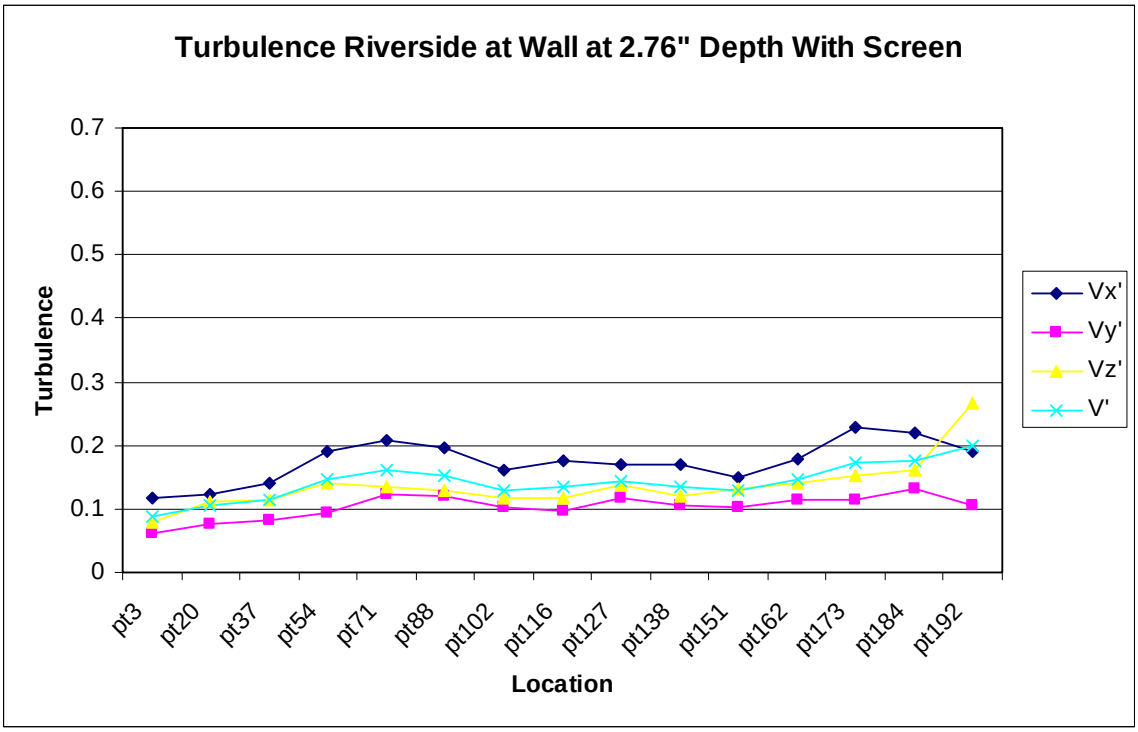

Figure C.15. Turbulence intensity along the Virginia side of the 11th geometry (river side at SAFL) at a depth of 2.76 inches from the surface. Streamflow is from left to right. Location numbers are shown in Figure 2.3.

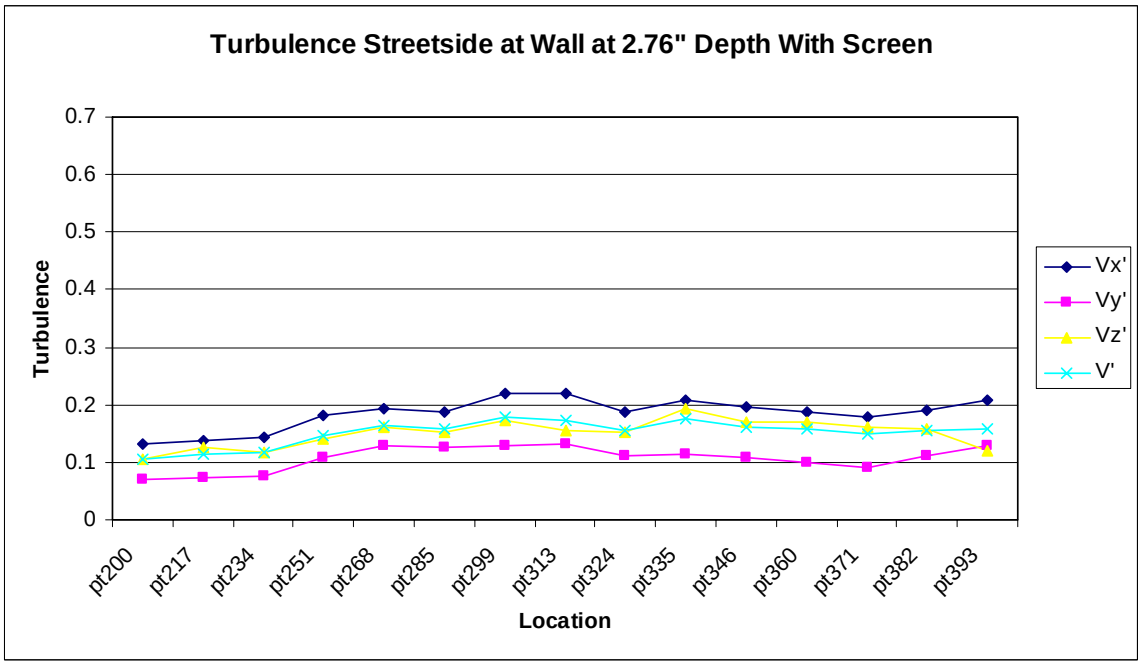

Figure C.16. Turbulence intensity along the Maryland side of the 11th geometry (street side at SAFL) at a depth of 2.76 inches from the surface. Streamflow is from left to right. Location numbers are shown in Figure 2.3.

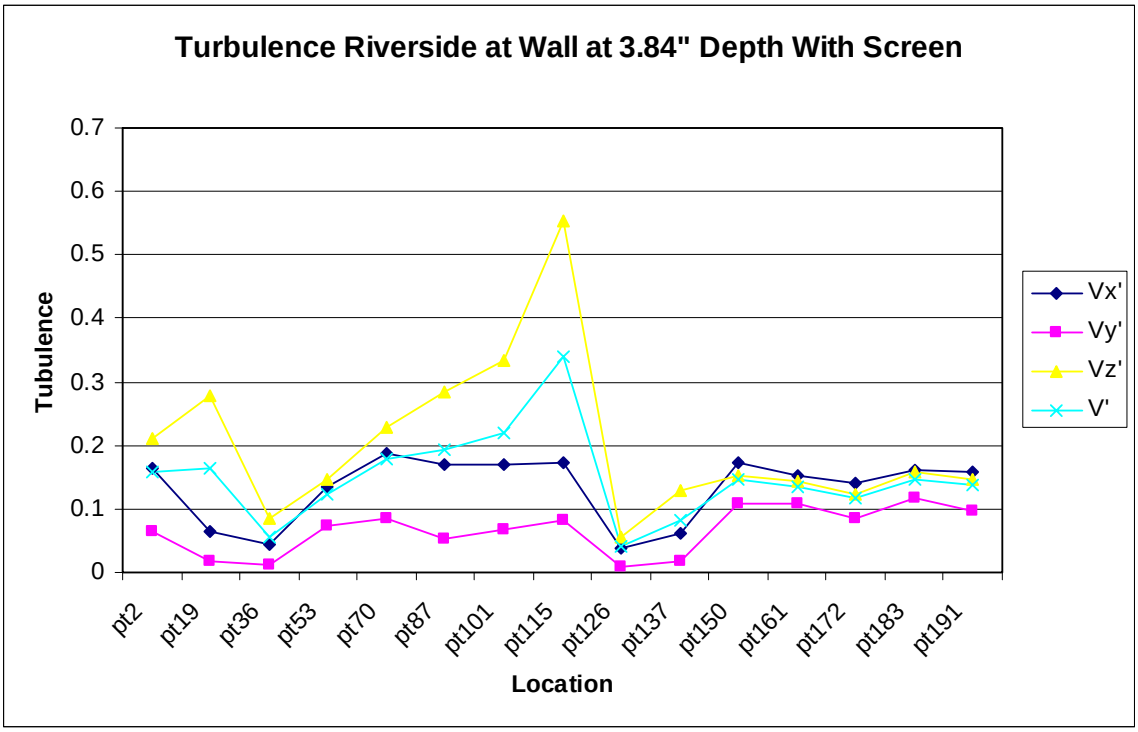

Figure C.17. Turbulence intensity along the Virginia side of the 11th geometry (river side at SAFL) at a depth of 3.84 inches from the surface. Streamflow is from left to right. Location numbers are shown in Figure 2.3.

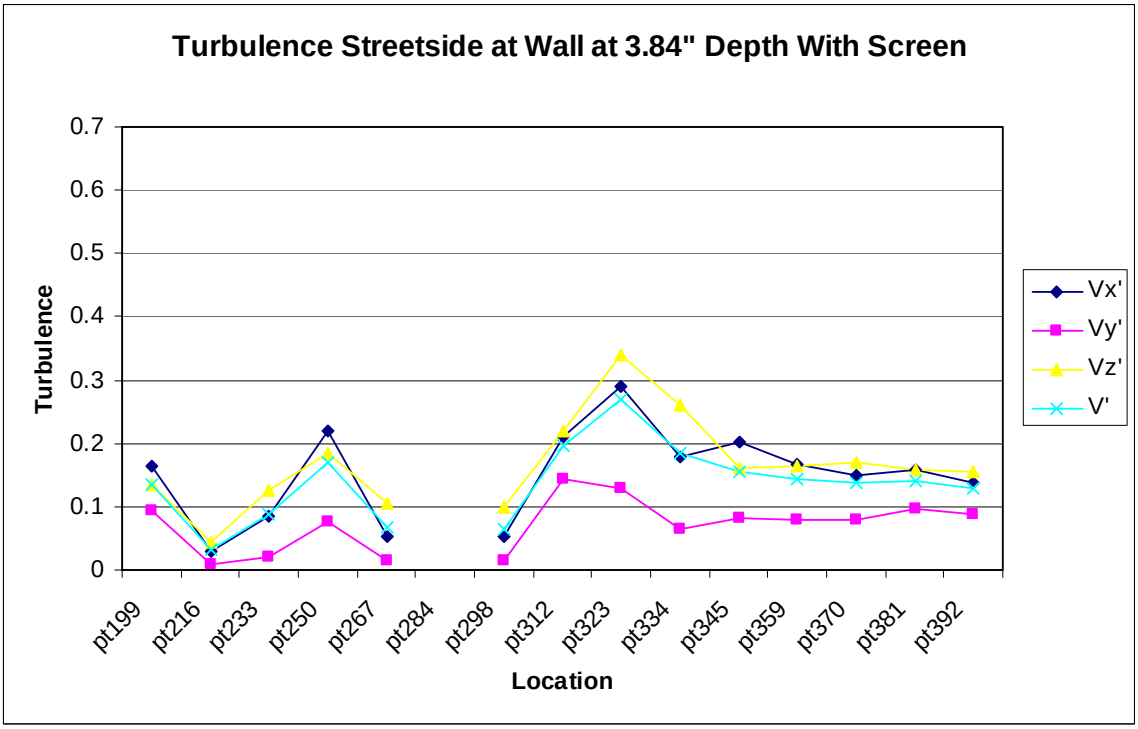

Figure C.18. Turbulence intensity along the Maryland side of the 11th geometry (street side at SAFL) at a depth of 3.84 inches from the surface. Streamflow is from left to right. Location numbers are shown in Figure 2.3.

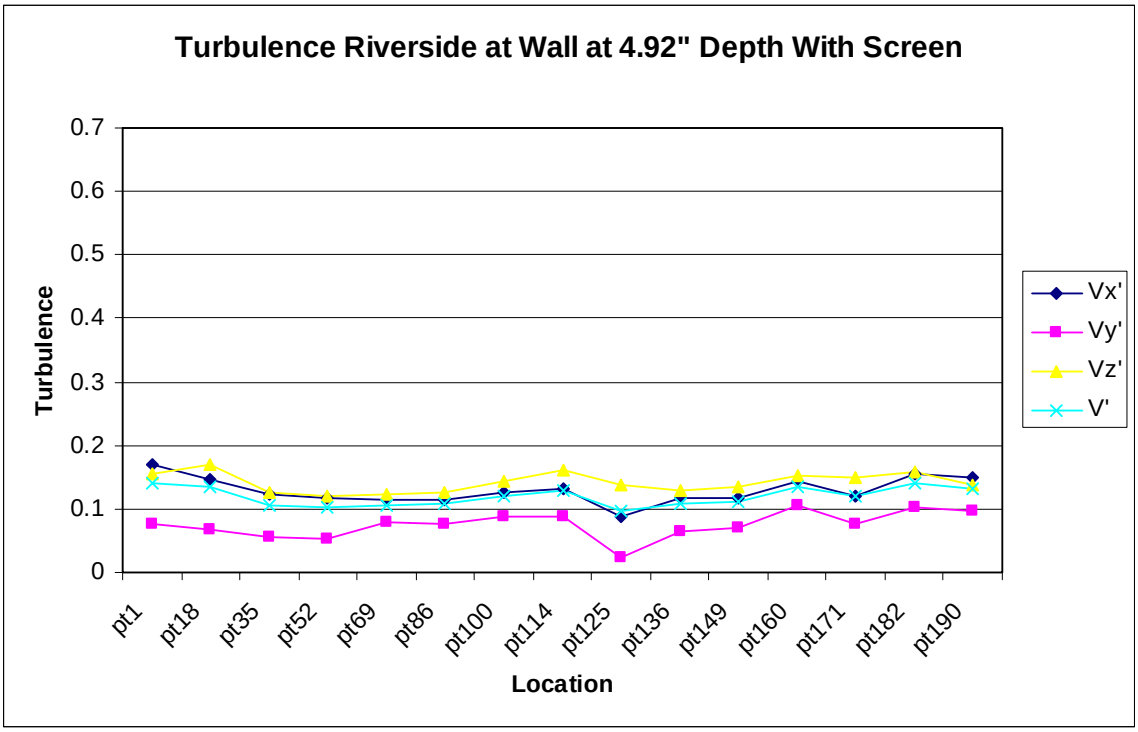

Figure C.19. Turbulence intensity along the Virginia side of the 11th geometry (river side at SAFL) at a depth of 4.92 inches from the surface. Streamflow is from left to right. Location numbers are shown in Figure 2.3.

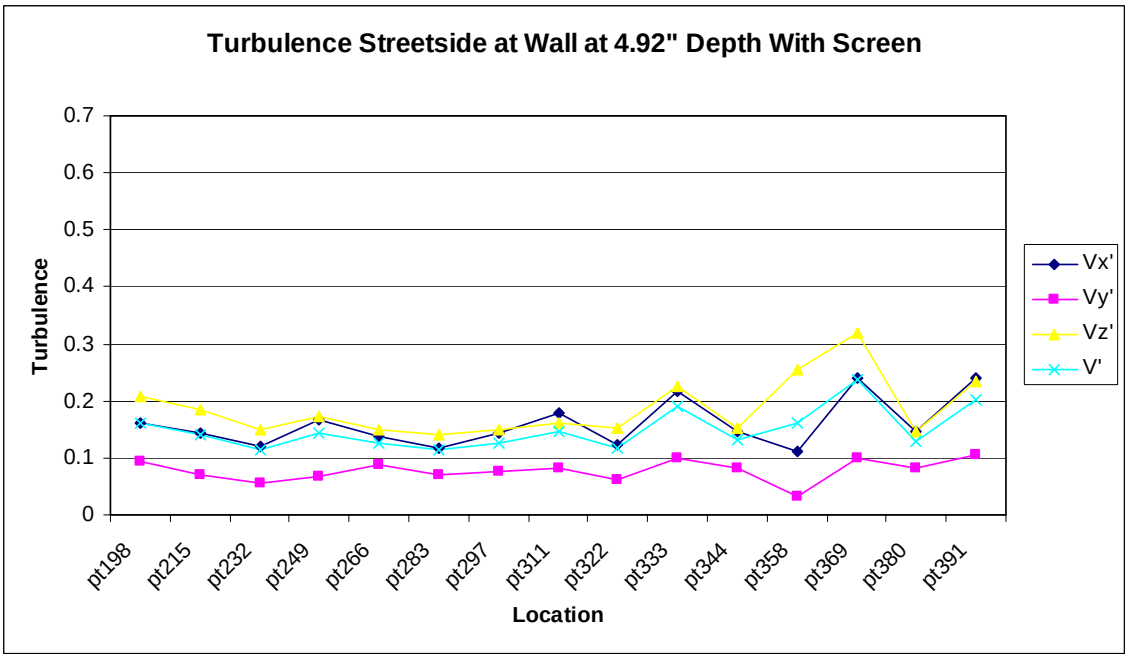

Figure C.20. Turbulence intensity along the Maryland side of the 11th geometry (street side at SAFL) at a depth of 4.92 inches from the surface. Streamflow is from left to right. Location numbers are shown in Figure 2.3.

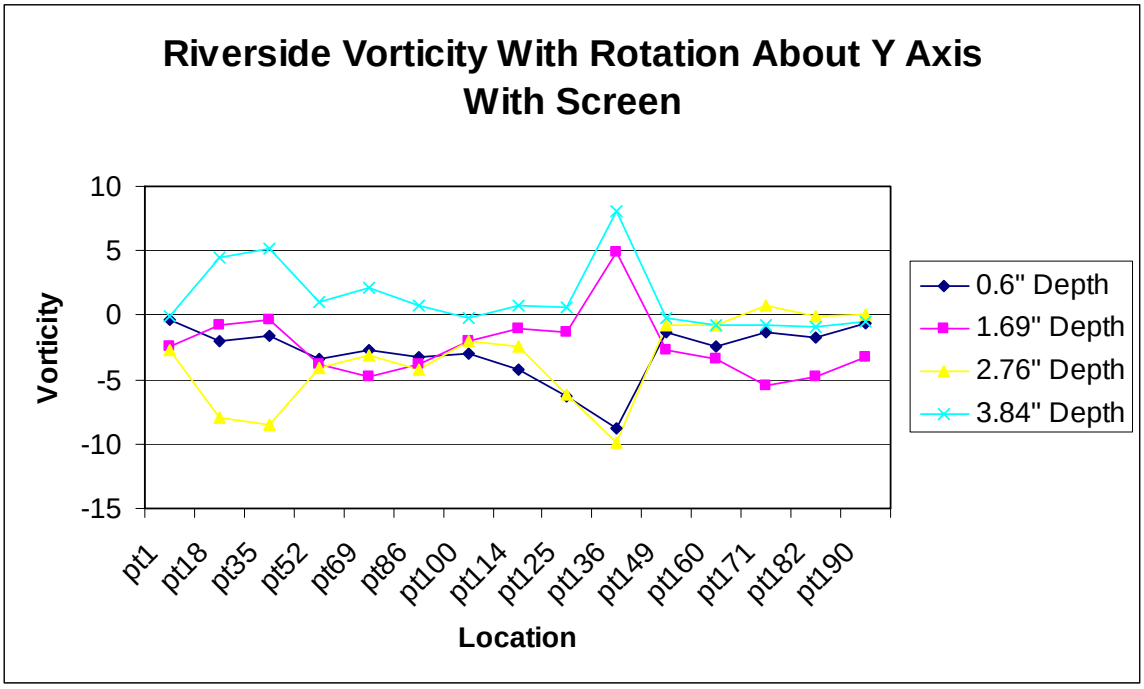

Figure C.21. Estimated vorticity about the y-axis along the Virginia side of the 11th geometry (riverside at SAFL). Streamflow is from left to right. Location numbers are shown in Figure 2.3.

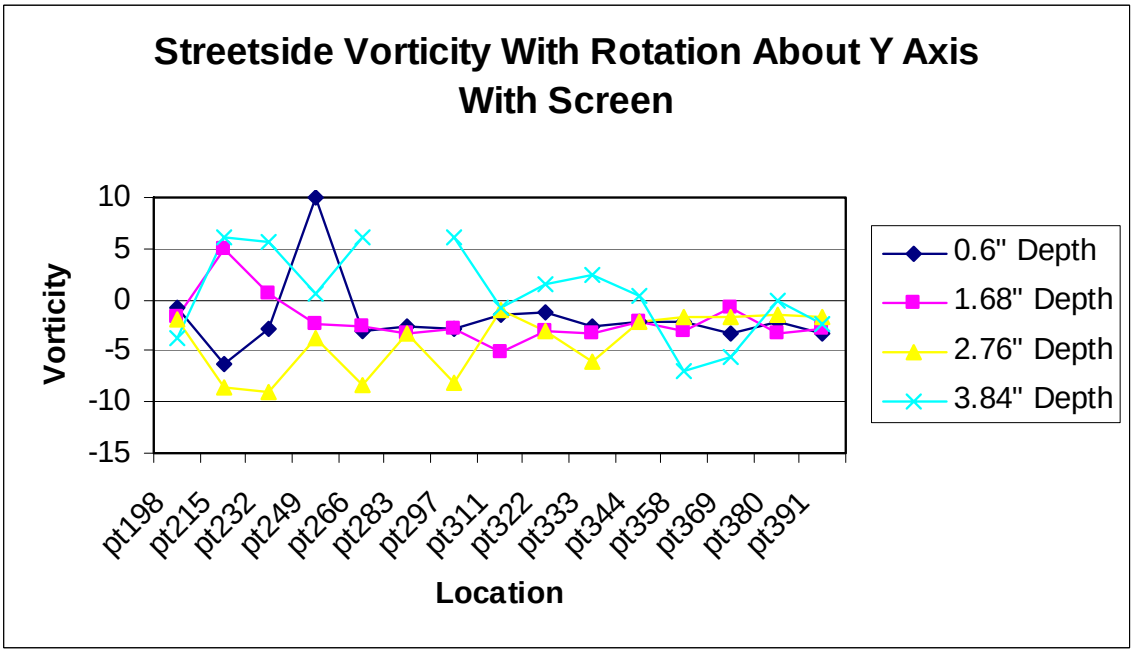

Figure C.22. Estimated vorticity about the y-axis along the Maryland side of the 11th geometry (street side at SAFL). Streamflow is from left to right. Location numbers are shown in Figure 2.3.